1. **Mechanics**

2. **Machine Building and Machine Science**

3. **Information Technology, Computer Science, and Management**

VESTNIK
of
DON STATE
TECHNICAL
UNIVERSITY

Vol. 18, № 3

CONTENT

MECHANICS
МЕХАНИКА

General scalarization method of dynamic elastic fields in transversally isotropic media and its new applications[*]

I. P. Miroshnichenko[1], V. P. Sizov[2][**]

[1] Don State Technical University, Rostov-on-Don, Russian Federation
[2] Rostov Scientific Research Institute for Radiocommunication, Rostov-on-Don, Russian Federation

Обобщенный метод скаляризации динамических упругих полей в трансверсально-изотропных средах и его новые применения[***]

И. П. Мирошниченко[1], В. П. Сизов[2][**]

[1] Донской государственный технический университет, г. Ростов-на-Дону, Российская Федерация
[2] Ростовский-на-Дону научно-исследовательский институт радиосвязи, г. Ростов-на-Дону, Российская Федерация

Introduction. An efficient technique of tensor field scalarization is successfully used while investigating tensor elastic fields of displacements, stresses and deformations in the layered structures of different materials, including transversally isotropic composites. These fields can be expressed through the scalar potentials corresponding to the quasi-longitudinal, quasi-transverse, and transverse-only waves. Such scalarization is possible if the objects under consideration are tensors relating to the subgroup of general coordinate conversions, when the local affine basis has one invariant vector that coincides with the material symmetry axis of the material. At this, the known papers consider structures where this vector coincides with the normal to the boundary between layers. However, other cases of the mutual arrangement of the material symmetry axis of the material and the boundaries between layers are of interest on the practical side.

Materials and Methods. The work objective is further development of the scalarization method application in the boundary value problems of the dynamic elasticity theory for the cases of an arbitrary arrangement of the material symmetry axis relative to the boundary between layers. The present research and methodological apparatus are developed through the general technique of scalarization of the dynamic elastic fields of displacements, stresses and strains in the transversally isotropic media.

Research Results. New design ratios for the determination of the displacement fields, stresses and deformations in the transversally isotropic media are obtained for the cases of an arbitrary arrangement of the material symmetry axes of the layer materials with respect to the boundaries between layers.

Введение. При исследовании тензорных упругих полей перемещений, напряжений и деформаций в слоистых конструкциях из различных материалов, включая трансверсально-изотропные композиты, успешно применяется эффективный метод скаляризации тензорных полей. Данные поля могут быть выражены через скалярные потенциалы, соответствующие квазипродольным, квазипоперечным и чисто поперечным волнам. Такая скаляризация возможна, если рассматриваемые объекты являются тензорами относительно подгруппы общих преобразований координат, когда локальный аффинный базис имеет один инвариантный вектор, который совпадает с осью материальной симметрии материала. При этом в известных работах рассматриваются конструкции, где этот вектор совпадает с нормалью к границе между слоями. Однако, для практики представляют интерес и другие случаи взаимного расположения оси материальной симметрии материала и границы между слоями.

Целью является дальнейшее развитие применения метода скаляризации в граничных задачах динамической теории упругости на случаи произвольного расположения оси материальной симметрии по отношению к границе между слоями.

Методы исследования. Предлагаемый научно-методический аппарат разработан на основе использования обобщенного метода скаляризации динамических упругих полей перемещений, напряжений и деформаций в трансверсально-изотропных средах.

Результаты исследования. Получены новые расчетные соотношения для определения полей перемещений, напряжений и деформаций в трансверсально-изотропных средах на случаи произвольного расположения осей материальной симметрии материалов слоев по отношению к границам между слоями.

Discussion and Conclusions. The present research and methodological apparatus are successfully used in determining the stress-strain state in the layered structures of transversally isotropic materials, and in analyzing the diagnosis results of the state of the plane-layered and layered cylindrical structures under operation.

Keywords: scalarization method, transversally isotropic medium, acoustic waves, composite materials.

Обсуждение и заключения. Предлагаемый научно-методический аппарат успешно использован при определении напряженно-деформированного состояния в слоистых конструкциях, выполненных из трансверсально-изотропных материалов, и при анализе результатов диагностики состояния плоскослоистых и слоистых цилиндрических конструкций, находящихся в эксплуатации.

Ключевые слова: метод скаляризации, трансверсально-изотропная среда, акустические волны, композиционные материалы.

Introduction. When investigating the displacement, stress, and strain tensor elastic fields in layered structures of various materials, including transversely isotropic composites [1-3], an efficient method for scalarization of tensor fields proposed in [4] is successfully used. Then, the checked fields can be expressed through scalar potentials corresponding to quasi-longitudinal, quasi-transverse, and transverse-only waves, respectively. This scalarization is possible if the objects under consideration are tensors relative to the subgroup of general coordinate transformations, when the local affine basis has one invariant vector that coincides with the material symmetry axis of the material. Structures where this vector coincides with the normal to the boundary between layers are considered in [5]. However, on the practical side, other cases of the mutual arrangement of the material symmetry axis of the material and the boundaries between layers are of interest.

Materials and Methods. The work objective is the further development of the application of the scalarization method for the boundary problems of the dynamic elasticity theory to the cases of an arbitrary arrangement of the material symmetry axis with respect to the boundary between layers.

At first, in the coordinate system with an admissible reference point, there are components of the displacement and stress tensors relative to this frame. Then, knowing all the components of the tensor fields in the given reference coordinates, we can find the normal and tangential displacement and stress components corresponding to the area lying on the boundary by passing to the coordinate system associated with the boundary between layers. These components are used later to satisfy the boundary problem conditions [5].

To dig deeper into the foregoing, we will discuss it in the context of solving problems for the plane-layered structures.

Let us consider the case when the principal symmetry axis of a transversally isotropic material makes angle α with the normal of the plane boundary surface between the layers (Fig. 1). At this, we assume that the field is independent of the coordinate $\bar{y}$.
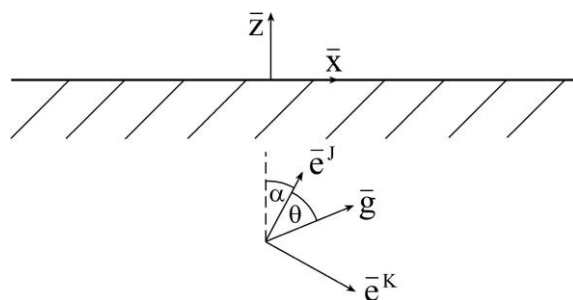
Fig. 1 Computational pattern

Design ratios

In accordance with [4]:

$$U_i = \left(\overset{(L)}{D_1}\nabla_i + \delta_i^J \overset{(L)}{D_2}\nabla_J \right)\phi + \left(\overset{(T)}{D_1} \frac{1}{\overset{(T)}{g}}\nabla_i\nabla_J + \overset{(T)}{g}\delta_i^J \right)w + \sqrt{g}(\delta_i^K\nabla^N - \delta_i^N\nabla^K)v \,;$$

$$\sigma_{ij} = (\overset{(L)}{d_1} g_{ij} + \overset{(L)}{d_2}\delta_i^J\delta_j^J + \overset{(L)}{d_3}\delta_{(i}^J\nabla_{j)}\nabla_J + \overset{(L)}{d_4}\nabla_i\nabla_j)\phi +$$
$$+ (\overset{(T)}{d_1} g_{ij}\nabla_J + \overset{(T)}{d_2}\delta_i^J\delta_j^J\nabla_J + \overset{(T)}{d_3}\delta_{(i}^J\nabla_{j)} + \overset{(T)}{d_4}\nabla_i\nabla_J\nabla_j)w +$$
$$+ 2\sqrt{g}[a_2(\nabla_{(i}\delta_{j)}^K\nabla^N - \nabla_{(i}\delta_{j)}^N\nabla^K) + a_4(\delta_{(i}^J\delta_{j)}^K\nabla^N - \delta_{(i}^J\delta_{j)}^N\nabla^K)\nabla_J]v \,. \tag{1}$$

Components of the tensor fields of displacements U_i and stresses σ_{ij} in the coordinate system associated with the anisotropy of the material x^J, x^K can be written as follows:

$$U_J = i\,\overset{(L)}{\xi}(\overset{(L)}{D_1} + \overset{(L)}{D_2})\phi + (-\overset{(T)}{D_1}\frac{\overset{(T)}{\xi^2}}{\overset{(T)}{g}} + \overset{(T)}{g})w \,;$$

$$U_K = i\,\overset{(L)}{\beta}\overset{(L)}{D_1}\phi - \overset{(T)}{D_1}\frac{\overset{(T)}{\xi}\overset{(T)}{\beta}}{\overset{(T)}{g}}w \,;$$

$$\sigma_{JJ} = [\overset{(L)}{d_1} + \overset{(L)}{d_2} - (\overset{(L)}{d_3} + \overset{(L)}{d_4})\overset{(L)}{\xi^2}]\phi + i\,\overset{(T)}{\xi}(\overset{(T)}{d_1} + \overset{(T)}{d_2} + \overset{(T)}{d_3} - \overset{(T)}{d_4}\overset{(T)}{\xi^2})w \,; \tag{2}$$

$$\sigma_{JK} = -(\frac{1}{2}\overset{(L)}{d_3}\overset{(L)}{\xi}\overset{(L)}{\beta} + \overset{(L)}{d_4}\overset{(L)}{\xi}\overset{(L)}{\beta})\phi + i\,\overset{(T)}{\beta}(\frac{1}{2}\overset{(T)}{d_3} - \overset{(T)}{d_4}\overset{(T)}{\xi^2})w \,;$$

$$\sigma_{KK} = (\overset{(L)}{d_1} + \overset{(L)}{d_4}\overset{(L)}{\beta^2})\phi + i\,\overset{(T)}{\xi}(\overset{(T)}{d_1} - \overset{(T)}{d_4}\overset{(T)}{\beta^2})w \,.$$

Here, the potentials of quasi-longitudinal ϕ and quasi-transverse w waves should satisfy the wave equation with the corresponding wave number g ($\overset{(L)}{g}$ or $\overset{(T)}{g}$), and they have the form:

$$\phi = \phi_0 e^{i\,\overset{(L)}{\xi}x^J} e^{i\,\overset{(L)}{\beta}x^K} \,;$$
$$w = w_0 e^{i\,\overset{(T)}{\xi}x^J} e^{i\,\overset{(T)}{\beta}x^K} \,, \tag{3}$$

Where $\xi^2 + \beta^2 = g^2$; $\qquad (\Delta + g^2)\begin{matrix}\phi\\w\end{matrix} = 0$. $\tag{4}$

The coefficients D and d entering (2) are determined in [5] and are as follows:

$$\overset{(L)}{D_1} = \frac{\overset{(L)}{g^2}(C_{13} + C_{44})}{\omega^2\rho - h^2\overset{(L)}{C_{44}} - (\overset{(L)}{g^2} - h^2)(C_{11} - C_{13} - C_{44})} \,;$$

$$\overset{(L)}{D_2} = \frac{\overset{(L)}{g^2}}{h^2}\frac{\omega^2\rho - h^2(2C_{44} + C_{13}) - (\overset{(L)}{g^2} - h^2)C_{11}}{\omega^2\rho - h^2\overset{(L)}{C_{44}} - (\overset{(L)}{g^2} - h^2)(C_{11} - C_{13} - C_{44})} = \frac{\overset{(L)}{g^2}}{\overset{(L)}{g^2} - h^2}\overset{(L)}{D_1} \,;$$

$$\overset{(T)}{D_1} = \frac{-\overset{(T)}{g^2}(C_{13} + C_{44})}{\omega^2\rho - h^2(2C_{44} + C_{13}) - (\overset{(T)}{g^2} - h^2)C_{11}} \,; \tag{5}$$

$$\overset{(L)}{d_1} = -\overset{(L)}{g^2}a_1 - h^2 a_3(\overset{(L)}{D_1} + \overset{(L)}{D_2}) \,; \qquad \overset{(L)}{d_2} = -\overset{(L)}{g^2}a_3 - h^2(2a_4\overset{(L)}{D_2} + a_5\overset{(L)}{D_2} + a_5\overset{(L)}{D_1}) \,;$$

$$\overset{(L)}{d_3} = 2a_2\overset{(L)}{D_2} + 2a_4(2\overset{(L)}{D_1} + \overset{(L)}{D_2}) \,; \qquad \overset{(L)}{d_4} = 2a_2\overset{(L)}{D_1} \,;$$

$$\overset{(T)}{d_1} = a_1\overset{(T)}{g}(1 - \overset{(T)}{D_1}) + a_3\left(\overset{(T)}{g} - \frac{h^2}{\overset{(T)}{g}}\overset{(T)}{D_1}\right) \,;$$

$$\overset{(T)}{d_2} = \overset{(T)}{a_3}\,\overset{(T)}{g}\,(1-\overset{(T)}{D_1}) + 2\overset{(T)}{a_4}\,\overset{(T)}{g} + a_5\left(\overset{(T)}{g} - \frac{\overset{(T)}{h^2}}{\overset{(T)}{g}}\overset{(T)}{D_1}\right);$$

$$\overset{(T)}{d_3} = 2\overset{(T)}{a_2}\,\overset{(T)}{g} + 2\overset{(T)}{a_4}\left(\overset{(T)}{g} - 2\overset{(T)}{D_1}\frac{\overset{(T)}{h^2}}{\overset{(T)}{g}}\right);\ \overset{(T)}{d_4} = 2\overset{(T)}{a_2}\,\overset{(T)}{D_1}\frac{1}{\overset{(T)}{g}}; \tag{6}$$

$$a_1 = C_{11} - 2a_2;\quad a_2 = \frac{1}{2}(C_{11}-C_{12});\qquad a_3 = -\frac{1}{2}(C_{11}+C_{12})+C_{13}+C_{44}-a_4;$$

$$a_4 = -\frac{1}{2}(C_{11}-C_{12})+C_{44};\ a_5 = C_{11}+C_{33}-2(C_{13}+2C_{44}), \tag{7}$$

where C_{ij} are elasticity moduli of the material written down by the contracted index [6-7].

In the formulas (5) and (6) for these coefficients:

$$h = \frac{\cos\theta}{\cos(\alpha+\theta)}g_z;\qquad \beta = \frac{\sin\theta}{\cos(\alpha+\theta)}g_z;\qquad g = \frac{g_z}{\cos(\alpha+\theta)}.$$

The boundary conditions of the dynamic elasticity problems include the components of displacements $\bar{U}_z$, $\bar{U}_x$, and stresses $\bar{\sigma}_{zz}$, $\bar{\sigma}_{zx}$ written in the coordinate system related to the boundary (Fig. 1).

The reference coordinates $\bar{z}$, $\bar{x}$ and x^J, x^K, u, are interlinked through the relations[8]:

$$\bar{z} = -x^K\sin\alpha + x^J\cos\alpha;\ \bar{x} = x^K\cos\alpha + x^J\sin\alpha \tag{8}$$

or:

$$x^K = \bar{x}\cos\alpha - \bar{z}\sin\alpha;\ x^J = \bar{x}\sin\alpha + \bar{z}\cos\alpha. \tag{9}$$

Using relations (8) and (9), from the formulas [5]:

$$\bar{U}_i = \frac{\partial x^m}{\partial \bar{x}^i}U_m;\ \bar{\sigma}_{ij} = \frac{\partial x^m}{\partial \bar{x}^i}\frac{\partial x^p}{\partial \bar{x}^j}\sigma_{mp}, \tag{10}$$

where the coefficients with a bar tab refer to the coordinate system $\bar{z}$, $\bar{x}$ (let us call them "new" coordinates), and without a bar tab – to the coordinate system x^J, x^K ("old" coordinates).

We can write the components of the displacement $\bar{U}_z$, $\bar{U}_x$ and stress $\bar{\sigma}_{zz}$, $\bar{\sigma}_{zx}$ fields entering the boundary conditions through the components (2):

$$\bar{U}_z = \cos\alpha\,U_J - \sin\alpha\,U_K;$$

$$\bar{U}_x = \sin\alpha\,U_J + \cos\alpha\,U_K; \tag{11}$$

$$\bar{\sigma}_{zz} = \cos^2\alpha\,\sigma_{JJ} - \sin 2\alpha\,\sigma_{JK} + \sin^2\alpha\,\sigma_{KK};$$

$$\bar{\sigma}_{zx} = \frac{1}{2}\sin 2\alpha(\sigma_{JJ}-\sigma_{KK}) + (1-2\sin^2\alpha)\sigma_{JK}. \tag{12}$$

In the "new" coordinates, the potential functions (3) have the form:

$$\bar{\phi} = \phi_0 e^{i\,\overset{(L)}{\xi}(\bar{x}\sin\alpha+\bar{z}\cos\alpha)}e^{i\,\overset{(L)}{\beta}(\bar{x}\cos\alpha-\bar{z}\sin\alpha)};$$

$$\bar{w} = w_0 e^{i\,\overset{(T)}{\xi}(\bar{x}\sin\alpha+\bar{z}\cos\alpha)}e^{i\,\overset{(T)}{\beta}(\bar{x}\cos\alpha-\bar{z}\sin\alpha)},$$

and the displacements (11) are written as follows:

$$\bar{U}_z = \cos\alpha[i\,\overset{(L)}{\xi}(\overset{(L)}{D_1}+\overset{(L)}{D_2})\bar{\phi} + (-\overset{(T)}{D_1}\frac{\overset{(T)}{\xi^2}}{\overset{(T)}{g}}+\overset{(T)}{g})\bar{w}] - \sin\alpha[i\,\overset{(L)}{\xi}\,\overset{(L)}{D_1}\bar{\phi} + (-\overset{(T)}{D_1}\frac{\overset{(T)}{\xi^2}}{\overset{(T)}{g}}+\overset{(T)}{g})\bar{w}] \tag{13}$$

$$\bar{U}_x = \sin\alpha[i(\overset{(L)}{D_1}+\overset{(L)}{D_2})\bar{\phi} + (-\overset{(T)}{D_1}\frac{\overset{(T)}{\xi^2}}{\overset{(T)}{g}}+\overset{(T)}{g})\bar{w}] + \cos\alpha[i\,\overset{(L)}{\beta}\,\overset{(L)}{D_1}\bar{\phi} - \overset{(L)}{D_1}\frac{\overset{(T)}{\xi}\overset{(T)}{\beta}}{\overset{(T)}{g}}\bar{w}] \tag{14}$$

Here, the wave numbers ξ, β, g are determined with respect to the "old" frame (Fig. 2).
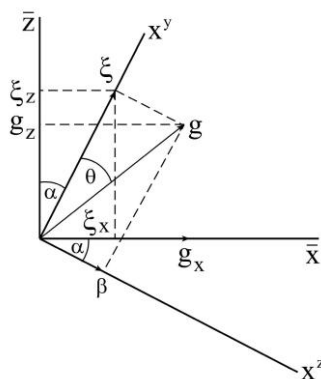
Fig. 2.Wave numbers "relations" diagram

The wave numbers ξ, β which are the projections of the vector $\bar{g}$ onto the "old" frame x^J, x^K, and the wave numbers g_x, g_z that are the projections of the vector $\bar{g}$ onto the "new frame" $\bar{z}$, $\bar{x}$ are interlinked through the following relations:

$$\xi = \frac{\cos\theta}{\sin(\alpha+\theta)}g_x = \frac{\cos\theta}{\cos(\alpha+\theta)}g_z \;;\;\; \beta = \frac{\sin\theta}{\sin(\alpha+\theta)}g_x = \frac{\sin\theta}{\cos(\alpha+\theta)}g_z \;;$$

$$g = \frac{g_x}{\sin(\alpha+\theta)} = \frac{g_z}{\cos(\alpha+\theta)}\;. \tag{15}$$

Substituting (15) into (14), we obtain expressions for displacements in the "new" coordinates:

$$\bar{U}_z = i\overset{(L)}{g_z}(\overset{(L)}{D_1} + \frac{\cos\theta\cos\alpha}{\cos(\alpha+\theta)}\overset{(L)}{D_2})\bar{\phi} + \overset{(T)}{g_z}(-\cos\theta\overset{(T)}{D_1} + \frac{\cos\alpha}{\cos(\alpha+\theta)})\bar{w}\;;$$

$$\bar{U}_x = i\overset{(L)}{g_z}[\frac{\cos\theta\sin\alpha}{\cos(\alpha+\theta)}(\overset{(L)}{D_1}+\overset{(L)}{D_2}) + \frac{\sin\theta\cos\alpha}{\cos(\alpha+\theta)}\overset{(L)}{D_1}]\bar{\phi} + \overset{(T)}{g_z}[-\frac{\sin(\alpha+\theta)\cos\theta}{\cos(\alpha+\theta)}\overset{(T)}{D_1} + \frac{\sin\alpha}{\cos(\alpha+\theta)}]\bar{w} \tag{16}$$

where, in accordance with (13) and (15):

$$\bar{\phi} = \phi_0 e^{i\overset{(L)}{g_x}\bar{x}}e^{i\overset{(L)}{g_z}\bar{z}} \;;\; \bar{w} = w_0 e^{i\overset{(T)}{g_x}\bar{x}}e^{i\overset{(T)}{g_z}\bar{z}}\;. \tag{17}$$

Similarly, using (2), (14), and (15), from (12), we obtain the relations for the stress components entering the boundary problem conditions:

$$\bar{\sigma}_{zz} = \{\cos^2\alpha[\overset{(L)}{d_1}+\overset{(L)}{d_2}-(\overset{(L)}{d_3}+\overset{(L)}{d_4})\frac{\cos^2\theta}{\cos^2(\alpha+\theta)}\overset{(L)}{g_z^2}] + \sin 2\alpha(\frac{1}{2}\overset{(L)}{d_3}+\overset{(L)}{d_4})\frac{\cos\theta\sin\theta}{\cos^2(\alpha+\theta)}\overset{(L)}{g_z^2} + \sin^2\alpha(\overset{(L)}{d_1}-\overset{(L)}{d_4})\frac{\sin^2\theta}{\cos^2(\alpha+\theta)}\overset{(L)}{g_z^2})\}\bar{\phi} +$$

$$+\{\cos^2\alpha\frac{\cos\theta}{\cos(\alpha+\theta)}i\overset{(T)}{g_z}(\overset{(T)}{d_1}+\overset{(T)}{d_2}+\overset{(T)}{d_3}-\overset{(T)}{d_4}\frac{\cos^2\theta}{\cos^2(\alpha+\theta)}\overset{(T)}{g_z^2}) - \sin 2\alpha\frac{\sin\theta}{\cos(\alpha+\theta)}i\overset{(T)}{g_z}(\frac{1}{2}\overset{(T)}{d_3}-\overset{(T)}{d_4}\frac{\cos^2\theta}{\cos^2(\alpha+\theta)}\overset{(T)}{g_z^2}) +$$

$$+\sin 2\alpha\frac{\cos\theta}{\cos(\alpha+\theta)}i\overset{(T)}{g_z}(\overset{(T)}{d_1}-\overset{(T)}{d_4}\frac{\cos^2\theta}{\cos^2(\alpha+\theta)}\overset{(T)}{g_z^2})\}\bar{w}\;;$$

$$\bar{\sigma}_{zx} = \{\frac{1}{2}\sin 2\alpha[\overset{(L)}{d_2}-(\overset{(L)}{d_3}+\overset{(L)}{d_4})\frac{\cos^2\theta}{\cos^2(\alpha+\theta)}\overset{(L)}{g_z^2}+\overset{(L)}{d_4}\frac{\sin^2\theta}{\cos^2(\alpha+\theta)}\overset{(L)}{g_z^2}] - (1-2\sin^2\alpha)(\frac{1}{2}\overset{(L)}{d_3}+\overset{(L)}{d_4})\frac{\cos\theta\sin\theta}{\cos^2(\alpha+\theta)}\overset{(L)}{g_z^2}\}\bar{\phi} +$$

$$+\{\frac{1}{2}\sin 2\alpha\frac{\cos\theta}{\cos(\alpha+\theta)}i(\overset{(T)}{d_2}+\overset{(T)}{d_3}-\overset{(T)}{d_4}\frac{\cos^2\theta-\sin^2\theta}{\cos^2(\alpha+\theta)}\overset{(T)}{g_z^2}) + (1-2\sin^2\alpha)\frac{\sin\theta}{\cos(\alpha+\theta)}i(\frac{1}{2}\overset{(T)}{d_3}-\overset{(T)}{d_4}\frac{\cos^2\theta}{\cos^2(\alpha+\theta)}\overset{(T)}{g_z^2})\}\bar{w}; \tag{18}$$

Thus, the displacement and stress components entering the boundary conditions (the coordinate system $\bar{z}$, $\bar{x}$ is associated with the boundary) are determined by the relations (16) - (18) where the projections of the wave vector $\bar{g}$ in the coordinate systems $\bar{z}$, $\bar{x}$ and x^J, x^K are linked through the relations (15).

The matrices C describing the wave properties of the layers [9-10] used in [5] and being the key elements in the development of concrete solutions to the boundary problems in the layered structures in this case, when the axes $\bar{z}$, $\bar{x}$ form the angle α with the frame components $\bar{e}^J$, $\bar{e}^K$, have the form:

$$C = \begin{pmatrix} c_{(1)} & c_{(2)} \\ c_{(3)} & c_{(4)} \end{pmatrix}, \tag{19}$$

where

$$
C = \begin{pmatrix} C_{(1)} = \begin{pmatrix} c_{11} & c_{12} \\ c_{21} & c_{22} \end{pmatrix} & C_{(2)} = \begin{pmatrix} -c_{11} & c_{12} \\ c_{21} & -c_{22} \end{pmatrix} \\ C_{(3)} = \begin{pmatrix} c_{31} & c_{32} \\ c_{41} & c_{42} \end{pmatrix} & C_{(4)} = \begin{pmatrix} c_{31} & -c_{32} \\ -c_{41} & c_{42} \end{pmatrix} \end{pmatrix} \begin{pmatrix} e^{i\overset{(L)}{g_z}z} & 0 & 0 & 0 \\ 0 & e^{i\overset{(T)}{g_z}z} & 0 & 0 \\ 0 & 0 & e^{-i\overset{(L)}{g_z}z} & 0 \\ 0 & 0 & 0 & e^{-i\overset{(T)}{g_z}z} \end{pmatrix} e^{ig_x x};
$$

$$
\overset{(T)}{g_x} = \overset{(L)}{g_x} = g_x ;
$$

(20)

$$
C_{11} = i\overset{(L)}{g_z}(\overset{(L)}{D_1} + \frac{\cos\theta\cos\alpha}{\cos(\alpha+\theta)}\overset{(L)}{D_2}) ;
$$

$$
C_{12} = \overset{(T)}{g_z}(-\cos\theta\overset{(T)}{D_1} + \frac{\cos\alpha}{\cos(\alpha+\theta)}) ;
$$

$$
C_{21} = i\overset{(L)}{g_z}[\frac{\cos\theta\sin\alpha}{\cos(\alpha+\theta)}(\overset{(L)}{D_1}+\overset{(L)}{D_2}) + \frac{\sin\theta\cos\alpha}{\cos(\alpha+\theta)}\overset{(L)}{D_1}] ;
$$

$$
C_{22} = \overset{(T)}{g_z}[-\frac{\sin(\alpha+\theta)\cos\theta}{\cos(\alpha+\theta)}\overset{(L)}{D_1} + \frac{\sin\alpha}{\cos(\alpha+\theta)}] ;
$$

$$
C_{31} = \cos^2\alpha[\overset{(L)}{d_1}+\overset{(L)}{d_2}-(\overset{(L)}{d_3}+\overset{(L)}{d_4})\frac{\cos^2\theta}{\cos^2(\alpha+\theta)}\overset{(L)}{g_z^2}] + \sin 2\alpha(\frac{1}{2}\overset{(L)}{d_3}+\overset{(L)}{d_4})\frac{\cos\theta\sin\theta}{\cos^2(\alpha+\theta)}\overset{(L)}{g_z^2} + +\sin^2\alpha(\overset{(L)}{d_1}-\overset{(L)}{d_4}\frac{\sin^2\theta}{\cos^2(\alpha+\theta)}\overset{(L)}{g_z^2})
$$

$$
C_{32} = \cos^2\alpha\frac{\cos\theta}{\cos(\alpha+\theta)}i\overset{(T)}{g_z}(\overset{(T)}{d_1}+\overset{(T)}{d_2}+\overset{(T)}{d_3}-\overset{(T)}{d_4}\frac{\cos^2\theta}{\cos^2(\alpha+\theta)}\overset{(T)}{g_z^2}) - \sin 2\alpha\frac{\sin\theta}{\cos(\alpha+\theta)}i\overset{(T)}{g_z}(\frac{1}{2}\overset{(T)}{d_3}-\overset{(T)}{d_4}\frac{\cos^2\theta}{\cos^2(\alpha+\theta)}\overset{(T)}{g_z^2}) +
$$

$$
+\sin^2\alpha\frac{\cos\theta}{\cos(\alpha+\theta)}i\overset{(T)}{g_z}(\overset{(T)}{d_1}-\overset{(T)}{d_4}\frac{\sin^2\theta}{\cos^2(\alpha+\theta)}\overset{(T)}{g_z^2}) ;
$$

$$
C_{41} = \frac{1}{2}\sin 2\alpha[\overset{(L)}{d_2}-(\overset{(L)}{d_3}+\overset{(L)}{d_4})\frac{\cos^2\theta}{\cos^2(\alpha+\theta)}\overset{(L)}{g_z^2}+\overset{(L)}{d_4}\frac{\sin^2\theta}{\cos^2(\alpha+\theta)}\overset{(L)}{g_z^2}] - (1-2\sin^2\alpha)(\frac{1}{2}\overset{(L)}{d_3}+\overset{(L)}{d_4})\frac{\cos\theta\sin\theta}{\cos^2(\alpha+\theta)}\overset{(L)}{g_z^2};
$$

$$
C_{42} = \frac{1}{2}\sin 2\alpha\frac{\cos\theta}{\cos(\alpha+\theta)}i(\overset{(T)}{d_2}+\overset{(T)}{d_3}-\overset{(T)}{d_4}\frac{\cos^2\theta-\sin^2\theta}{\cos^2(\alpha+\theta)}\overset{(T)}{g_z^2}) + (1-2\sin^2\alpha)\frac{\sin\theta}{\cos(\alpha+\theta)}i(\frac{1}{2}\overset{(T)}{d_3}-\overset{(T)}{d_4}\frac{\cos^2\theta}{\cos^2(\alpha+\theta)}\overset{(T)}{g_z^2}) .
$$

(21)

Where $\alpha = 0$, the elements (21) of the matrix C coincide with the corresponding elements of this matrix for the case of coincidence of the normal to the boundary and the material symmetry axis direction that are represented by the formulas (3.82) in [5]. If $\alpha = \frac{\pi}{2}$, then we get the case when the symmetry axis of the material is tangent to the boundary surface, and the formulas (21) coincide with the expressions (3.89) - (3.91) in [5].

Knowing the expressions for matrices C, one can construct solutions to various problems using the research and methodological apparatus described in [5].

Conclusions. The present research and methodological apparatus were successfully used for determining the stress-strain state in the layered structures made of transversely isotropic materials, and for analyzing the diagnostics results of the state of flat-layered and layered cylindrical structures in operation.

References

1. Tarnopolskiy, Y.M., Zhigun, I.G., Polyakov, V.A. Prostranstvenno-armirovannye kompozitsionnye materialy. [Spatially reinforced composite materials.] Moscow: Mashinostroenie, 1987, 224 p. (in Russian).

2. Geller, B.E., ed. Spravochnik po kompozitsionnym materialam. Kn.1 [Handbook in composite materials. Book 1.] Moscow: Mashinostroenie, 1988, 448 p. (in Russian).

3. Vasilyev, V.V., Protasov, V.D., Bolotin, V.V., et al. Kompozitsionnye materialy. Spravochnik. [Composite materials. Handbook.] Moscow: Mashinostroenie, 1990, 512 p. (in Russian).

4. Sizov, V.P. O skalyarizatsii dinamicheskikh uprugikh poley v transversal'no-izotropnykh sredakh. [On scalarization of dynamic elastic fields in transversely isotropic media.] Izvestia: Mechanics of Solids, 1988, no. 5pp. 55–58 (in Russian).

5. Sizov, V.P., Miroshnichenko, I.P. Vozbuzhdenie uprugikh voln v sloistykh anizotropnykh konstruktsiyakh. Monografiya. [Excitation of elastic waves in layered anisotropic structures. Monograph.] Saarbrucken: LAP LAMBERT Academic Publishing, 2012, 270 p. (in Russian).

6. Sirotin, Y.I., Shaskolskaya, M.P. Osnovy kristallofiziki. [Basic crystallophysics.] Moscow: Nauka, 1979, 640 p. (in Russian).

7. Fedorov, F.I. Teoriya uprugikh voln v kristallakh. [Theory of elastic waves in crystals.] Moscow: Nauka, 1965, 386 p. (in Russian).

8. Corn, G., Corn, T. Spravochnik po matematike dlya nauchnykh rabotnikov i inzhenerov. [Handbook in Mathematics for Scientists and Engineers.] Moscow: Nauka, 1968, 720 p. (in Russian).

9. Brekhovskikh, L.M. Volny v sloistykh sredakh. [Waves in layered media.] Moscow: AN SSSR, 1957, 502 p. (in Russian).

10. Vinogradova, M.B., Rudenko, O.V., Sukhorukov, A.P. Teoriya voln. [Wave theory.] Moscow: Nauka, 1979, 384 p. (in Russian).

Authors:

Miroshnichenko, Igor P.,
Head of the Machine Design Principles
Department, Don State Technical University (1, Gagarin
Square, Rostov-on-Don, 344000, RF), Cand.Sci. (Eng.),
associate professor,
ORCID: https://orcid.org/0000-0001-9450-2500
Ipmir@rambler.ru

Sizov, Valery P.,
Leading research scholar, Rostov Scientific Research Institute for Radiocommunication (130, Nansena St.,
Rostov-on-Don, 344038, RF), Dr.Sci. (Eng.), professor,
ORCID: https://orcid.org/0000-0003-4816-0145

MECHANICS
МЕХАНИКА

Contact problem for a two-layered cylinder[*]

D. A. Pozharskii[1], N. B. Zolotov[2], I. Ye. Semenov[3], E. D. Pozharskaya[4], M. I. Chebakov[5]**

[1,2,4] Don State Technical University, Rostov-on-Don, Russian Federation
[2,5] Southern Federal University, Rostov-on-Don, Russian Federation

Контактная задача для двухслойного цилиндра[***]

Д. А. Пожарский[1], Н. Б. Золотов[2], И. Е. Семенов[3], Е. Д. Пожарская[4], М. И. Чебаков[5]**

[1,3,4] Донской государственный технический университет, г. Ростов-на-Дону, Российская Федерация
[2,5] Южный федеральный университет, г. Ростов-на-Дону, Российская Федерация

Introduction. The investigation of the contact problems for cylindrical bodies is urgent due to the engineering contact strength analysis on shafts, cores and pipe-lines. In the present paper, a new contact problem of elastostatics on the interaction between a rigid band and an infinite two-layered cylinder, which consists of an internal continuous cylinder and an outer hollow one, with a frictionless contact between the cylinders, is studied. The outer cylindrical band of finite length is press fitted. By using a Fourier integral transformation, the problem is reduced to an integral equation with respect to the unknown contact pressure.

Materials and Methods. Different combinations of linearly elastic materials of the composite cylinder are considered. Asymptotics of the symbol function of the integral equation kernel at zero and infinity is analyzed. This plays an important role for the application of the analytical solution methods. A key dimensionless geometric parameter is introduced, and a singular asymptotic technique is employed to solve the integral equation.

Research Results. On the basis of the symbol function properties, a special easily factorable approximation being applicable in a wide variation range of the problem parameters is suggested. The Monte-Carlo method is used to determine the approximation parameters. The asymptotic formulas are derived both for the contact pressure, and for its integral characteristic. Calculations are made for different materials and for various relative thickness of the cylindrical layer including thin-walled layers.

Discussion and Conclusions. The asymptotic solutions are effective for relatively wide bands when the contact zone length is bigger than the diameter of the composite cylinder. It is significant that the method is applicable also for those cases

Введение. Актуальность исследования контактных задач для цилиндрических тел обусловлена необходимостью проведения инженерных расчетов на контактную прочность валов, стержней и трубопроводов. В настоящей работе изучается новая контактная задача статической теории упругости о взаимодействии жесткого бандажа с бесконечным двухслойным цилиндром, состоящим из внутреннего сплошного и внешнего полого цилиндров, между которыми выполняются условия гладкого контакта. Наружный цилиндрический бандаж посажен с натягом и имеет конечную длину. При помощи интегрального преобразования Фурье задача сводится к интегральному уравнению относительно неизвестного контактного давления.

Материалы и методы. Рассматриваются разные комбинации линейно-упругих материалов составного цилиндра. Исследуется асимптотика функции-символа ядра интегрального уравнения в нуле и бесконечности, играющая важную роль для использования аналитических методов решения. Для решения интегрального уравнения вводится основной безразмерный геометрический параметр и применяется сингулярный асимптотический метод.

Результаты исследования. В соответствии со свойствами функции-символа предложена специальная легко факторизуемая аппроксимация этой функции, пригодная в широком диапазоне изменения параметров задачи. При помощи метода Монте-Карло рассчитаны параметры этой аппроксимации. Получены асимптотические формулы как для контактных давлений, так и для их интегральной характеристики. Расчеты сделаны для разных материалов и относительных толщин цилиндрического слоя, в том числе для тонкостенных слоев.

Обсуждение и заключения. Полученные асимптотические решения эффективны для относительно широких бандажей, когда размер области контакта превышает диаметр составного цилиндра. Важно, что используемый метод остается применимым и для случаев, когда внешний ци-

---

when the outer cylindrical layer is treated as a cylindrical shell. The asymptotic solutions can be recommended to engineers for the contact strength analysis of the elastic barrels with a flexible coating of another material.

линдрический слой можно рассматривать как цилиндрическую оболочку. Асимптотические решения можно рекомендовать инженерам для анализа контактной прочности упругих деталей цилиндрической формы с упругим покрытием из другого материала.

Introduction. A dynamic contact problem for a prestressed elastic liquid-filled cylinder is studied in the paper [1]. Static contact problems for homogeneous elastic cylindrical bodies were considered in the papers [2-6] using regular and singular asymptotic methods. It was found [4] that for cylindrical bodies, kernel symbols of integral equations of the contact problems are characterized by a more complex asymptotic behavior at zero and infinity than, for example, in contact problems for resilient strip. This required applying complicated approximations of the symbols easily factored by functions when using the singular asymptotic method. The approximation for hollow thin-walled cylinders is particularly complicated [6]. The suggested approximation [6] is advantageous even for the cases when a thin-walled elastic cylinder can be considered as a cylindrical shell [7]. The contact problem on the interaction of an elastic ring and a flexible cylinder was studied [8]. The elastic cylinder wear was analyzed in the paper [9]. This work objective is to obtain a solution to the contact problem for a composite two-layer elastic cylinder on the basis of a singular asymptotic technique and an effective approximation of the kernel symbol of the integral equation.

Materials and Methods. In the cylindrical coordinates r, z (with axisymmetry), we consider an infinite elastic composite cylinder of outer radius R which consists of an inner solid cylinder of radius $R1 < R$ with elastic parameters ν_1, G_1 (Poisson's ratio and shear modulus) and an outer cylindrical layer with elastic parameters ν, G. Between the layer and the inner cylinder, the sliding binding conditions are met. We consider the contact problem on the interaction of the described composite cylinder and a rigid band in the domain $|z| \le a$. For the given band preload δ, it is required to estimate contact pressures $\sigma_r = -q(z)$ $(|z| \le a)$. Using the integral Fourier transform to solve the properly mixed (contact) boundary-value problem for Lame's elastic equilibrium equations and introducing non-dimensional notations (the primes are further omitted)

$$\lambda = \frac{R}{a}, \quad \delta' = \frac{\delta}{a}, \quad \zeta' = \frac{z}{a}, \quad q'(\zeta') = \frac{q(\zeta)(1-\nu)}{G}, \quad \varepsilon = \frac{G_1}{G}, \quad k = \frac{R_1}{R} < 1, \tag{1}$$

we obtain the following integral equation for $q(\zeta)$:

$$\int_{-1}^{1} q(\xi) k\left(\frac{\zeta - \xi}{\lambda}\right) d\xi = \pi\delta \quad (|\zeta| \le 1), \qquad k(t) = \int_{0}^{\infty} L(u)\cos(ut)du, \tag{2}$$

where the kernel symbol takes the form

$$L(u) = -\frac{d_1}{d}I_1 - \frac{d_2}{d}K_1, \tag{3}$$

$$d = (A_{55}A_{66} - A_{56}A_{65})[(A_{12}A_{31} - A_{11}A_{32})(A_{23}A_{44} - A_{24}A_{43}) -$$
$$- A_{13}A_{31}(A_{22}A_{44} - A_{24}A_{42}) + A_{14}A_{31}(A_{22}A_{43} - A_{23}A_{42}) +$$
$$+ A_{13}A_{32}(A_{21}A_{44} - A_{24}A_{41}) - A_{14}A_{32}(A_{21}A_{43} - A_{23}A_{41})] +$$
$$+ A_{35}A_{56}[(A_{23}A_{44} - A_{24}A_{43})(A_{12}A_{61} - A_{11}A_{62}) +$$
$$+ (A_{22}A_{44} - A_{24}A_{42})(A_{11}A_{63} - A_{13}A_{61}) + (A_{22}A_{43} - A_{23}A_{42})(A_{14}A_{61} - A_{11}A_{64}) +$$
$$+ (A_{21}A_{44} - A_{24}A_{41})(A_{13}A_{62} - A_{12}A_{63}) + (A_{21}A_{43} - A_{23}A_{41})(A_{12}A_{64} - A_{14}A_{62}) +$$
$$+ (A_{21}A_{42} - A_{22}A_{41})(A_{14}A_{63} - A_{13}A_{64})],$$

$$d_1 = (A_{13}A_{44} - A_{14}A_{43})[A_{32}(A_{56}A_{65} - A_{55}A_{66}) - A_{35}A_{56}A_{62}] -$$
$$- A_{35}A_{56}[A_{12}(A_{43}A_{64} - A_{44}A_{63}) - A_{42}(A_{13}A_{64} - A_{14}A_{63})],$$

$$d_2 = -(A_{13}A_{44} - A_{14}A_{43})[A_{31}(A_{56}A_{65} - A_{55}A_{66}) - A_{35}A_{56}A_{61}] +$$
$$+ A_{35}A_{56}[A_{11}(A_{43}A_{64} - A_{44}A_{63}) - A_{41}(A_{13}A_{64} - A_{14}A_{63})],$$

$$A_{11} = uI_0 - 2(1-\nu)I_1, \quad A_{12} = -uK_0 - 2(1-\nu)K_1, \quad A_{13} = uI_1, \quad A_{14} = -uK_1,$$

$$A_{21} = (3-2\nu)uI_0 - (u^2 + 4(1-\nu))I_1, \quad A_{22} = -(3-2\nu)uK_0 - (u^2 + 4(1-\nu))K_1,$$

$$A_{23} = u(I_1 - uI_0), \quad A_{24} = -u(K_1 + uK_0),$$

$$A_{31} = 2(1-\nu)I_1^*, \quad A_{32} = 2(1-\nu)K_1^*, \quad A_{35} = -4(1-\nu_1)I_1^*,$$

$$A_{41} = ukI_0^* - 2(1-\nu)I_1^*, \quad A_{42} = -ukK_0^* - 2(1-\nu)K_1^*, \quad A_{43} = uI_1^*, \quad A_{44} = -uK_1^*,$$

$$A_{55} = ukI_0^* - 2(1-\nu_1)I_1^*, \quad A_{56} = uI_1^*,$$

$$A_{61} = (3-2\nu)uI_0^* - (u^2k + 4(1-\nu)k^{-1})I_1^*,$$

$$A_{62} = -(3-2\nu)uK_0^* - (u^2k + 4(1-\nu)k^{-1})K_1^*,$$

$$A_{63} = uk^{-1}I_1^* - u^2I_0^*, \quad A_{64} = -uk^{-1}K_1^* - u^2K_0^*,$$

$$A_{65} = -\varepsilon[(3-2\nu_1)uI_0^* - (u^2k + 4(1-\nu_1)k^{-1})I_1^*], \quad A_{66} = -\varepsilon u(I_1^*k^{-1} - uI_0^*),$$

$$I_n = I_n(u), \quad K_n = K_n(u), \quad I_n^* = I_n(uk), \quad K_n^* = K_n(uk), \quad n = 0, 1.$$

Here, $I_n(u)$, $K_n(u)$ are modified Bessel functions. The dimensionless parameter λ characterizes a relative width of the contact region.

Function $L(u)$ at zero and infinity behaves as follows:

$$\lim_{u \to 0} L(u) = L(0) = \frac{(\nu-1)(1+\varepsilon-\nu_1+\varepsilon\nu_1) + k^2\varepsilon_1}{2(\nu-1)[(\nu+1)(1+\varepsilon-\nu_1+\varepsilon\nu_1) + k^2\varepsilon_1]}, \quad \varepsilon_1 = (\nu+1)(\nu_1-1) - \varepsilon(\nu-1)(\nu_1+1). \tag{4}$$

$$L(u) = \frac{1}{u} + \frac{D}{u^2} + o(u^{-2}) \quad (u \to +\infty), \quad D = 1-2\nu.$$

At $k=0$, value $L(0)$ is the same as the known value for the homogeneous solid cylinder [4].

To solve the equation (2), we apply the singular asymptotic method [3,4] effective for sufficiently small values of λ. To apply the Wiener-Hopf technique [10], we used an easily factorable approximation of the function $L(u)$ (3) by the expression

$$L^*(u) = \frac{\sqrt{u^2 + B^2}}{u^2 + C^2} \exp\left(\frac{D}{\sqrt{u^2 + 10^4}}\right) \frac{u^2 + A^2G^2}{u^2 + G^2}, \quad C^2 = \frac{A^2B}{L(0)}\exp\left(\frac{D}{10^2}\right). \tag{5}$$

At calculations, two cases were taken: 1) iron inside, zinc outside ($\varepsilon=2.126$, $\nu=0.27$, $\nu_1=0.28$); 2) aluminum inside, zinc outside ($\varepsilon=0.779$, $\nu=0.27$, $\nu_1=0.34$). Table 1 gives the approximation parameters values (5), its relative error on the real axis θ (%) calculated using the Monte Carlo method for different relative thicknesses of the outer layer k.

Table 1

Approximation parameters

k	A	B	G	θ	A	B	G	θ
	Iron inside zinc				Aluminum inside zinc			
0.01	1.230	1.549	4.638	2.5	0.451	6.113	3.394	3
0.03	1.291	1.563	4.042	2.5	0.888	5.977	3.029	3
0.05	1.296	1.851	5.006	3	2.399	1.467	2.524	5
0.07	1.258	2.057	6.376	3	0.720	7.945	2.512	7
0.09	1.024	4.360	92.381	5	1.481	9.890	9.369	5
0.099	3.540	24.178	5.347	7	1.178	5.535	235.946	10

Considering, as follows from (4),

$$\lim_{k \to 1} L(0) = \frac{1 - \nu_1}{2\varepsilon(1-\nu)(1+\nu_1)},$$
(6)

then, in the case of small ε, the approximation (5) for thin outer layers is to be complicated by increase in number of the parameters included into it.

Research Results. As a result of applying the Wiener-Hopf technique, the principal term of the asymptotic solution to the integral equation (2) for small λ can be constructed in the form of

$$q(\zeta) = \frac{\delta}{\lambda}\left[\omega\left(\frac{1+\zeta}{\lambda}\right) + \omega\left(\frac{1-\zeta}{\lambda}\right) - \frac{1}{L(0)} \right] \quad (|x| \le 1),$$
(7)

$$\omega(s) = \frac{W(s) + I(s)}{\sqrt{L(0)}}, \quad I(s) = -\frac{D}{\pi}\int_0^s W(s-\tau)K_0(10^2\tau)d\tau,$$

$$W(s) = \frac{\exp(-Bs)}{\sqrt{\pi s}} + \frac{C}{\sqrt{B}}\operatorname{erf}(\sqrt{Bs}) + \left(\frac{1}{A} - 1\right)Q(AG, s),$$

$$Q(F, s) = \frac{F-C}{\sqrt{B-F}}\exp(-Fs)\operatorname{erf}(\sqrt{(B-F)s}) + \frac{C}{\sqrt{B}}\operatorname{erf}(\sqrt{Bs}).$$

Here, $\operatorname{erf}(x)$ is error function integral.

For the integral characteristic of the solution

$$P = \int_{-1}^{1} q(\zeta)d\zeta$$
(8)

on the basis of the formulas (7), we obtain the expression

$$\frac{P}{\delta} = \frac{2}{\sqrt{L(0)}}\left[Z\left(\frac{2}{\lambda}\right) + J\left(\frac{2}{\lambda}\right) \right] - \frac{2}{\lambda L(0)}, \quad J(s) = -\frac{D}{\pi}\int_0^s Z(s-\tau)K_0(10^2\tau)d\tau,$$
(9)

$$Z(s) = \frac{C}{\sqrt{B}}\left[\left(s - \frac{1}{2B} + \frac{1}{C}\right)\operatorname{erf}(\sqrt{Bs}) + \sqrt{\frac{s}{\pi B}}\exp(-Bs) \right] + \left(\frac{1}{A} - 1\right)T(AG, s),$$

$$T(F, s) = \frac{C}{\sqrt{B}}\left[\left(s - \frac{1}{2B} + \frac{1}{C} - \frac{1}{F}\right)\operatorname{erf}(\sqrt{Bs}) + \sqrt{\frac{s}{\pi B}}\exp(-Bs) \right] -$$

$$- \left(1 - \frac{C}{F}\right)\frac{\exp(-Fs)}{\sqrt{B-F}}\operatorname{erf}(\sqrt{(B-F)s}).$$

Calculations show that the asymptotics (7), (9) error for $\lambda < 1$ does not exceed $(5+\theta)$ %, where θ is the approximation (5) error.

Table 2 shows the values of the integral characteristic $P\delta^{-1}$ calculated from the formulas (9) at different values of k and λ.

Table 2

Values of $P\delta^{-1}$

λ=	2	1	0.5	0.25	2	1	0.5	0.25
k	Iron inside zinc				Aluminum inside zinc			
0.1 [,]	3.25	5.77	10.9	21.1	3.22	5.71	10.8	20.9
0.03	3.37	6.02	11.4	22.2	3.20	5.65	10.7	20.7
0.05	3.67	6.65	12.7	24.8	3.09	5.51	10.5	20.4
0.07	4.22	7.78	15.0	29.4	2.96	5.33	10.2	19.9
0.09	5.60	10.3	19.6	38.2	2.93	5.28	9.99	19.4
0.099	6.91	12.3	23.2	44.9	2.99	5.31	9.94	19.2

Discussion and Conclusions. As Table 2 shows, with decrease in λ, the integral characteristic of the contact pressures increases, which is associated with the extension of the contact area. For the case of a stronger material inside zinc (iron), contact pressures are higher than for aluminum inside zinc.

With thinning the zinc layer around the iron (with increasing *k*), the contact pressures increase essentially. This is hardly in evidence during thinning the layer of zinc around aluminum, since the modulus of longitudinal elasticity (and also shear modulus) of aluminum is slightly less than that of zinc. The asymptotics found can be recommended to engineers for analyzing the contact strength characteristics of the coated cylindrical parts.

References

1. Belyankova, T.I., Kalinchuk, V.V. The dynamic contact problem for a prestressed cylindrical tube filled with a fluid. Journal of Applied Mathematics and Mechanics, 2009, vol. 73, no. 2, pp. 209–219. DOI: https://doi.org/10.1016/j.jappmathmech.2009.04.011.

2. Aleksandrov, V.M., Romalis, B.L. Kontaktnye zadachi v mashinostroenii. [Contact tasks in mechanical engineering.] Moscow: Mashinostroenie, 1986, 176 p. (in Russian).

3. Aleksandrov, V.M., Pozharskii, D.A. An asymptotic method in contact problems. Journal of Applied Mathematics and Mechanics, 1999, vol. 63, no. 2, pp. 283–290. DOI: https://doi.org/10.1016/j.jappmathmech.2016.03.011.

4. Alexandrov, V.M., Pozharskii, D.A. Three-dimensional contact problems. Dordrecht: Kluwer academic publishers, 2001, 406 p.

5. Pozharskii, D.A., Zolotov, N.B. K odnoy zadache Belokonya A.V. [To one A.V. Belokon's problem.] Vestnik of DSTU, 2017, vol. 17, no. 2, pp. 7–11 (in Russian). DOI: https://doi.org/10.23947/1992-5980-2017-17-2-7-11.

6. Zolotov, N.B., v Pozharskii, D.A., Pozharskaya, E.D. K kontaktnym zadacham dlya tsilindra. [To contact problems for a cylinder.] Izvestiya vuzov. Severo-Kavkazskiy region. Natural Sciences. 2017, no. 2, pp. 12–14 (in Russian). DOI: https://doi.org/10.23683/0321-3005-2017-2-12-14.

7. Grigolyuk, E.I., Tolkachev, V.M. Kontaktnye zadachi teorii plastin i obolochek. [Contact problems of the theory of plates and shells.] Moscow: Mashinostroenie, 1980, 411 p. (in Russian).

8. Arutyunyan, N.Kh. On the contact interaction of an elastic ring with an elastic cylinder. Mechanics of Solids, 1994, vol. 29, no. 2. Pp. 194–197.

9. Goriacheva, I. G. Contact problem in the presence of wear for a piston ring inserted into cylinder. Journal of Applied Mathematics and Mechanics, 1980, vol. 44, no. 2, pp. 255–257.

10. Noble. B. Metod Vinera-Khopfa. [Wiener-Hopf technique.] Moscow: Izd-vo inostrannoy literatury, 1962, 276 p. (in Russian).

Authors:

Pozharskii, Dmitry A.,
Head of the Applied Mathematics Department, Don State
Technical University (1, Gagarin Square, Rostov-on-Don,
344000, RF), Dr.Sci. (Phys.-Math.), professor,
ORCID: https://orcid.org/0000-0001-6372-1866
pozharda@rambler.ru

Zolotov, Nikita B.,
graduate student, Vorovich Institute for Mathematics,
Mechanics, and Computer Science, Southern Federal
University (8-a, ul. Milchakova, Rostov-on-Don,
 344090, RF),
ORCID: https://orcid.org/0000-0002-2193-0616
zolotov.nikita.borisovich@gmail.com

Mechanics

Semenov, Ivan E.,
student of the Applied Mathematics Department, Don
State Technical University (1, Gagarin Square,
Rostov-on-Don, 344000, RF),
ORCID: https://orcid.org/0000-0002-9247-0055
ivan.sk6@gmail.com

Pozharskaya, Elizaveta D.,
student of the Applied Mathematics Department, Don
State Technical University (1, Gagarin Square,
Rostov-on-Don, 344000, RF),
ORCID: https://orcid.org/0000-0002-5745-6135
pozharskaya.elizaveta@rambler.ru

Chebakov, Mikhail I.,
Chief Research Scholar, Vorovich Institute for Mathemat-
ics, Mechanics, and Computer Science, Southern Federal
University (8-a, ul. Milchakova, Rostov-on-Don,
344090, RF), Dr.Sci. (Phys.-Math.), professor,
ORCID: https://orcid.org/0000-0003-2075-1760
chebakov@math.sfedu.ru

MACHINE BUILDING AND MACHINE SCIENCE
МАШИНОСТРОЕНИЕ И МАШИНОВЕДЕНИЕ

Reliability-based design optimization using optimum safety factors for large-scale problems[*]

Ghias Kharmanda [1], I. R. Antypas[2][**]
[1] Lund University, Lund, Sweden
[2] Don State Technical University, Rostov-on-Don, Russian Federation

Надежность оптимизации дизайна с использованием оптимальных факторов безопасности для крупномасштабных задач[***]

Харманда М. Г.[1], Антибас И. Р.[2][**]
[1] Лундский университет, г. Лунд, Швеция
[2] Донской государственный технический университет, г. Ростов-на-Дону, Российская Федерация

Introduction. Reliability-Based Design Optimization (RBDO) model reduces the structural weight in uncritical regions, does not only provide an improved design but also a higher level of confidence in the design.

Materials and Methods. The classical RBDO approach can be carried out in two separate spaces: the physical space and the normalized space. Since very many repeated researches are needed in the above two spaces, the computational time for such an optimization is a big problem. An efficient method called Optimum Safety Factor (OSF) method is developed and successfully put to use in several engineering applications.

Research Results. A numerical application on a large scale problem under fatigue loading shows the efficiency of the developed RBDO method relative to the Deterministic Design Optimization (DDO). The efficiency of the OSF method is also extended to multiple failure modes to control several output parameters, such as structural volume and damage criterion.

Discussion and Conclusions. The simplified implementation framework of the OSF strategy consists of a single optimization problem to evaluate the design point, and a direct evaluation of the optimum solution considering OSF formulations. It provides designers with efficient solutions that should be economic, satisfying a required reliability level with a reduced computing time.

Введение. Модель, основанная на оптимизации надёжности, (RBDO) уменьшает структурный вес в некритических регионах, обеспечивает не только улучшенную конструкцию, но и более высокий уровень уверенности в дизайне.

Материалы и методы. Классический подход RBDO может быть выполнен в двух отдельных пространствах: физическом пространстве и нормированном пространстве. Поскольку в вышеупомянутых двух пространствах требуется очень много повторных исследований, расчётное время для такой оптимизации является большой проблемой. Эффективный метод, называемый Optimum Safety Factor (OSF), разработан и успешно применяется к нескольким инженерным приложениям.

Результаты исследования. Численное приложение по крупномасштабной задаче при усталостной загрузке показывает эффективность разработанного метода RBDO относительно детерминированной оптимизации дизайна (DDO). Эффективность метода OSF также распространяется на несколько режимов отказоустойчивости для управления несколькими выходными параметрами, такими как структурный объем и атрибут повреждения.

Обсуждение и заключения. Упрощенная стратегия внедрения структуры OSF состоит из единственной задачи по оптимизации оценки проектной точки и прямой оценки оптимального решения с учетом составов OSF. Он предоставляет разработчикам эффективные решения, которые должны быть экономичными, удовлетворяющими требуемому уровню надежности с сокращённым расчётным временем.

Keywords: Reliability-Based Design Optimization, Structural Reliability, Safety Factors

Ключевые слова: оптимизация на основе надежности, структурная надежность, факторы безопасности

1. Introduction

When Deterministic Design Optimization (DDO) methods are used, deterministic optimum designs are usually pushed to the design constraint boundary, leaving little or no room for tolerances (or uncertainties) in design, manufacture, and operating processes. So, deterministic optimum designs obtained without consideration of uncertainties may lead to unreliable designs, therefore calling for Reliability-Based Design Optimization (RBDO). An RBDO solution that reduces the structural weight in uncritical regions does not only provide an improved design but also a higher level of confidence in the design. The basic idea is to couple the reliability analysis with optimization problems. This coupling is a complex task, drawing on a high computing time and convergence stability, which seriously limits its applicability in real problems. To overcome these difficulties, several methods have been elaborated [1]. These methods can be classified into two categories: numerical and semi-numerical methods. An efficient numerical method called Hybrid Method is based on simultaneous solution to the reliability and the optimization problem. It has successfully reduced the computational time problem. The advantage of the hybrid method allows us to satisfy a required reliability level for different cases (static, dynamic, …), but the vector of variables here contains both deterministic and random variables. To overcome both difficulties, an efficient semi-numerical method called Optimum Safety Factor (OSF) method has been proposed to solve problems in statics [2], and also an efficient alternative semi-numerical method called Safest Point Method (SP) has been proposed to solve problem in dynamics [3]. Recently, a Robust Hybrid Method (RHM) is also developed to overcome the HM difficulties in order to solve multiaxial fatigue damage analysis problems [4]. The RHM leads to robust solution comparing with the HM, but the computing time is still a big drawback.

2. Reliability-Based Design Optimization

2.1 Developments

The computational cost of sequential RBDO approaches is much higher than the DDO procedure. Several developments accelerated the use of the RBDO model. The Reliability Index Approach (RIA) and the Performance Measure Approach (PMA) have been proposed [5]. Next, the sequential optimization and reliability assessment (SORA) is developed to improve the efficiency of probabilistic optimization [6]. The SORA method employs a single-loop strategy with a serial of cycles of deterministic optimization and reliability assessment. The major difficulty lies in the evaluation of the probabilistic constraints, which is prohibitively expensive and even diverges for many applications. It is clear that efforts were directed towards the development of efficient techniques to perform the reliability analysis. Here, the reliability index is computed iteratively that leads to an enormous amount of computer time in the whole design process.

2.2 Basic RBDO formulations

Traditionally, for the reliability-based design optimization procedure, two spaces are used: the physical space and the normalized space [7,8]. Therefore, the reliability-based design optimization is performed by nesting the following two problems:

1. Optimization problem:

$$
\begin{aligned}
&\min_{x} && f(x) \\
&\text{subject to} && g_k(x) \le 0 \;,\; k = 1,...,K \\
&\text{and} && \beta(x,u) \ge \beta_t
\end{aligned}
\tag{1}
$$

where $f(x)$ is the objective function, $g_k(x) \le 0$ are the associated constraints, $\beta(x,u)$ is the reliability index of the structure, and β_t is the target reliability.

2. Reliability analysis: the reliability index $\beta(x,u)$ is the minimum distance between the limit state function $H(\mathbf{u})$ and the origin, see Figure 1b. This index is determined by solving the minimization problem:

$$
\begin{aligned}
&\min_{u} && d(u) \\
&\text{subject to} && H(u) = 0
\end{aligned}
\tag{2}
$$

where $d(\mathbf{u})$ is the distance in the normalized random space, given by $d = \sqrt{\sum u_i^2}$, and $H(\mathbf{u})$ is the performance function (or limit state function) in the normalized space, defined such that $H(\mathbf{u}) \leq 0$ implies failure, see Figure 1b. In the physical space, the image of $H(\mathbf{u})$ is the limit state function $G(\mathbf{x},\mathbf{y})$, see Figure 1a. Using the classical approach, the RBDO process is carried out in two spaces. That leads to a high computational time problem. Therefore, there is a strong need to develop efficient methods [9].

a)   *b)*
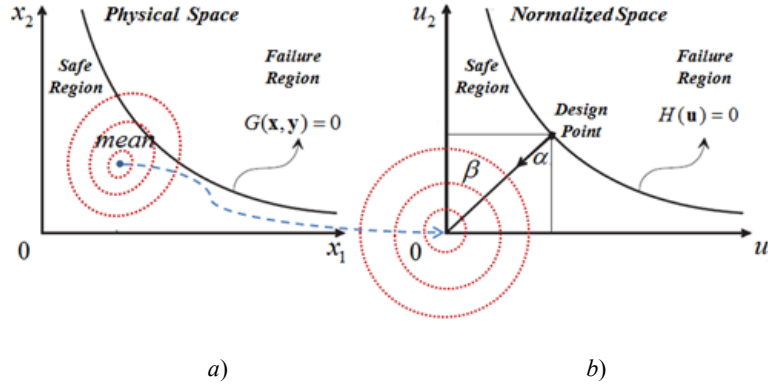
Fig. 1. Physical and normalized spaces

In the field of reliability-based design optimization, we distinguish between two types of variables:

1. **The optimization variables**, which are deterministic variables to be adjusted with a view to optimizing the sizing; they represent the control parameters of the mechanical system (i.e. dimensions, materials, loads, etc.), and the probabilistic model (i.e. means and standard deviations of random variables);
2. **The random variables**, which represent the uncertainties in the system. Each of these variables is identified by the type of distribution law and the associated parameters. These variables may be the geometric dimensions, the characteristics of the material or the external loads.

3. Optimum Safety Factor (OSF)

The Partial Safety Factors (PSF) presented in [10] use the calibration methods that need to propose some constraints during the calibration process to increase the efficiency and the accuracy. The resulting solution when using PSF may not represent a global or even local optimum. It may satisfy the required reliability level because of the efficiency of the used optimization algorithm. An efficient OSF method essentially depends on the satisfaction of the optimality conditions of the reliability index problem (2). This method provides the designer at least with a local reliability-based optimum without additional computing cost. This method has been basically developed for a normal distribution case [11]. In this work, it is generalized to be applied to a single and multiple failure cases.

3.1 Single Failure Mode (SFM)

The SFM reliability problem can be written as:

$$\beta^{SFM} = \min d(u_i) = \sqrt{u_1^2 + u_2^2 + \ldots + u_n^2} \quad \text{s.t.:} \quad H\left(u_1, u_2, \ldots, u_n\right) \leq 0 \tag{3}$$

where $d(u_i)$ is the minimum distance between the design point and the optimal solution. And $H\left(u_i\right) \leq 0$ represent the failure mode. The corresponding analytical formulation using OSF can be written as follows:

$$u_i^* = \beta_t \sqrt{\dfrac{\left|\dfrac{\partial G}{\partial y_i}\right|}{\sum_{j=1}^{n} \left|\dfrac{\partial G}{\partial y_j}\right|}}, \quad i = 1, \ldots, n \tag{4}$$

where the sign of $\pm$ depends on the sign of the derivative, i.e.,

$$\frac{\partial G}{\partial y_i} > 0 \Leftrightarrow u_i^* > 1 \quad \text{and} \quad \frac{\partial G}{\partial y_i} < 0 \Leftrightarrow u_i^* < 1, \quad\quad i = 1, \ldots, n$$

Formulation (4) provides different optimum values of the normalized variables at the design point and taking into account a single failure mode. In [2], a similar formulation can be found for several distributions.

3.2 Multiple Failure Mode (MFM)

Using the same OSF developments for a single failure mode [2], the MFM problem can be written as:

$$\beta^{MFM} = \min d(u_i) = \sqrt{u_1^2 + u_2^2 + ... + u_n^2} \quad \text{s.t.:} \quad H_j\left(u_1, u_2, ..., u_m\right) \le 0 \tag{5}$$

$H_j\left(u_i\right) \le 0$ represent the different failure modes. The corresponding analytical formulation using OSF can be written as follows:

$$u_i^* = \pm\beta_t \sqrt{\dfrac{\left|\sum_{j=1}^{m} \dfrac{\partial G_j}{\partial y_i}\right|}{\sum_{i=1}^{n}\left|\sum_{j=1}^{m} \dfrac{\partial G_j}{\partial y_i}\right|}} \tag{6}$$

Formulation (6) provides different optimum values of the normalized variables at the design point and taking into account several failure modes.

3.3 OSF algorithm

The Optimum Safety Factor (OSF) algorithm can be easily implemented in three principal steps (Fig. 2). The first step is to determine the design point considering the most active constraint as a limit state function G(y). The optimization problem is to minimize the objective function subject to the limit state and the deterministic constraints. The resulting solution is termed the design point. The second step is to compute the safety factors using the equations (4) and (6). The third step is to calculate the optimal solution including the values of the safety factors in the computation of the values of the design variables and then determine the optimum design of the structure.
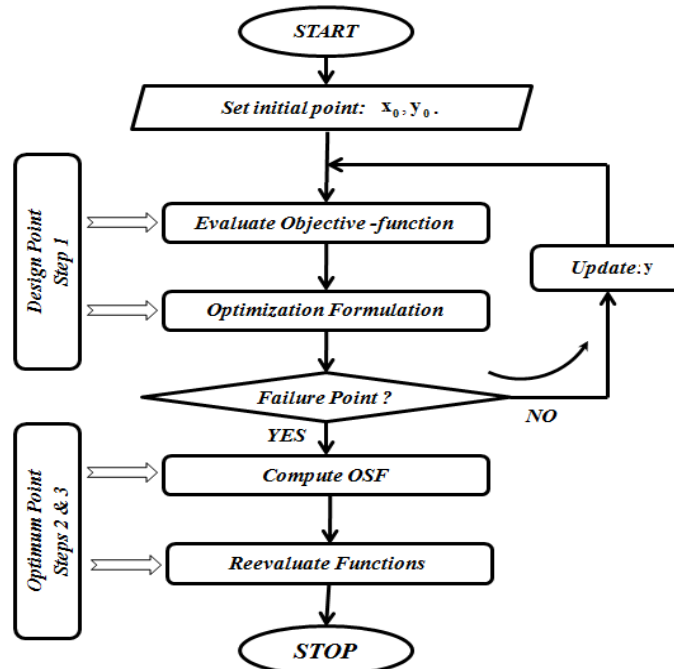
Fig. 2. OSF algorithm

4.   Numerical Application

The objective of this application is to show the advantage of the RBDO by OSF relative to the DDO when dealing with SFM and MFM. The corresponding material properties are: Young's modulus E = 206.8GPa, Poisson's ratio ν = 0.29 and density ρ = 7820 kg/m^3. The endurance limits for the reversed tension stress and torsion stress f-1 and t-1

stated after 2.106 cycles are equal to 252MPa and 182MPa, respectively. For more details about the fatigue data and methods of this example, the interested reader can refer to [12]. The length and the height of the studied plate are: L=0.14 m and H=0.1 m, respectively (Fig. 3a). In finite element analysis, the plate is supposed simply fixed on its four edges and is modelled by 32 eight-node square elements which produce no out-of-plane stress (Fig. 3b). Here, the thickness of each element T_i is considered as a random variable and its mean as a deterministic variable that leads to 32 deterministic variables and 32 random variables.
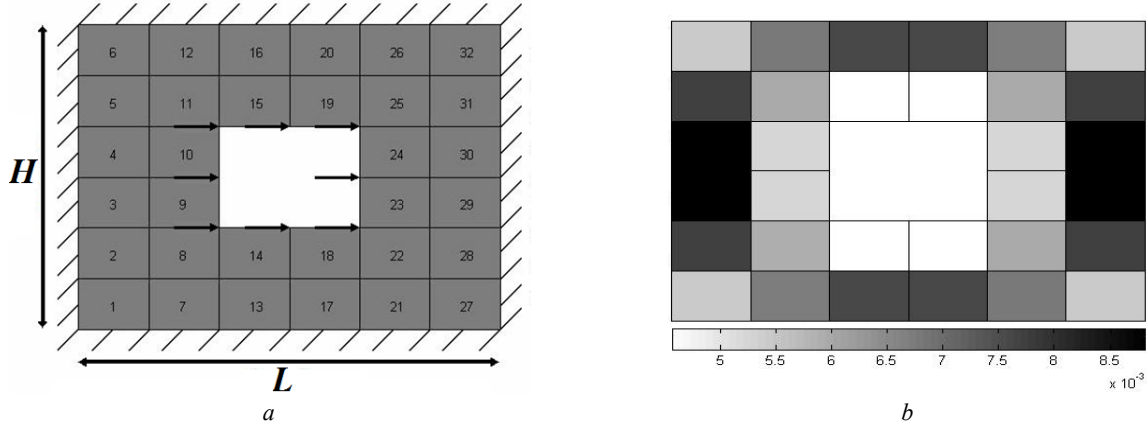
Fig. 3:
a - Dimensions of the perforated plate and
b - Thickness distribution for resulting optimum design

The objective of the DDO procedure is to minimize the volume subject to the fatigue damage constraints. Here, we consider a global safety factor $S_f = 1.25$ applied to the damage D_{max} and based on the engineering experience. The RBDO procedure cannot control not only the reliability level but several output parameters. In [2], the reliability level has been controlled considering a target reliability level, however, here we seek to control the other output parameters such as the structural volume and the damage criterion.

The DDO and RBDO results in table (1) show that the DDO cannot provide the designer with a required reliability level while RBDO by OSF allow controlling the safety levels. According to the problems 3 and 5, the value of the global safety factor is applied to the upper damage limit $D_U = 1$ to be $S_f = 1.25$. This way the allowable damage will be: $D_w = 0.8$. The standard deviations are considered as proportional of the mean values: $\sigma_i = 0.5 m_i$, i=1,...,32. After having optimized the structure, the resulting DDO volume (Table 1) was found to be $V_{DDO}=105.64$cm^3. The corresponding reliability index was found to be: $\beta_{DDO} = 2.73$. This resulting value does not belong to the standard structural engineering norm $\beta_{DDO} = 2.73 \notin [3-4.25]$. However, for the same optimum volume, the RBDO for multiple failure modes (using 5 and 6) provides the designer with a more reliable optimum structure with $\beta_{RBDO^v} = 3.64$. Figures 4a and b show the interval of the damage distribution of all structure thickness for DDO and RBDO in the same volume $V_{DDO} \approx V_{RBDO}^v$. The resulting damage distribution interval of RBDO by OSF [0.52,0.8] is better than the resulting one by DDO [0.4,0.8]. While Figures 4b and c show the interval of the damage distribution of all structure thickness for DDO and RBDO for the same maximum damage values $D_{DDO}=D_{RBDO}^v=0.8$. The RBDO by OSF provides the designer with an optimum structure with an increase 7% but more reliable by 45% relative to the resulting structure by DDO ($\beta_{RBDO^D} = 3.78 > \beta_{DDO} = 2.73$). Here, the resulting damage distribution interval of RBDO by OSF [0.56,0.84] is also better than the resulting one by DDO [0.4,0.8]. Thus, when obtaining a better damage distribution interval, the volume is reduced in the non-critical structural regions that leads to economic and reliable designs.

Table 1

DDO and RBDO results for β^{SFM}

Parameters	Design Point	Optimum Solutions		
		$RBDO^V$	DDO	$RBDO^D$
Volume	81.9770	105.53	105.64	112.70
$D_{U\max}$	$0.9945 \approx 1$	0.84	0.8	0.8
β^{SFM}	*0*	3.64	2.73	3.78
T_1	5.5784	8.914	7.7839	9.665
T_2	7.7249	11.477	9.2979	12.434
T_3	8.7796	8.340	10.1057	8.732
T_4	8.7876	8.328	10.1055	8.718
T_5	7.7435	11.571	9.2976	12.536
T_6	5.604	9.001	7.7838	9.759
T_7	6.8081	12.024	8.6421	13.129
T_8	6.0581	8.675	8.1291	9.265
T_9	5.3822	3.715	7.5599	3.738
T_{10}	5.3866	3.745	7.5597	3.770
T_{11}	6.0644	8.678	8.1290	9.266
T_{12}	6.8267	12.063	8.6422	13.169
T_{13}	7.605	10.503	9.2265	11.214
T_{14}	4.7228	4.081	7.1685	4.157
T_{15}	4.7194	4.061	7.1689	4.136
T_{16}	7.608	10.507	9.2268	11.218
T_{17}	7.6074	10.504	9.2267	11.214
T_{18}	4.7191	4.057	7.1688	4.131
T_{19}	4.7231	4.082	7.1685	4.159
T_{20}	7.6056	10.509	9.2264	11.220
T_{21}	6.8256	12.057	8.6421	13.162
T_{22}	6.0637	8.675	8.1290	9.262
T_{23}	5.3861	3.738	7.5597	3.762
T_{24}	5.3825	3.721	7.5599	3.745
T_{25}	6.0588	8.680	8.1291	9.270
T_{26}	6.8093	12.031	8.6421	13.137
T_{27}	5.6029	8.992	7.7838	9.749
T_{28}	7.7425	11.557	9.2976	12.521
T_{29}	8.7871	8.311	10.1055	8.699
T_{30}	8.7799	8.351	10.1057	8.744
T_{31}	7.7257	11.491	9.2979	12.450
T_{32}	5.5794	8.922	7.7839	9.674

The structural reliability level is improved because the OSF-based solution essentially depends on the sensitivity study which determines the role of each parameter relative to the failure probability. For the computing time, the DDO procedure needs to solve two sequential optimization problems (1) and (2) while the RBDO by OSF can realize the operation in only one single optimization problem.
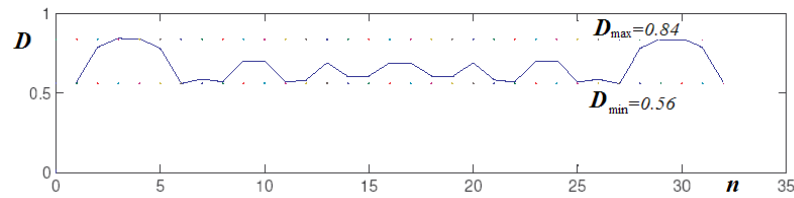
a) Optimum Solution by $RBDO^V$, Dmax=0.84 Volume=105, β =3.64, D $\in$ [0.56,0.84]
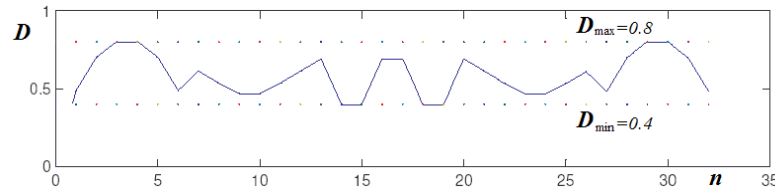
b) Optimum Solution by DDO, D_{max}=0.8, *Volume*=105, β =2.73, D $\in$ [0.4,0.8]
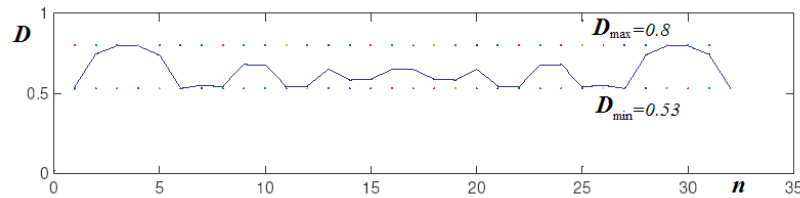
c) Optimum Solution by $RBDO^D$, Dmax=0.8, Volume=112, β =3.78, D $\in$ [0.53,0.8]

Figure 4. Resulting damage distribution intervals by DDO and RBDO procedures

Table 2 presents the different OSF results considering the linear and nonlinear distributions (normal, lognormal, uniform, Weilbull and Gumbel distributions), see [2], satisfying a required reliability level $\beta = 3$. The required reliability level can be considered as a given data and the algorithm converges to the optimum design that verifies the requirements (controllable designs: reliability, volume, damage …). For the computing time consumption, for a single failure mode, when using DDO procedure, two optimization processes are used (the first is to find the optimum solution and the second is to find the design point). The problem becomes much more complex for multiple failure modes where each failure mode needs a separate optimization process to find the corresponding design point. However, the RBDO by OSF needs only a single optimization process to find the design point and next the optimum solution is analytically computed using OSF-SFM or OSF-MFM formulations. The RBDO by OSF is then carried out without additional computing time because it has a single variable vector that defines the design point.

Table 2

Linear and nonlinear RBDO result for required reliability index $\beta = 3$

Structural Parameters	Design Point	Optimum RBDO solutions				
		Normal	Lognormal	Uniform	Weibull	Gumbel
Volume	81.97	86.63	86.92	88.22	85.59	83.28
D_{max}	$0.99 \approx 1$	0.94	0.93	0.92	0.95	0. 98
β	0	3.00	3.00	3.00	3.00	3.00
P_f	50%	$\approx 0.1\%$	$\approx 0.1\%$	$\approx 0.1\%$	$\approx 0.1\%$	$\approx 0.1\%$
T_1	5.5784	5.8679	5.8890	5.9694	5.7954	5.6604
T_2	7.7249	8.1947	8.2203	8.3520	8.0980	7.8541
T_3	8.7796	9.3409	9.3684	9.5255	9.2330	8.9342
T_4	8.7876	9.3488	9.3763	9.5334	9.2407	8.9428
T_5	7.7435	8.2130	8.2387	8.3704	8.1160	7.8739
T_6	5.6040	5.8933	5.9145	5.9949	5.8204	5.6873
T_7	6.8081	7.1965	7.2204	7.3293	7.1097	6.9176

T_8	6.0581	6.3822	6.4046	6.4950	6.3039	6.1518
T_9	5.3822	5.6633	5.6836	5.7618	5.5934	5.4579
T_{10}	5.3866	5.6677	5.6880	5.7662	5.5978	5.4625
T_{11}	6.0644	6.3885	6.4109	6.5013	6.3101	6.1584
T_{12}	6.8267	7.2148	7.2389	7.3476	7.1277	6.9374
T_{13}	7.6050	8.0591	8.0848	8.2121	7.9634	7.7337
T_{14}	4.7228	4.9483	4.9670	5.0288	4.8862	4.7866
T_{15}	4.7194	4.9451	4.9638	5.0257	4.8831	4.7830
T_{16}	7.6080	8.0621	8.0877	8.2151	7.9663	7.7369
T_{17}	7.6074	8.0615	8.0872	8.2145	7.9657	7.7362
T_{18}	4.7191	4.9448	4.9635	5.0254	4.8828	4.7827
T_{19}	4.7231	4.9486	4.9673	5.0291	4.8864	4.7869
T_{20}	7.6056	8.0597	8.0854	8.2127	7.9640	7.7343
T_{21}	6.8256	7.2137	7.2378	7.3466	7.1267	6.9362
T_{22}	6.0637	6.3878	6.4103	6.5007	6.3094	6.1577
T_{23}	5.3861	5.6672	5.6875	5.7657	5.5973	5.4620
T_{24}	5.3825	5.6636	5.6838	5.7620	5.5937	5.4583
T_{25}	6.0588	6.3828	6.4052	6.4956	6.3045	6.1525
T_{26}	6.8093	7.1976	7.2216	7.3304	7.1109	6.9189
T_{27}	5.6029	5.8922	5.9135	5.9938	5.8193	5.6861
T_{28}	7.7425	8.2121	8.2378	8.3695	8.1151	7.8729
T_{29}	8.7871	9.3483	9.3759	9.5329	9.2402	8.9422
T_{30}	8.7799	9.3412	9.3687	9.5257	9.2332	8.9345
T_{31}	7.7257	8.1954	8.2210	8.3527	8.0987	7.8550
T_{32}	5.5794	5.8689	5.8899	5.9704	5.7964	5.6615

The OSF method is shown as a distinctive tool for RBDO problems. It shows the following advantages:

- The obtained reliability-based optimum solutions should be more reliable than those obtained by DDO procedure for the same optimum volumes,
- The OSF procedure needs only a single optimization process for the design point without additional computing time because it has a single variable vector that defines the design point while the DDO procedure needs two optimization processes.
- Since the major difficulty lies in the evaluation of the probabilistic constraints, which is prohibitively expensive and even diverges for many applications, the OSF procedure provides the designer with an analytical evaluation with small computing time relative to DDO and other RBDO procedures.
- All reliability index evaluations for RBDO-MFM studies can be analytically carried out for different probabilistic distributions. There is no need to optimization processes.

7. Conclusions

The RBDO using OSF has several advantages: small number of optimization variables, good convergence stability, small computing time, satisfaction of the required reliability levels and global optima and more economic solution for the same reliability index relative to the DDO process. The OSF-MFM formulation can be applied easily to different distribution laws. In fatigue analysis, the use of the classical method leads to an extremely high computing time and also local optima.

References

1. Kharmanda, G., El-Hami, A. Reliability-Based Design Optimization, In edited book Multidisciplinary Design Optimization in Computational Mechanics. Piotr Breitkopt and Rajan Filomeno Coelho, eds. Chapter 11: Wiley & Sons, April 2010, ISBN: 9781848211384, Hardback, 576 p.

2. Kharmanda, G., Antypas, I. Reliability-Based Design Optimization Strategy for Soil Tillage Equipment Considering Soil Parameter Uncertainty. Vestnik of DSTU, 2016, vol. 16, no. 2 (85), pp. 136−147.

3. Kharmanda, G. The safest point method as an efficient tool for reliability-based design optimization applied to free vibrated composite structures. Vestnik of DSTU, 2017, vol. 17 (2), pp. 46−55. DOI: https://doi.org/10.23947/1992-5980-2017-17-2-46-55

4. Yaich, A., Kharmanda, G., El Hami, A., Walha, L. Reliability-based design optimization for multi-axial fatigue damage analysis using robust hybrid method. Journal of Mechanics, Haddar Online 6 July, 2017. – Available at: doi: https://doi.org/10.1017/jmech.2017.44.

5. Tu, J. ,Choi, K.K., Park, Y.H. A new study on reliability-based design optimization. ASME Journal of Mechanical Design, 1999, vol. 121, no. 4, pp. 557−564.

6. Du, X., Chen, W. Sequential Optimization and Reliability Assessment method for Efficient Probabilistic Design. ASME J. Mech. Des., 2004, vol. 126(2), pp. 225−233.

7. Steenackers, G.,Versluys, R., Runacres, M., Guillaume, P. Reliability-based design optimization of computation-intensive models making use of response surface models. Quality and Reliability Engineering International, 2011, vol. 27 (4), pp. 555–568.

8. Lopez, R.H., Beck, A.T. Reliability-Based Design Optimization Strategies Based on FORM: A Review, J. of the Braz. Soc. of Mech. Sci. & Eng., 2012, vol. 34 (4), pp. 506−514.

9. Kharmanda, G., Antypas, I. Integration of Reliability Concept into Soil Tillage Machine Design. Vestnik of DSTU, 2015, vol. 15, no. 2 (81), pp. 22−31.

10. Gayton, N., Pendola, M., Lemaire, M. Partial safety factors calibration of externally pressurized thin shells. In: CNES editor. Third European conference on launcher technology, Strasbourg, France; 2001.

11. Kharmanda, G., Olhoff, N., El-Hami, A. Optimum values of structural safety factors for a predefined reliability level with extension to multiple limit states. Structural and Multidisciplinary Optimization, 2004, vol. 27, pp. 421–434.

12. Ibrahim, M-H., Kharmanda, G., Charki, A. Reliability-based design optimization for fatigue damage analysis. The International Journal of Advanced Manufacturing Technology, 2015, vol. 76, pp. 1021−1030.

Authors:

Ghias Kharmanda,

guest researcher of the Biomedical Engineering Department, Lund University (Ole Römersväg 1, Box 118, 221 00 Lund, Sweden),
ORCID: http://orcid.org/0000-0002-8344-9270
ghias.kharmanda@bme.lth.se

Antypas, Imad Rizakalla,

associate professor of the Machine Design Principles Department, Don State Technical University (1, Gagarin sq., Rostov-on-Don, 344000, RF), Cand.Sci. (Eng.), associate professor,
ORCID: http://orcid.org/0000-0002-8141-9529
imad.antypas@mail.ru

Machine building and machine science

MACHINE BUILDING AND MACHINE SCIENCE
МАШИНОСТРОЕНИЕ И МАШИНОВЕДЕНИЕ

Mechanical properties of servovite films formed in aqueous solutions of carboxylic acids under friction[*]

V. E. Burlakova[1], E. G. Drogan[2], A. I. Tyurin[3], T. S. Pirozhkova[4]**

[1,2] Don State Technical University, Rostov-on-Don, Russian Federation
[3,4] Research Institute of Nanotechnologies and Nanomaterials, G.R. Derzhavin Tambov State University, Tambov, Russian Federation

Механические свойства сервовитных пленок, формирующихся при трении в водных растворах карбоновых кислот[***]

В. Э. Бурлакова[1], Е. Г. Дроган[2], А. И. Тюрин[3], Т. С. Пирожкова[4]**

[1,2] Донской государственный технический университет, г. Ростов-на-Дону, Российская Федерация
[3,4] НИИ «Нанотехнологии и наноматериалы» Тамбовского государственного университета им. Г. Р. Державина, Тамбов, Российская Федерация

Introduction. The effect of the organic component nature in the systematic series of monocarboxylic acids on the tribological characteristics of the brass-steel friction pair in aqueous solutions is described. Dependence of the mechanical-and-physical properties of the antifriction films formed during friction on the nature of the lubricating composition is investigated. The work objectives are to study the applicability of carboxylic acids as an antifriction lubricant component; to assess their effect on the mechanical properties of the servovite film formed under the brass – steel friction.

Materials and Methods. Tribological studies of the brass-steel friction pair on the AE-5 end-type friction machine are carried out. Roughness parameters of the servovite film were determined through the optical profilometry. The microgeometry and the object structure at the nanoscale were considered using atomic force microscopy. The mechanical characteristics of the antifriction film were investigated using the instrument nanoindentation.

Research Results. Tribological characteristics of the brass-steel tribocoupling and mechanical-and-physical properties of the servovite film formed during friction in the "brass – aqueous solution of carboxylic acid – steel" system were studied. It is established that the friction factor reduces when increasing the hydrocarbon radical length. The dimensional effects are found in the mechanical and tribological properties of the servovite film formed on the surface of the friction interaction in the carboxylic acids.

Discussion and Conclusions. The study results show that the

Введение. В работе показано, каким образом природа органической компоненты в систематическом ряду одноосновных карбоновых кислот влияет на трибологические характеристики пары трения «латунь — сталь» в водных растворах. Изучена зависимость физико-механических свойств антифрикционных пленок, формирующихся при трении, от природы смазочной композиции. Цели работы: изучить возможности использования карбоновых кислот как антифрикционных компонентов смазочного материала; оценить их влияние на механические свойства сервовитной пленки, формирующейся при трении латуни по стали.

Материалы и методы. Проведены трибологические исследования пары трения «латунь — сталь» на машине трения торцевого типа АЕ-5. Параметры шероховатости сервовитной пленки определялись с помощью оптической профилометрии. Микрогеометрия и структура объекта на наноуровне исследовались с помощью атомно-силовой микроскопии. Механические характеристики антифрикционной пленки изучали с помощью инструментального наноиндентирования.

Результаты исследования. Изучены трибологические характеристики трибосопряжения «латунь — сталь» и физико-механические характеристики сервовитной пленки, формирующейся при трении в системе «латунь — водный раствор карбоновой кислоты — сталь». Установлено, что при увеличении длины углеводородного радикала коэффициент трения снижается. Обнаружены размерные эффекты в механических и трибологических свойствах сервовитной пленки, формирующейся на поверхности фрикционного взаимодействия в водных растворах карбоновых кислот.

friction interaction on the wearing surface in the aqueous solutions of carboxylic acids forms a nanostructured servovite film which drops the friction factor. Its mechanical, physical and tribological parameters depend on the composition of the model lubricating medium. It is determined that the local mechanical-and-physical properties depend on the method of producing the servovite layer, the load and the size of the deformation zone. The results obtained can be used in the development of lubricants.

Обсуждение и заключения. Результаты исследования показывают, что при фрикционном взаимодействии на поверхности трения в водных растворах карбоновых кислот формируется наноструктурная сервовитная пленка, резко снижающая коэффициент трения. Ее физико-механические и трибологические параметры зависят от состава модельной смазочной среды. Определено, что локальные физико-механические свойства зависят от способа получения сервовитного слоя, нагрузки и размера зоны деформирования. Полученные результаты могут быть использованы при разработке смазочных материалов.

Introduction. A rapid development of modern machine building increases opportunities of constructing machines that operate under the extreme conditions. Thus, the motivation of the life growth of the friction units rises with the demanding requirements for the mechanical properties of materials.

The friction conditions with high energy density impose a number of specific requirements on the machines and equipment in terms of the tribological characteristics, reliability and service life. The critical working conditions of tribo-mating surfaces affect the flow of force, loss of energy, and, eventually, dynamic behavior of the complete mechanism. Space distributions of topographic irregularities, as a rule, negatively affect the operational capabilities of machines and mechanisms. In other words, the load-bearing capacity of friction units hinges on the basic parameters of the surface state. They affect the interaction conditions in the contact area, adhesion, and deformation, thereby generating vibrations during the friction process [1] and causing uneven wear.

In this case, the greatest antifriction efficiency is demonstrated by the lubricants [2-6] containing metal additives, such as copper, aluminum, silver. These materials form protective metal plaque shells on the tribo-mating surfaces in the process of friction. Thus, a low friction factor and a medium low wear are provided in a wide range of contact pressures and slip velocities [2, 3]. The process of metal plaque filming of the surface layers in-service enables to "heal" surface defects (cracks, pores, accumulated fatigue damage). This essentially increases the antifriction characteristics and improves the mechanical-and-physical properties, which is of prime importance for the reliable operation of the friction units, and the lifetime extension.

It is notable that the formation of transfer films is possible under friction in aqueous-alcoholic media with no visible total wear of the mating surfaces [7, 8]. In the engineering practice, the use of selective transfer gives a real opportunity for designing long-life and effective friction units in the movable mating of parts and components of machines and mechanisms [8].

In this context, it is interesting to consider the effect of the lubricating medium composition on the mechanical and tribological parameters of the servovite film forming in the "brass-steel" tribo-pair (aqueous solutions of carboxylic acids are used as a lubricant medium).

Materials and Methods. Evolution of the friction factor of the "brass 59 – aqueous solution of carboxylic acid – steel 40X" system was investigated in the "Hybrid Functional Graphene-Based Materials" laboratory of the Research and Education Center (REC) "Materials" on the AE-5 end-type friction machine. The experiments were carried out under the following conditions: rotation speed was 180 rpm; axleload was 98 N; the test time was 10 hours. The

monocarboxylic acids of the limiting series with the general formula of $R - COOH$ ($R = C_nH_{2n+1}$) were used as an organic component of the lubricant composition.

The mechanical characteristics (hardness – H and Young modulus – E) of servovite films were determined by the instrument indentation method [9, 10]. Thereat, we used:

–Nanotest Platform 3 (Micromaterials, UK) nanoindentation tester with the attached function unit that enables to impose loads from 0.01 mN to 500 mN;

– *Nanotest Platform* 3 (*Micromaterials*, *UK*) tribological nanoindentation tester, a multifunctional system for mechanical testing of materials through the dynamic nanoindentation.

The nanoindentation technique makes it possible to study the package of mechanical properties of light boundary layers of solids and films up to a few tens of nm thick [9-15]. The mechanical characteristics were studied using a diamond Berkovich indenter. Taking into account the specific thickness of the investigated films (from several hundred nanometers to units of micrometers), the operational mechanical parameters were measured at the nanoscale at indentation depths from 20 nm to the micron units. At the nanoscale, the friction coefficient was investigated on the *Triboindenter* TI-950 with simultaneous application of normal and lateral loads to the indenter [11, 16, 17]. The normal and lateral components of the forces (F_N and F_L) and displacements (h_N and h_L) implemented during the replication of the tribo contacts by the indenter were recorded continuously. The recorded data were analyzed, which permitted to describe the friction and wear processes. The friction coefficient k_{mp} was an evaluation item.

The *Contour GT-K1* optical profilometer with *Vision 64* analytical software installed in the REC "Materials" was used to determine the servovite film thickness and roughness parameters. The measurements were taken using vertical scanning interferometry (*VSI*) at the scan rate of 0.1 μm / s with the repeatability of *RMS* 0.01 nm.

The servovite film surface topography was studied using the *PHYWE Compact* atomic-force microscope (AFM) in a semi-contact mode with a single-crystal silicon aluminum-coated probe.

Research Results. A servovite film, spontaneously arising under the friction interaction in the glycerin solution in the copper-steel alloy, is studied fairly well [8, 18]. It is common knowledge that it is formed on the friction face under the topographically unequal conditions. Thus, in different places of frictional contact, the properties of the servovite film are different. Its thickness is less than 2 μm, and the mechanical, physical and tribological properties differ from those of base compact copper.

It should be mentioned that one of the glycerin tribooxidation [19] products is carboxylic acid. In that context, it is interesting to consider the effect of the lubricating medium composition on the mechanical and tribological properties of the "brass-steel" tribo-pair under friction in the systematic series of monocarboxylic acids.

Long-term evolutionary tribological studies of the "brass-steel" friction pair in aqueous solutions of carboxylic acids have revealed the following dependence of the tribological characteristics on the lubricating medium composition: the length of the hydrocarbon chain of the acid radical increases from C_0 to C_5, and the friction factor decreases to 0.007.

At that, the lowest value of the friction factor, which is characteristic for the systems implementing the wearlessness effect [20, 21], is obtained in aqueous solutions of the valeric and caproic acids. At the same time, the "brass-steel" tribo-pair wear is reduced by 25 times. As a result of the selective transfer under the tribo-mating surfaces friction, a copper film with different roughness and surface coating density is formed.

The friction surface was scanned under transition conditions in the series of the "formic - acetic - propionic - oil - valeric – caproic" acids. At that, optical profilometry has revealed, first, a decrease in the servovite film roughness. Secondly, the dependence of roughness on the initial topography of the of the test steel disc surface (its R_a is equal to 118 nm) and on the lubricant composition was determined [22, 23] (Fig. 1).

— scan profile;　　— roughness profile;　　— undulation profile
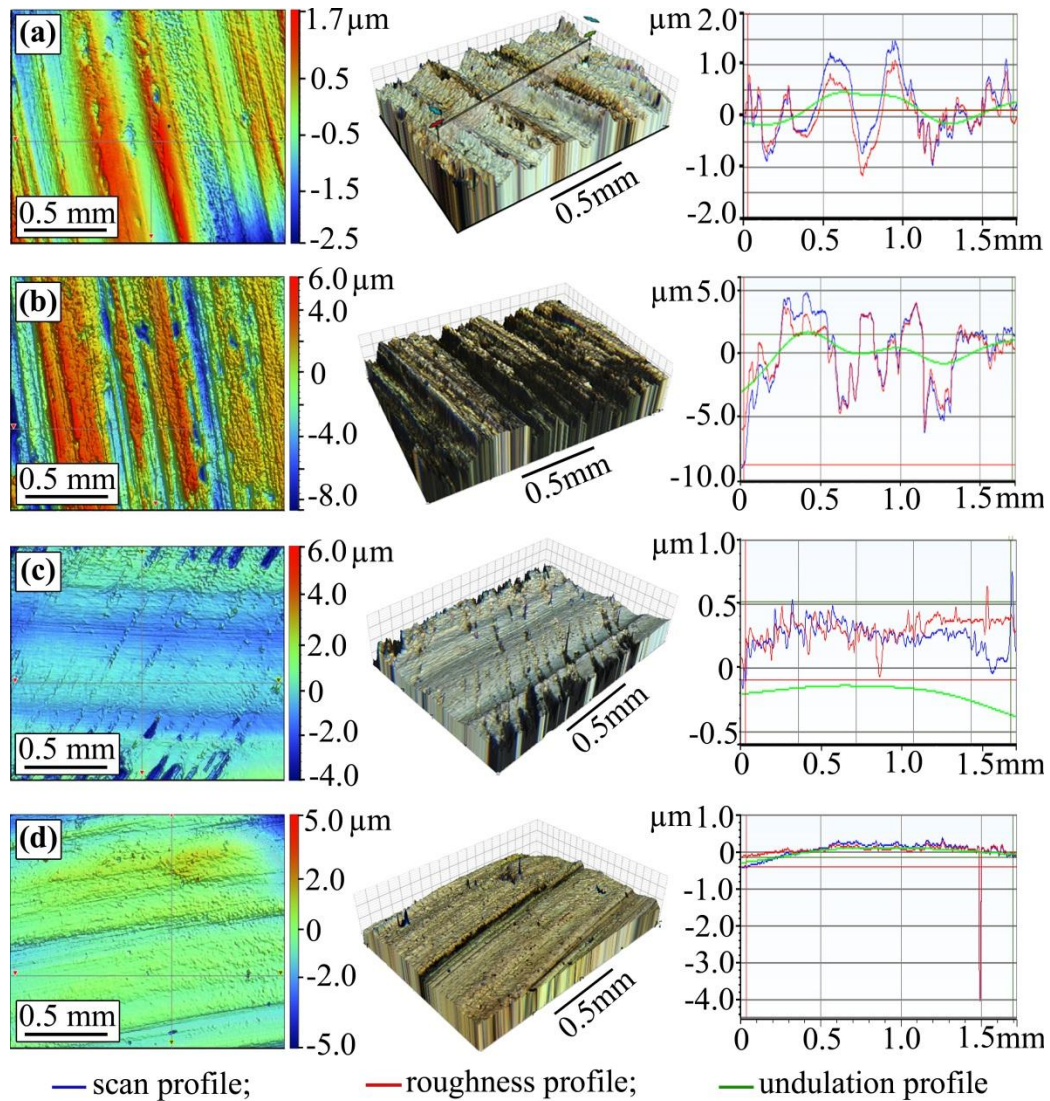
Fig. 1. 2D visualization, 3D visualization and surface profile from steel (*a*), (*c*) and brass-59 (*b*), (*d*) after friction in aqueous solutions of acetic (*a*), (*b*) and caproic (*c*), (*d*) acids

Roughness R_a at the base length (L = 800 μm) of the servovite film decreases, for example, in the aqueous caproic acid, up to 69 nm. (For comparison: this index comes up to 580 nm in an aqueous solution of formic acid and to 401 nm – in an acetic acid solution.) The difference is due to the corrosive activity of the medium.

In the formic and acetic acid solutions, scores of scratches, irregularities and pores occur on the tribo-mating surfaces, as well as areas with a copper film formed in the island growth mode. In the cross-section of the friction surface, deep longitudinal grooves are revealed, which goes to show the abrasive wear pattern of the tribocoupling [23, 24].

A more detailed scanning of the surface using the AFM method and image visualization discovers considerable damage under friction in the formic and acetic acid solutions. On a 3D image, they are visualized as macroscopic dark bands corresponding to the areas of intense frictional stress accompanied by strong abrasive wear of tribo-combinations (Fig. 2).
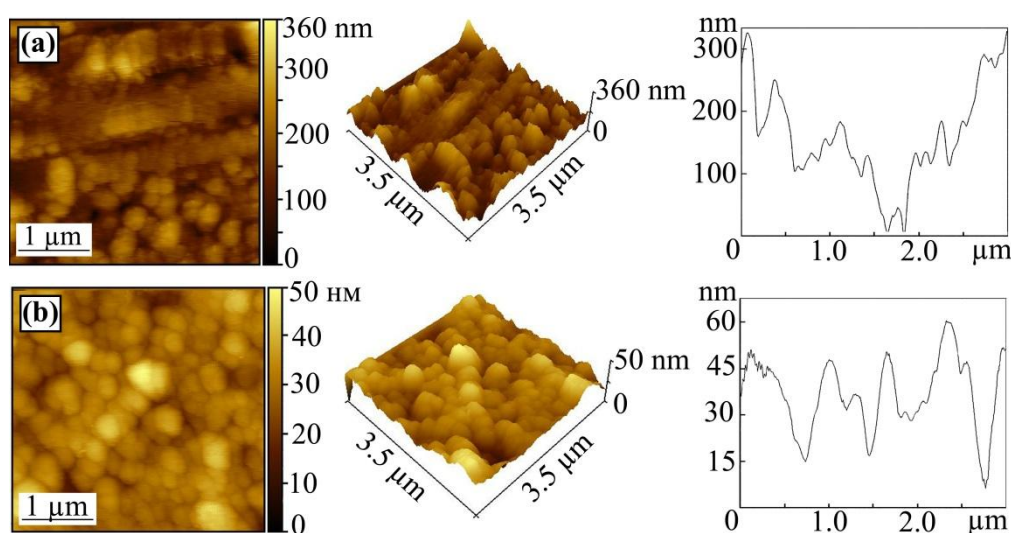
Fig. 2. Topography of servovite film surface obtained under friction in aqueous solution of acetic (*a*) and caproic (*b*) acid

A comparative analysis of the friction surface morphology upon transition to the acids with a longer hydrocarbon radical, suggests the wear pattern transition, and the structural modification of a thin subsurface film of tribocoupling.

It follows from the mass transfer of the components of the contacting bodies, as well as from the adsorption of copper nanoclusters from the working medium to the counterbody as a result of tribo-electrochemical processes in the friction zone during the implementation of the selective transfer. At this, a copper film of fine-grained copper nanoclusters is formed on the steel surface under the friction interaction in the aqueous solutions of caproic and valeric acids. The layer formed on the surface is fairly dense, with a small spread of particles in size (see Fig. 1, 2).

By now, a significant amount of experimental data has been accumulated [25-29] implying a major change in the mechanical properties with reducing the characteristic dimensions of the elements of the object structure of less than 100 nm. This permits to assume a change in the mechanical parameters of the servovite films as compared to those for copper in the volume [30]. To identify this fact, an instrument indentation was carried out.

The hardness values of *H* and Young's modulus *E* were determined by the Oliver-Pharr method [10] from the characteristic *P-h* diagrams (Fig. 3) in accordance with the standards [9].
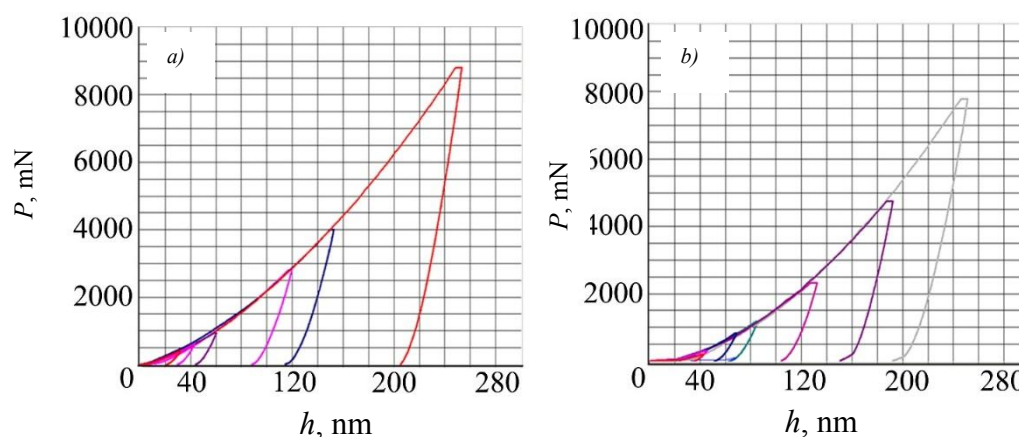
Fig. 3. Representative *P-h* diagrams for servovite film obtained through friction of "brass-steel" pair in aqueous solution of valeric acid (*a*), caproic acid (*b*)

The undertaken studies showed an increase in the values of *H* and *E* films compared to the similar characteristics of the copper sample.

The increase in the hardness *H* and the elasticity modulus *E* of the film formed on the friction surface can be ascribed to the change in the plastic deformation mechanism. A high vacancy concentration at the grain boundaries during friction interaction promotes grain-boundary sliding of building blocks relative to each other. In this case, the non-dislocation plasticity mechanism is implemented [31-34], which results in improving strength characteristics of the copper surface layer, and in increasing ductility during the transition in the series of the "formic - acetic - propionic - oil - valeric – caproic" acids.

Besides, the analysis of the dependence of the *H* and *E* values of the servovite film on the depth of the h_c plastic impression shows that the hardness is affected by the scale factor. The Young's modulus values remain practically constant up to the depths associated with the servovite layer thickness. The films formed through friction in valeric acid are of much evidence (Fig. 4).
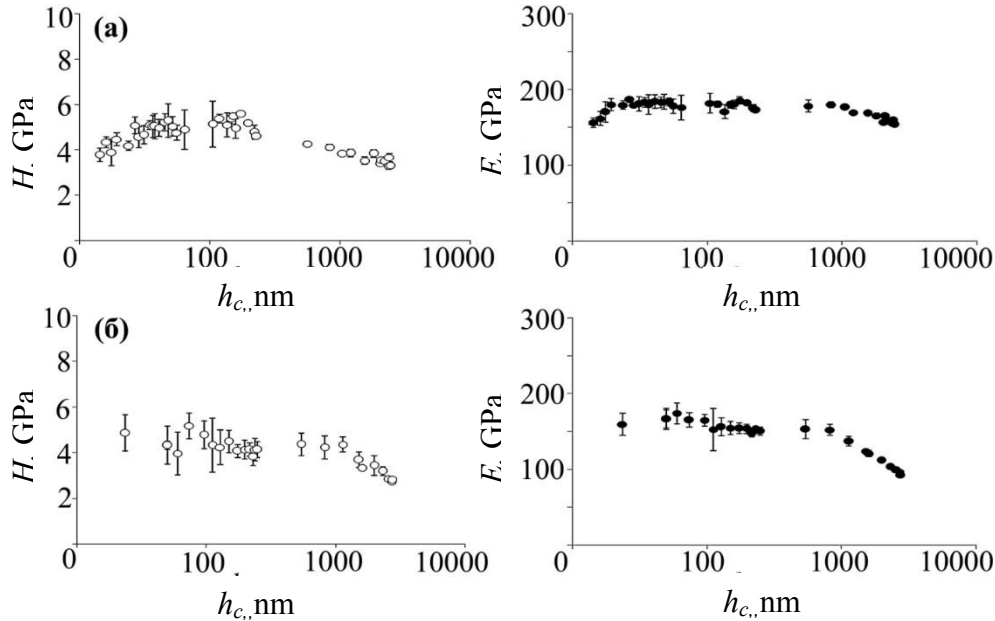
Fig. 4. Dependence of hardness (*H*) and Young's modulus (*E*) on the depth of plastic impression (h_c) (shown in semilog coordinates) when indenting servovite film obtained in aqueous solution of valeric acid (*a*), caproic acid (*b*)

The following dimensional effect is identified:
- *H* value increases with growth of h_c in the shallow depth-region;
- with further growth of h_c, *H* falls dramatically.

For other samples, the dimensional effects are feebly-marked. Thus, for example, for the film formed in caproic acid, the values of *H* and *E* remain practically constant within the full tested range of h_c (from 23 nm to 1.1 μm). Then, with increasing h_c, the values of *H* and *E* decrease. Obviously, this is due to the increase in the deformation zone size: the properties of the transition layer and the substrate material start to affect *H* and *E*. And, in the region of deep depths of the indentation ($h_c > 1.1$ μm), the values of *H* and *E* decrease (see Fig. 4).

The dimensional effect [35, 36] is also found under studying the dependence of the friction factor on the applied load in the nano- and microscale [11, 16, 17] (Fig. 5).
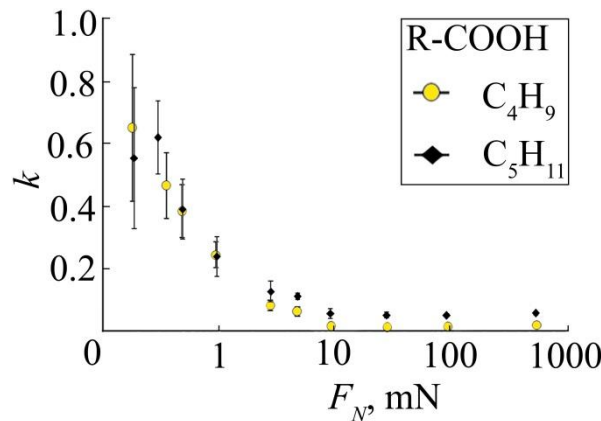
Fig. 5. Dependence of friction factor *k* of servovite film on load in nanoscale

First, it is expressed in a sharp drop in the friction coefficient with an increase in the normal load, up to some value of F_{Nonm}. Then, the friction coefficient increases smoothly with increasing F_N. So, the dependences $k = f(F_N)$ have sharp minimum if some value of F_{Nonm} is reached [11, 16, 17].

The experimental data obtained can be compared to the theoretical dependence of the friction factor on the normal load. Hence, it is becoming apparent that they are in good qualitative agreement to all the film samples under

study. The F_{Nonm} value is affected by the type of carboxylic acid used as a lubricant. For example, for caproic acid, $F_{Nonm} = 30$ mN, and for valerian acid, $F_{Nonm} = 100$ mN.

Discussion and Conclusions. The mechanical properties of servovite films formed in the "brass-steel" friction pair are studied. The dimensional effects in the mechanical (hardness) and tribological (friction factor) properties are identified in the nano- and microscale. It is shown that the properties studied and the nature of their changes depend on the type of carboxylic acid used. The decrease in the average size of crystallites in the composition of film nanoparticles leads to an increase in its strength and the development of superplasticity under tension and shear.

The results obtained in the paper permit to draw the following conclusions.

1. During the friction interaction of the "brass-steel" pair in aqueous solutions of carboxylic acids, an antifriction servovite film is formed on the friction surfaces, which contributes to a sharp decrease in the friction factor.

2. The servovite film, which is formed under the tribo-interaction of the "brass-steel" pair, is nanostructured.

3. The tribological parameters of the "brass – aqueous carboxylic acid – steel" system depend on the length of the hydrocarbon radical of carboxylic acid used as a lubricant.

4. The lubricating medium composition affects the roughness parameters of the servovite film: in the transition from formic to caproic acid, the film surface roughness is reduced to one-quarter.

5. Local physical and mechanical properties depend on the conditions for obtaining the servovite layer, the load, and the size of the deformation zone (the indentation depth).

6. The detected dimensional effects (dependence of the determined values on the indentation depth) verify the conclusion on the nanostructured character of the servovite film formed in the "brass – aqueous carboxylic acid – steel" tribosystem.

References

1. Duvefelt, K., Olofsson, U., Johannesson, C.-M. Model for contact between finger and sinusoidal plane to evaluate adhesion and deformation component of friction. Tribology International, 2016, vol. 96, pp. 389–394.

2. Jen, T.-C., Nemecek, D.-J. Thermal analysis of a wet-disk clutch subjected to a constant energy engagement. International Journal of Heat and Mass Transfer, 2008, vol. 51, no. 7/8, pp. 1757–1769.

3. Ost, W., De Baets, P., Degrieck, J. The tribological behaviour of paper friction plates for wet clutch application investigated on SAEII and pin-on-disk test rigs. Wear, 2001, vol. 249, pp. 361–371.

4. Asnida, M., et al. Copper (II) oxide nanoparticles as additive in engine oil to increase the durability of piston-liner contact. Fuel, 2018, vol. 212, pp. 656–667.

5. Borda, F.-L.-G. Experimental investigation of the tribological behavior of lubricants with additive containing copper nanoparticles. Tribology International, 2018, vol. 117, pp. 52–58.

6. Safonov, V.V., Venskaitis, V.V., Azarov, A.S. Evaluation of the antiwear properties of transmission oil with nanoscale powder additives. Surface Engineering and Applied Electrochemistry, 2017, vol. 53, no. 4, pp. 311–321.

7. Burlakova, V.E., Kosogova, Y.P., Drogan, E.G. Vliyanie nanorazmernykh klasterov medi na tribotekhnicheskie svoystva pary treniya «stal' — stal'» v vodnykh rastvorakh spirtov. [Effect of copper nanoclusters on the tribological properties of steel-steel friction pair in alcohol aqueous solutions.] Vestnik of DSTU, 2015, vol. 15, no. 2 (81), pp. 41–47 (in Russian).

8. Kuzharov, A.S. Kontseptsiya bezyznosnosti v sovremennoy tribologii. [The concept of wearless in modern tribology.] University News. North-Caucasian region. Technical Sciences Series. 2014, no. 2 (177), pp. 23–31 (in Russian).

9. Metallic materials — Instrumented indentation test for hardness and materials parameters: ISO 14577-4 (2007). International Organization for Standardization. Geneva: ISO, 2007, 11 p.

10. Oliver, W.-C., Pharr, G.-M. Measurement of hardness and elastic modulus by instrumented indentation: Advances in understanding and refinements to methodology. Journal of materials research, 2004, vol. 19, no. 1, pp. 3–20.

11. Tyurin, A.I., Pirozhkova, T.S., Shuvarin, I.A. Issledovanie protsessov deformirovaniya pri formirovanii otpechatka i treniya v mikro- i nanoshkale. [Study of deformation in imprinted and friction in micro- and nanoscale.] Russian Physics Journal, 2016, vol. 59 (7-2), pp. 243–247 (in Russian).

12. Surmeneva, M.A., et al. Effect of silicate doping on the structure and mechanical properties of thin nanostructured RF magnetron sputter-deposited hydroxyapatite films. Surface and Coatings Technology, 2015, vol. 27, pp. 176–184.

13. Surmeneva, M.A., et al. Enhancement of the mechanical properties of az31 magnesium alloy via nanostructured hydroxyapatite thin films fabricated via radio-frequency magnetron sputtering. Journal of the Mechanical Behavior of Biomedical Materials, 2015, vol. 46, pp. 127–136.

14. Ivanova, A.A., et al. Fabrication and physico-mechanical properties of thin magnetron sputter deposited silver-containing hydroxyapatite films. Applied Surface Science, 2016, vol. 360, pp. 929–935.

15. Yurkevich, O., et al. Protective radiolucent aluminium oxide coatings for beryllium x-ray optics. Journal of Synchrotron Radiation, 2017, vol. 24, no. 4, pp. 775–780.

16. Tyurin, A.I., et al. Issledovanie kinetiki i mekhanizmov deformirovaniya, treniya i iznosa odnorodnykh i neodnorodnykh tverdykh tel v nanoshkale metodami dinamicheskogo mikro- i nanoindentirovaniya. [Study on kinetics and mechanisms of deformation, friction, and wear of homogeneous and inhomogeneous solids in nanoscale by methods of dynamic micro- and nanoindentation.] Deformirovanie i razrushenie strukturno neodnorodnykh sred i konstruktsiy: mat-ly III vseros. konf., posvyashchennoy 100-letiyu so dnya rozhdeniya akademika Yu. N. Rabotnova. [Deformation and destruction of structurally inhomogeneous media and structures: Proc. III All-Russ. Conf. on the occasion of centenary of the birth of Academician Yu. N. Rabotnov.] Novosibirsk: Lavrentyev Institute of Hydrodynamics, 2014, pp. 108–110 (in Russian).

17. Tyurin, A.I., Pirozhkova, T.S. Issledovanie protsessov treniya i iznosa tverdykh tel v mikro- i nanoshkale. [Study of deformation in imprinted and friction in micro- and nanoscale.] Transactions of TSTU, 2016, vol. 21, no. 3, pp. 1375–1380 (Natural and Technical Sciences) (in Russian).

18. Kragelskii, I.V., et al. The mechanism of the initial stage of selective transfer during frictional contact. Wear, 1978, vol. 47, no. 1, pp. 133–138.

19. Belikova, M.A. Elektrokhimicheskie svoystva poverkhnosti treniya pri samoorganizatsii v usloviyakh izbiratel'nogo perenosa: avtoref. dis. ... kand. tekhn. nauk. [Electrochemical properties of the friction surface during self-organization under conditions of selective transfer: Cand.Sci. (Eng.), diss., author's abstract.] Rostov-on-Don, 2007, 19 p. (in Russian).

20. Burlakova, V.E., et al. Vliyanie prirody organicheskoy komponenty na tribotekhnicheskie svoystva sistemy «bronza — vodnyy rastvor karbonovoy kisloty — stal'». [Effect of organic component nature on tribological properties of "bronze-aqueous solution of carboxylic acid-steel" system.] Vestnik of DSTU, 2015, vol. 15, no. 4 (83), pp. 63–68 (in Russian).

21. Kuzharov, A.S., et al. Nanotribologiya vodnykh rastvorov karbonovykh kislot pri trenii bronzy po stali. [Nanotribology of aqueous solutions of carboxylic acids in under bronze - steel friction.] Innovatsii, ekologiya i resursosberegayushchie tekhnologii: mat-ly XI mezhdunar. nauch.-tekhn. foruma. [Innovations, ecology and resource-saving technologies: Proc. XI Int. Sci.-Tech. Forum.] 2014, pp. 712–717 (in Russian).

22. Drogan, E.G. Issledovanie topografii poverkhnosti i mekhanicheskikh svoystv servovitnoy plenki. [Study of surface topography and mechanical properties of servovite film.] Perspektivy razvitiya fundamental'nykh nauk: sb. nauch. tr. XIII mezhdunar. konf. studentov, aspirantov i molodykh uchenykh. [Prospects for the development of fundamental sciences: Proc. XIII Int. Conf. of students, postgraduates and young scientists.] 2016, pp. 148–150 (in Russian).

23. Jiang, J., Arnell, R.-D. The effect of substrate surface roughness on the wear of DLC coatings. Wear, 2000, vol. 239, no. 1, pp. 1–9.

24. Dayson, C. The friction of very thin solid film lubricants on surfaces of finite roughness. ASLE transactions, 1971, vol. 14, no. 2, pp. 105–115.

25. Andrievski, R.A., Glezer, A.M. Prochnost' nanostruktur. [Strength of nanostructures.] Physics – Uspekhi, 2009, vol. 179, pp. 337–358 (in Russian).

26. Koch, C.-C. Nanostructured materials: processing, properties and applications. Norwich: William Andrew, 2006, 784 p.

27. Glezer, A.M., Permyakova, I.E., Fedorov, V.A. Crack resistance and plasticity of amorphous alloys under microindentation. Bulletin of the Russian Academy of Sciences: Physics, 2006, vol. 70, no. 9, pp. 1599–1603.

28. Malygin, G.A. Plasticity and strength of micro-and nanocrystalline materials. Physics of the Solid State, 2007, vol. 49, no. 6, pp. 1013–1033.

29. Valiev, R.Z., Aleksandrov, I.V. Ob"emnye nanostrukturnye metallicheskie materialy. [Bulk nanostructured metallic materials.] Moscow: Akademkniga, 2007, 398 p. (in Russian).

30. Golovin, Y.I. Vvedenie v nanotekhniku. [Introduction to nanotechnology.] Moscow: Mashinostroenie, 2008, 496 p. (in Russian).

31. Panin, V.E., et al. Nanostructuring of surface layers and production of nanostructured coatings as an effective method of strengthening modern structural and tool materials. The Physics of Metals and Metallography, 2007, vol. 104, no. 6, pp. 627–636.

32. Andrievski, R.A., Glezer, A.M. Strength of nanostructures. Physics-Uspekhi, 2009, vol. 52, no. 4, pp. 315–334.

33. Dub, S.N., Novikov, N.V. Ispytaniya tverdykh tel na nanotverdost'. [Tests of solids for nanohardness.] Journal of Superhard Materials, 2004, no. 6, pp. 16–33.

Machine building and machine science

34. Vakulenko, K., Kazak, I., Matsevityi, V. Effect of the state of surface layer on 40X steel fatigue characteristics. Eastern-European Journal of Enterprise Technologies, 2016, vol. 3, no. 5, pp. 18–24.

35. Stoyanov, P., Chromik, R.-R. Scaling effects on materials tribology: from macro to micro scale. Materials, 2017, vol. 10, no. 5, pp. 550.

36. Manini, N., et al. Current trends in the physics of nanoscale friction. Advances in Physics: X, 2017, vol. 2, no. 3, pp. 569–590.

Authors:

Burlakova, Victoria E.,
Head of the Chemistry Department, Don State Technical
University (1, Gagarin Square, Rostov-on-Don, 344000,
RF), Dr.Sci. (Eng.), professor,
ORCID: https://orcid.org/0000-0003-3779-7079
vburlakova@donstu.ru

Drogan, Ekaterina G.,
teaching assistant of the Chemistry Department, Don State
Technical University (1, Gagarin Square, Rostov-on-Don,
344000, RF),
ORCID: https://orcid.org/0000-0002-4002-2082
Ekaterina.drogan@gmail.com

Tyurin, Alexander I.,
Associate director for Research, Research Institute of
Nanotechnologies and Nanomaterials, G.R. Derzhavin
Tambov State University (33, Ul. Internatsionalnaya,
Tambov, 392000, RF), Cand.Sci. (Phys.-Math.), associate
professor,
ORCID: https://orcid.org/0000-0001-8020-2507
tyurin@tsu.tmb.ru

Pirozhkova, Tatyana S.,
engineer, Research Institute of Nanotechnologies and
Nanomaterials, G.R. Derzhavin Tambov State University
(33, Ul. Internatsionalnaya, Tambov, 392000, RF),
ORCID: https://orcid.org/0000-0002-4231-0213
t-s-pir@ya.ru

MACHINE BUILDING AND MACHINE SCIENCE
МАШИНОСТРОЕНИЕ И МАШИНОВЕДЕНИЕ

Experimental study on power parameters of "rolling - ECA-pressing" combined process[*]

A. B. Naizabekov[1], S. N. Lezhnev[2], T. A. Koinov[3], E. A. Panin[4][**]

[1,2] Rudny Industrial Institute, Rudny, Republic of Kazakhstan
[3] University of Chemical Technology and Metallurgy, Sofia, Republic of Bulgaria
[4] Karaganda State Industrial University, Temirtau, Republic of Kazakhstan

Экспериментальное исследование энергосиловых параметров совмещенного процесса «прокатка — равноканальное угловое прессование»[***]

А. Б. Найзабеков[1], С. Н. Лежнев[2], Т. А. Койнов[3], Е. А. Панин[4][**]

[1,2] Рудненский индустриальный институт, г. Рудный, Республика Казахстан
[3] Университет химической технологии и металлургии, г. София, Республика Болгария
[4] Карагандинский государственный индустриальный университет, г. Темиртау, Республика Казахстан

Introduction. Power parameters of the "rolling − equal-channel angular pressing" (ECA) combined process are studied. The work objective is to determine forces of rolling and pressing in the deformation by the combined method.

Materials and Methods. The die strength calculation and the experiment on deformation of AISI 6063 aluminum samples were carried out. During the experiment, the force values were recorded using a strain-gauge station.

Research Results. The strength analysis results show that this die design is suitable for creating an experimental stand of the "rolling − ECA-pressing" combined process, since the calculated safety margin is sufficient to implement the pressing under extreme conditions. The rolling forces at all stages of the deformation exceed the corresponding pressing forces, which is a necessary condition for the combined process.

Discussion and Conclusions. The obtained results can be used in the design of experimental stands that implement the investigated combined process. Herewith, the given strain-gauge method for studying strength characteristics is suitable for the case of calibrated rolls.

Введение. Статья посвящена исследованию энергосиловых параметров совмещенного процесса «прокатка — равноканальное угловое прессование (РКУ)». Цель работы — определение возникающих усилий прокатки и прессования при деформировании совмещенным способом.

Материалы и методы. Был проведен прочностной расчет матрицы и эксперимент по деформированию образцов из алюминия марки AISI 6063. В ходе опытов значения усилий фиксировались с помощью тензометрической станции.

Результаты исследования. Результаты прочностного анализа позволяют утверждать, что данная конструкция матрицы пригодна для создания экспериментальной установки совмещенного процесса «прокатка — РКУ-прессование», поскольку рассчитанного запаса прочности вполне достаточно для реализации прессования на предельных условиях. Усилия прокатки на всех этапах деформирования превышают соответствующие усилия прессования, что является необходимым условием совмещенного процесса.

Обсуждение и заключения. Полученные результаты могут быть использованы при проектировании экспериментальных установок, реализующих исследуемый совмещенный процесс. При этом тензометрический метод исследования прочностных характеристик пригоден и при использовании калиброванных валков.

Keywords: combined process, rolling, equal channel angular pressing, force, strength analysis, tensometry.

Ключевые слова: совмещенный процесс, прокатка, равноканальное угловое прессование, усилие, прочностной анализ, тензометрия.

Machine building and machine science

289

Introduction. Improvement of the deformable metal quality is one of the major tasks when creating a new metal forming process (MFP) or improving the known one. No matter which type (rolling or blacksmithing) the process belongs to, it is recommended to apply a deformation scheme implementing a pure shear. In this case, a minimum amount of energy is expended on the metal deformation; maximum and uniform workpiece processing through the section is performed; and internal defects are closed.

Over the past two decades, forming techniques have been actively developed. They enable to obtain ultrafine-textured blanks. Their analysis shows that they are based on the principles of implementation of shear or alternating deformations. Processes that are a combination of these principles are worthy of special mention. These processes allow for the implementation of an unconventional forming operation which is called "severe plastic deformation" (SPD). SPD implements such methods as torsion under high pressure [1-3], equal-channel angular (ECA) pressing [4-8], screw extrusion [9-12] and others. Special attention should be given to an echelon ECA-die (or ECA-die with parallel channels) [13-14]. It enables to realize a shear deformation when the workpiece passes through its channels and concurrently two alternating deformation zones, provided that the input and output channels are codirectional. In comparison with the usual angular die, the echelon ECA-die is energy-saving, since it allows for implementing a greater degree of deformation in one pass with the equal force.

The MFP methods discussed above belong to the discrete press forming techniques. These technologies for the molded articles production have a number of shortcomings. The principle ones are due to:

- press operation discreteness (discontinuity);
- occurrence of reactive frictional forces on the metal-to-container contact.

Thus, due to uneven deformation and high energy intensity of the press operation, the length of the pressed products is limited, and their quality is reduced. The application of the continuous pressing scheme enables to eliminate these drawbacks. This method differs fundamentally from the previous ones in that active friction forces are used to deform and extrude the workpiece through the die hole. The length of the workpiece is thus not limited.

In recent years, the so-called "combined" MFP processes, which are a combination of two or more deformation processes, are being developed.

Crucially, the most important feature of the combined MFP process is that shortcomings of the components of individual processes are often reduced or completely eliminated under its implementation.

Besides, more and more attention has been recently paid to the energy-saving technologies based on the use of active friction forces for deformation.

The authors of the study have developed a combined technique of rolling and pressing in an equal-channel echelon die, which, in comparison to the conventional pressing in an equal-channel echelon die, removes the limitations on the dimensions of the initial blanks [15]. It seems to be one of the most advanced and understudied on the practical level rolling and pressing processes, and it in many ways surpasses the known forming methods. The principle of this straining method is as follows. The workpiece, pre-heated up to the temperature of the deformation onset, is fed to the cast rolls. The first pair of rolls, due to the contact friction forces, bites the workpiece and pushes it on exit through the channels of an equal-channel echelon die. After the workpiece completely leaves the die channels, it is bitten by the second pair of rolls, which completely pull the workpiece out of the die also by contact friction forces. Thus, in this case, pressing the workpieces is provided by the friction contact forces that arise on the surface of the metal-to-rotating rollers contact. Previously, various studies of this combined process have been carried out – both theoretical [16-19] and laboratory ones (on a single-roll machine) [20-23].

This paper presents the results of the power analysis performed during the development of a pilot plant with two pairs of rolls (Fig. 1).
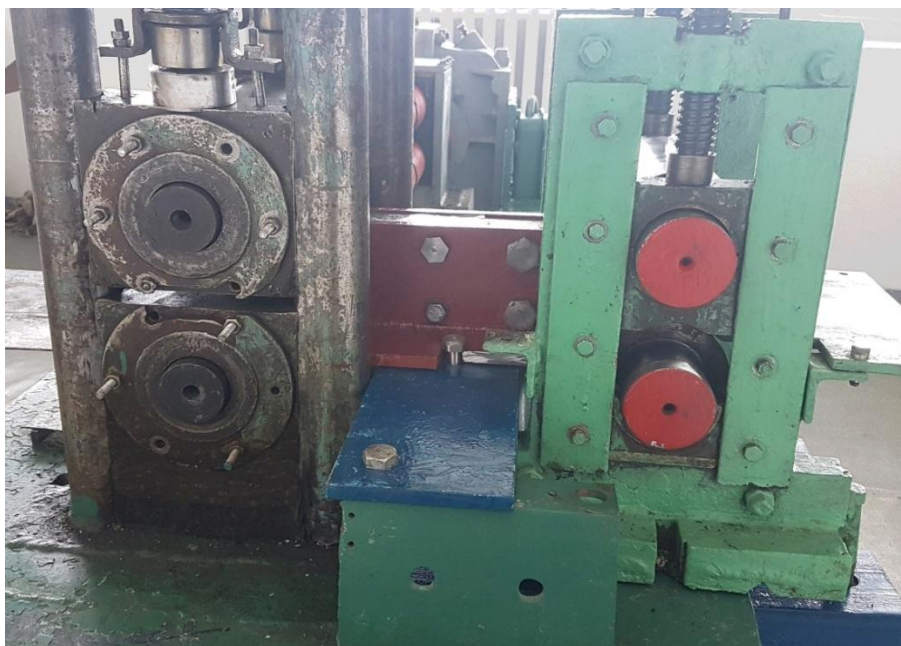
Fig. 1. Pilot plant for "rolling – ECA-pressing" combined process implementation

Strength analysis of the ECA-die. When implementing the combined process of the "rolling – ECA-pressing", a pilot plant created on the basis of the laboratory rolling mills DUO-200 and DUO-250 was used. Their power characteristics enable to cold-form aluminum and copper alloys.

When designing a new technology of deformation at the pilot stage, strength analysis is essential. It enables to determine the tool durability and rigidity, and to estimate its strength margin which will give information on its service life. Theoretical studies of the "rolling – ECA-pressing" combined process were performed using computer simulation in the DEFORM program. As a result, it was established [17, 18] that the most loaded part is the pressing die. This is explained by the fact that the most rigid straining conditions occur in the joint mouth zone. Thuswise, a strength analysis was carried out to test the selected die design validity. For this purpose, a model of a joint die mouth with 150 degree angle represented in [20], was constructed.

When implementing the combined process, it is appropriate to select the workpiece width in such a way that under forming in the die, the metal does not contact with its sidewalls. This will significantly reduce the die total back force. However, one cannot completely exclude such a case. Thus, an ECA-pressing model, in which the workpiece height and width correspond to the height and width of the die mouth, was created in the DEFORM software. This case of deformation is limiting and is almost impracticable. Therefore, if the die is hard enough, it will be suited for a combined process, the conditions of which are much "softer". In particular, the workpiece height and width is somewhat less than the height and width of the die mouth, which is a necessary condition for the metal passage through the mouth.

The initial blank dimensions are $10 \times 40 \times 90$ mm. The conditions and assumptions used in modeling:

- initial material is isotropic, it does not have any stress or strain;
- workpiece is divided into 24,000 finite elements, average length of the element edge is 1.5 mm;
- initial temperature of the workpiece is 700 °C, besides, strain warming-up, and heat transfer from workpiece to tool and into the environment are considered;
- instrument is taken as an absolutely rigid body;
- dummy blank is taken as elastoplastic;
- workpiece material is AISI 1045, corresponding to steel 45;
- friction factor at the workpiece-die contact is 0.1;
- punch speed is 10 mm / sec.

As a result of the calculation, the deformation force on all die elements was determined to find the most strained structural members. The greatest forces occur in the direction of the normal stresses action (Fig. 2).

Machine building and machine science
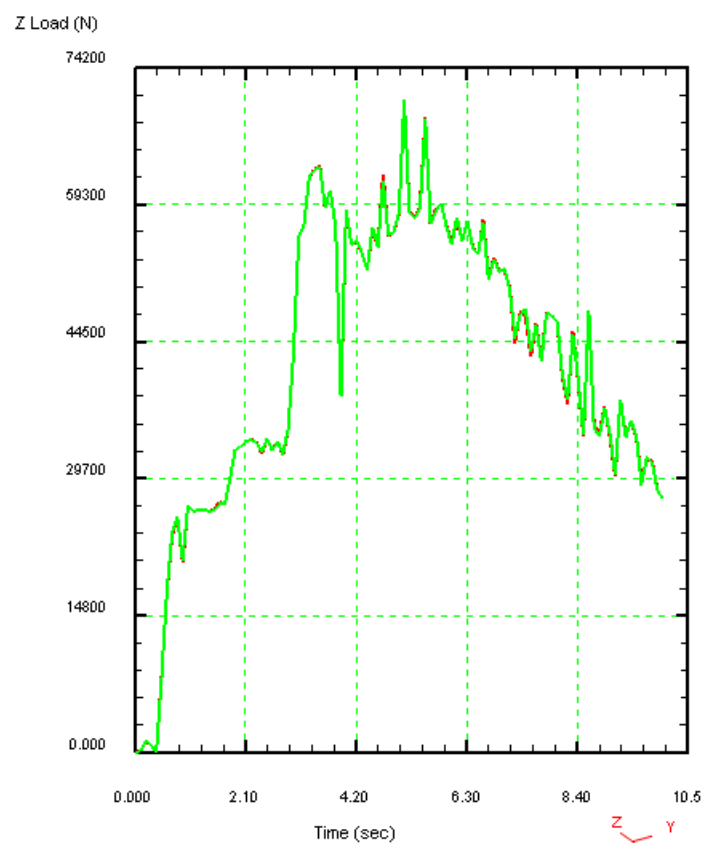
a)
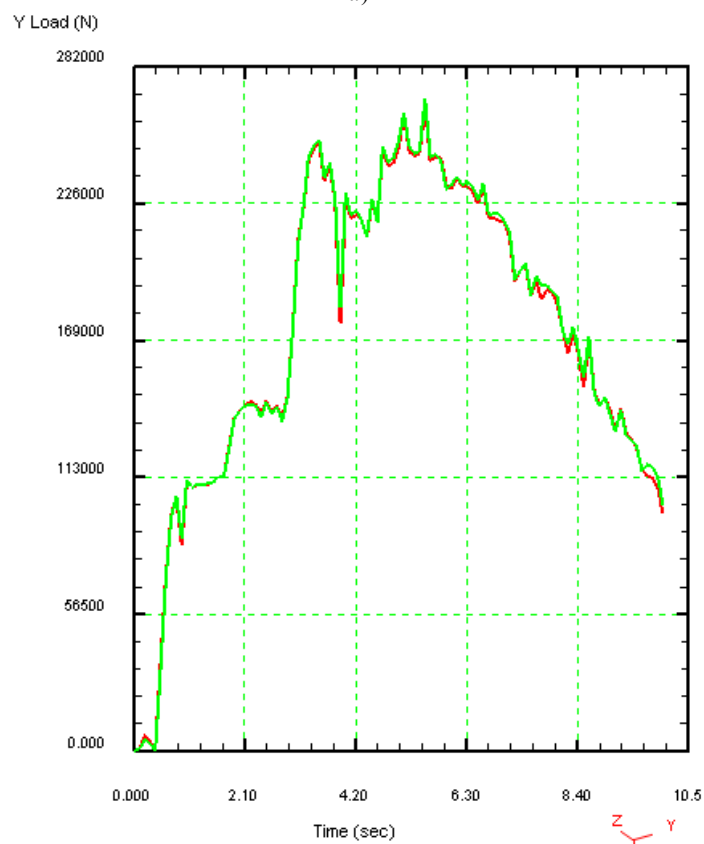
b)

Fig. 2. ECA-pressing force curves for sidewalls (*a*) and central segments (*b*)

Fig. 2 shows that the most strained die elements are the central segments. At deformation, the force up to 260 kN occurs on them, while it does not exceed 75 kN on the sidewalls. Based on these data, the stress analysis of the tool

was carried out in the DEFORM program using a dedicated module. This analysis approach implies that absolutely rigid model elements become elastic bodies taking stress. Interpolation of operating forces on the tool is carried out from the workpiece. Then, fixation points are defined so that the elastic bodies do not scatter under the action of forces. In our case, the fixation points are ring openings for holding elements. In addition, in this calculation, it is required to specify the tool material. 5ХВ2С instrument steel was used to make the die. It is used for manufacturing:
- complex dies operating with high impact loads,
- knives for cold metal cutting,
- thread-rolling dies,
- punches and swaging dies for cold operation.

As a result, the following data were obtained (Fig. 3).

a)

b)

c)
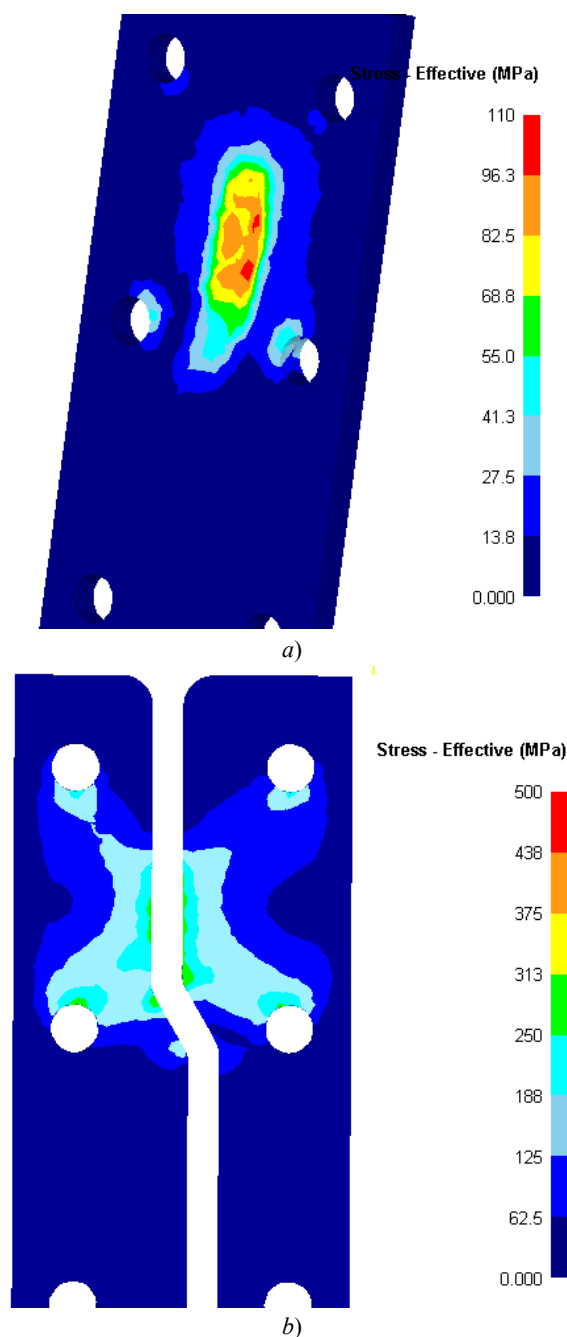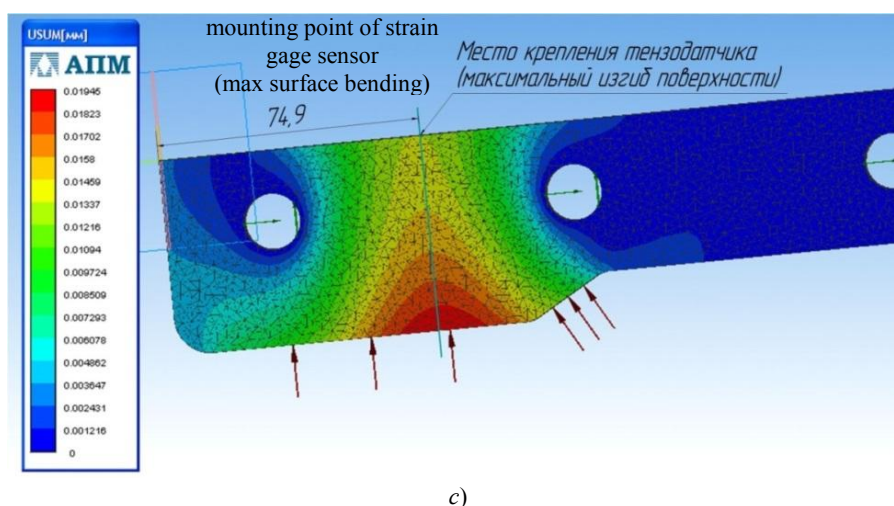
Fig. 3. Strength analysis results: stress on sidewalls (*a*); tension in central segments (*b*); linear displacement (*c*)

Fig. 3 shows that the most loaded zones in the central segments are surface areas near the die mouth joints and arc zones around the first two pairs of openings. Here, voltage up to 250 MPa occurs.

In the areas between openings, the voltage is within 125 ÷ 150 MPa (see Fig. 3, *a*).

On the sidewalls, peak voltage occurs in the contact zone with the deformable metal, and it is equal to 95 ÷ 100 MPa (see Fig. 3, *b*).

The results of calculating the linear displacements of structural elements under the action of elastic deformation were considered [24] in the specialized calculation APM library to study the structure rigidity. The investigation of elastic deformation shows its greatest value in the surface region near the die mouth joints. Two facts should be mentioned. The first: operating stresses on all die elements are much lower than the 5XB2C steel yield limit. The second: peak value of linear displacement reaches 0.019 mm (Fig. 3, c), which is negligible and allows us to speak about the increased rigidity of the proposed structure. In light of this, we can conclude that this matrix design is suitable for creating a pilot plant of the "rolling – ECA-pressing" combined process, since the estimated safety margin is sufficient for ECA-pressing implementation under extreme conditions.

Laboratory experiments to study forcing. As a result of the strength analysis, the location of the strain gage sensors in the matrix was determined for measuring the deformation force. The mounting spots are at a distance of 75 mm from the leading edge of the central segment where peak linear displacements occur.

The following equipment was used to measure the emerging deformation forces:

- ZET-017-T8 strain-gauge station ("ETSM" CJSC, Russia);

- force sensors with TKFO1-2-200 strain gages ("ETSM" CJSC, Russia);

- laptop computer to control the strain gage and to record the signal.

The strain-gauge station manufactured by "ETSM" CJSC (Moscow) is designed to measure power and other parameters on several channels with a time resolution of writeenable up to 20 kHz [25].

On investigating the power parameters of the "rolling – ECA-pressing" combined process, it is planned to study the deformation forces at the stages of rolling and molding in dies. This calls for installation of strain gauges on the die and on the measuring cells of the roll mill. The principle of tensometry is that during the deformation process, the rolling and pressing forces affect the rolls and the die. As a result, the rolls and the die are bent. Strain gages attached to the die and measuring cells are deformed along with them. Their electrical resistance value changes. The strain-gauge station records this variation and, according with the results of the predetermined calibration of the sensors, converts it automatically into the force pattern.

For the predetermined calibration of the strain gages, the die central segment and measuring cell were tested by compression on the MI-40KU hydraulic torsion-tensile machine. Usage of a torsion-stretching machine enables to develop considerable forces (35-40 kN). Herewith, their values are fixed accurately and reliably. The change in the onloading stress-strain state causes deformation and a linear resistance variation of the strain gages. The principle of cali-

bration is in the construction of the circuit electrical voltage – applied force relationship. This dependence always has a strictly linear character.

To perform the calibration, the elements under study were sequentially loaded in increments of 5 kN in the zero – 35 kN range. The corresponding values of the circuit voltage on-load and after unloading were fixed. In order to increase the accuracy, three passes were performed over the specified range – up-down-up (42 measurements). As a result, for each element, the "force – displacement" relationship was obtained ("displacement" corresponds to the value of the upper striker travel). The calibration test data were statistically processed, and the linear regression equations that connect the force applied to the tool (P_i, H) and the voltage (U_i, mV) in the circuit were obtained from them.

The equation for measuring the rolling force is as follows:

$$P_i = -4852{,}7U_i + 23538.$$

The coefficient of determination $R^2 = 0.998$. The standard measurement error based on the results of 42 tests was less than 0.2%.

The equation for measuring the pressing force is as follows:

$$P_i = -4120{,}2U_i + 21609.$$

The determination factor $R^2 = 0{,}997$. The standard measurement error based on the results of 42 tests was less than 0.3%.

The data obtained were entered on the program of registration and processing of measurements of the ZET-017-T8 strain-gauge station. This enabled to record the signal as a schedule of effort.

After the calibration operations, the die with the strain gage was placed on the pilot plant (Fig. 4).

Fig. 4. Force measurement under "rolling – ECA-pressing" combined process"

Here, on the measuring cells of the first stand, strain gages were also installed to measure the rolling force which was performed only on the first stand. This is a key parameter according to the process concept. When implementing the combined process, the rolling force should exceed the resulting pressing force.

The basic material used was 6063aluminum alloy (analog of AD31aluminum deformable alloy) at room temperature. Its chemistry and mechanical behavior are given in Table 1.

Table 1

Chemistry and mechanical characteristics of 6063aluminum alloy

Weight content of elements, %								
Si	Fe	Cu	Mn	Mg	Cr	Zn	Ti	Other
0.2–0.6	0.35	0.1	0.1	0.45–0.9	0.1	0.1	0.1	0.15
Mechanical properties at 20 °C								
Tensile stress, MPa		Yield stress, MPa			Hardness, HB		Stretching, %	
90		48			25		20	

Blanks of equal size (15 × 25 × 450 mm) were rolled with the thickness of 9 mm in the first stand. In the second stand, the roller gap was 7 mm. The blank length was selected so that its lead end was bit by the second pair of rolls, whereas the back end was being still rolled in the first stand (Fig. 5).

a)

b)

Fig. 5. Force variation under deformation of 6063aluminum alloy: rolling in the first stand (*a*); pressing in the die (*b*)

The force measurement data are presented in Table 2.

Table 2

Force measurement results

	1st stage	2nd stage	3rd stage
Rolling step, kN	205	217	242
Pressing step, kN	59	104	172
Difference (friction margin), %	247	108	40

The difference between the values of the rolling and pressing forces was also determined. In this case, this difference characterizes the level of active friction force margin:

$$\Delta = (\frac{P_{ПРОК}}{P_{ПРЕСС}} - 1) \cdot 100\% ,$$

where $P_{ПРОК}$ is rolling force in the first stand; $P_{ПРЕСС}$ is back force in the die.

A comparative analysis of the values of the arising forces has shown that the rolling forces at all three stages exceed the values of the corresponding pressing forces. Thus, the necessary condition for implementing the combined process is satisfied. Herewith, the active friction forces margin in the first stand with the advancing of the blank along the die mouths reduces dramatically.

Conclusions. The study results indicate that the die strength margin is quite sufficient for the ECA-pressing implementation under the limiting conditions. It should also be mentioned that the rolling forces at all stages of deformation exceed the pressing forces, and thus, the necessary condition for implementing the combined process is satisfied. At this, the active friction forces margin in the first stand with the advancing of the blank along the die mouths reduces dramatically.

The results obtained can be used for designing the experimental facilities that implement the combined process of interest. The stain-gauge analysis of strength characteristics is also suitable for the calibrated rolls.

References

1. Jahedi, M., Knezevic, M., Paydar, M.-H. High-Pressure Double Torsion as a Severe Plastic Deformation Process: Experimental Procedure and Finite Element Modeling. Journal of Materials Engineering and Performance, 2015, vol. 24, iss. 4, pp. 1471–1482.

2. Straska, J., et al. Evolution of microstructure and hardness in AZ31 alloy processed by high pressure torsion. Materials Science and Engineering: A, 2015, vol. 625, pp. 98–106.

3. Alhamidi, A., Horita, Z. Grain refinement and high strain rate superplasticity in aluminium 2024 alloy processed by high-pressure torsion. Materials Science and Engineering: A, 2015, vol. 622, pp. 139–145.

4. Valiev, R.-Z., Langdon, T.-G. Principles of equal-channel angular pressing as a processing tool for grain refinement. Progress in Materials Science, 2006, vol. 51, pp. 881–981.

5. Shaeri, M.-H., et al. Microstructure and mechanical properties of Al-7075 alloy processed by equal channel angular pressing combined with aging treatment. Materials & Design, 2014, vol. 57, pp. 250–257.

6. Zhang, X., et al. Effect of route on tensile anisotropy in equal channel angular pressing. Materials Science and Engineering: A, 2016, vol. 676, pp. 65–72.

7. Wei, W., et al. Microstructure and tensile properties of Cu-Al alloys processed by ECAP and rolling at cryogenic temperature. Journal of Alloys and Compounds, 2016, vol. 678, pp. 506–510.

8. Mostaed, E., et al. Microstructural, texture, plastic anisotropy and superplasticity development of ZK60 alloy during equal channel angular extrusion processing. Metallurgia Italiana, 2015, iss. 11–12, pp. 5–12.

9. Kalahroudi, F.-J., et al. Inhomogeneity in strain, microstructure and mechanical properties of AA1050 alloy during twist extrusion. Materials Science and Engineering: A, 2016, vol. 667, pp. 349–357.

10. Kim, J.-G., et al. Finite element analysis of the plastic deformation in tandem process of simple shear extrusion and twist extrusion. Materials & Design, 2015, vol. 83, pp. 858–865.

11. Bar Bahadori, S.-R., Dehghani, K., Mousavi, S.-A.-A.-A. Comparison of microstructure and mechanical properties of pure copper processed by twist extrusion and equal channel angular Pressing. Materials Letters, 2015, vol. 152, pp. 48–52.

12. Latypov, M.I., et al. Modeling and Characterization of Texture Evolution in Twist Extrusion. Metallurgical and Materials Transactions: A, 2016vol. 47A, iss. 3, pp. 1248–1260.

13. Raab, I., et al. Ustroystvo dlya obrabotki metallov davleniem: patent 2181314 Ros. Federatsiya: 7 B21D25/02. [Device for metal forming.] Ufa State Aviation Technical University. RF patent, no. 2181314, 2002 (in Russian).

Machine building and machine science

14. Naizabekov, A.B., Lezhnev, S.N., Volokitina, I.E. Change in Copper Microstructure and Mechanical Properties with Deformation in an Equal Channel Stepped Die. Metal Science and Heat Treatment, 2015, vol. 57, iss. 5–6, pp. 254–260.

15. Naizabekov, A.B., Lezhnev, S.N., Panin, E.A. Ustroystvo dlya nepreryvnogo pressovaniya metalla: patent 25863 Respublika Kazakhstan: B21J 5/00. [Device for continuous metal pressing.] Patent of Republic of Kazakhstan, no. 25863, 2012 (in Russian).

16. Naizabekov, A., et al. Theoretical grounds of the combined "rolling — equal - channel step pressing" process. Journal of Chemical Technology and Metallurgy, 2016, vol. 51, iss. 5, pp. 594–602.

17. Naizabekov, A.B., Lezhnev, S.N., Panin, E.A. Modelirovanie sovmeshchennogo protsessa «prokatka — pressovanie» s ispol'zovaniem ravnokanal'noy stupenchatoy matritsy. [Simulation of the combined "rolling-pressing" process using an equal-channel step die.] University's Works, 2008, no. 3, pp. 16–19 (in Russian).

18. Lezhnev, S., Panin, E. Investigation of the Influence of Geometric and Technological Factors on the Stress - Strain State of Metal in the Implementation of the Combined Rolling - Pressing Process. Advanced Materials Research, 2014, vol. 936, pp. 1918–1924.

19. Lezhnev, S., et al. Evaluation of the effectiveness of the use of horizontal and vertical rolls in the "Rolling — pressing" process on the basis of the stress - strain state studying. IOP Conf. Series: Materials Science and Engineering, 2017, vol. 179, no. 012047, 5 p.

20. Naizabekov, A., et al. Study of broadening in a combined process "rolling — pressing" using an equal - channel step die. Journal of Chemical Technology and Metallurgy, 2015, vol. 50, iss. 3, pp. 308–313.

21. Lezhnev, S., Panin, A., Volokitina, I. Research of combined process "Rolling — pressing" influence on the microstructure and mechanical properties of aluminium. Advanced Materials Research, 2013, vol. 814, pp. 68–75.

22. Naizabekov, A., et al. Influence of Combined Process «Rolling — pressing» on Microstructure and Mechanical Properties of Copper. Procedia Engineering, 2014, vol. 81, pp. 1499–1504.

23. Naizabekov, A., et al. The Role of Preliminary Heat Treatment in the Formation of Ultrafine — Grained Structure in the Implementation of the Combined Process "Rolling — Equal Channel Angular Pressing". Materials Science Forum, 2016, vol. 879, pp. 1093–1098.

24. Sistema prochnostnogo analiza APM FEM dlya KOMPAS-3D. [APM FEM for COMPASS-3D Strength analysis system.] APM Research and Software Development Centre, LLC. Available at: http://apm.ru/produkti/programmnie_kompleksi/APM_FEM (accessed: 14.07.18) (in Russian).

25. Tenzometricheskaya stantsiya ZET 017-T8. [ZET 017-T8 Strain-gauge station.] "Electronic technologies and metrological systems" Enterprise (ZETLAB Company). Available at: https://zetlab.com/shop/izmeritelnoe-oborudovanie/tenzostantsii/tenzostanciya-zet-017-t8. (accessed: 14.07.18) (in Russian).

Authors:

Naizabekov, Abdrakhman B.,
rector, Rudny Industrial Institute (38, 50 let Oktyabrya St.,
Rudny, Kostanay region, 111500, Republic of Kazakh-
stan), Dr.Sci. (Eng.), professor,
ORCID: https://orcid.org/0000-0002-8517-3482
naizabekov57@mail.ru

Lezhnev, Sergey N.,
associate professor of the Metallurgical Engineering and Mining Department, Rudny Industrial Institute (38, 50 let Oktyabrya St., Rudny, Kostanay region, 111500, Republic of Kazakhstan), Cand.Sci. (Eng.),
ORCID: https://orcid.org/0000-0002-1737-9825
sergey_legnev@mail.ru

Koinov, Toncho A.,
professor of the Physical Metallurgy and Thermal Generating Units Department, University of Chemical Technology and Metallurgy(8, Kliment Ohridsky Blvd., Sofia, 1756, Bulgaria), Dr.Sci. (Eng.), professor,
ORCID: https://orcid.org/0000-0001-9577-3732
toni309@koinov.com

Panin, Evgeny A.,
senior lecturer of the Metal Forming Department, Karaganda State Industrial University (30, Republic Ave., Temirtau, Karaganda region, 101400, Republic of Kazakhstan),
ORCID: https://orcid.org/0000-0001-6830-0630
cooper802@mail.ru

MACHINE BUILDING AND MACHINE SCIENCE
МАШИНОСТРОЕНИЕ И МАШИНОВЕДЕНИЕ

Effect of sawdust volume on mechanical properties of composite material[*]

A. G. Dyachenko[1], T. P. Savostina[2], B. I. Saed [3][**]
[1, 2] Don State Technical University, Rostov-on-Don, Russian Federation
[3] University of Aleppo, Aleppo, Syrian Arab Republic

Влияние объема древесных опилок на механические свойства композитного материала[***]

А. Г. Дьяченко[1], Т. П. Савостина[2], Б. И. Саед [3][**]
[1, 2] Донской государственный технический университет, г. Ростов-на-Дону, Российская Федерация
[3] Университет Алеппо, г. Алеппо, Сирийская Арабская Республика

Introduction. Generation of composite materials with addition of sawdust is considered. The wood component of the composites is treated with water to enhance the surface roughness. This increases the contact area resulting in intensifying the sawdust – polymer fibers interaction. The work objective is to study the possibility of strengthening composites obtained from sawdust.

Materials and Methods. Samples are made of composite materials based on the unsaturated polyester resins, reinforced with wood chips. Water treatment was carried out at room temperature for 2, 4, 6 and 8 days. Then the samples were tested for bending and compression.

Research Results. As a result of testing the samples, changes in their mechanical properties were recorded. It is determined how the bending and compression resistance depends on the water treatment time. Graphs that reflect these dependences are constructed.

Discussion and Conclusions. After water treatment, the composites reinforced with sawdust show a higher resistance to bending. This is due to the increased roughness of the sawdust surface and, as a consequence, to the extension of the surface area adhesion with the composite base. Besides, the water treatment enhances the specimen resistance under compression. The samples created on the basis of large sawdust come into particular prominence. This is due to the formation of holes on the sawdust surface which also enhances the adhesion between them and the composite polymer base.

Keywords: wood fibers, sawdust, polymer, composite material.

Введение. Рассматриваются вопросы создания композиционных материалов с добавлением древесных опилок. Древесная составляющая композитов обрабатывается водой для усиления шероховатости поверхности. Это увеличивает площадь контакта, вследствие чего усиливается взаимодействие между опилками и волокнами полимера. Цель исследования — изучение возможности упрочнения композиционных материалов, полученных из опилок.

Материалы и методы. Образцы изготовлены из композитных материалов на основе ненасыщенных полиэфирных смол, армированных древесной стружкой. Обработка водой проводилась при комнатной температуре в течение 2, 4, 6 и 8 дней. Затем образцы проходили испытания на изгиб и сжатие.

Результаты исследования. В результате испытаний образцов зафиксированы изменения их механических свойств. Определено, каким образом сопротивления изгибу и прочности при сжатии зависят от времени обработки водой. Построены графики, отражающие указанные зависимости.

Обсуждение и заключения. После обработки водой композиты, армированные древесными опилками, демонстрируют более высокую стойкость при изгибе. Это объясняется усилением шероховатости поверхности опилок и, как следствие, увеличением поверхности сцепления с композитной основой. Кроме того, обработка водой повышает стойкость образцов при сжатии. Особенно заметно упрочняются образцы, созданные на основе крупных опилок. Это объясняется образованием углублений на поверхности древесных опилок, что также усиливает адгезию между ними и полимерной основой композита.

Ключевые слова: древесные волокна, опилки, полимер, композитный материал.

Introduction. Composite materials based on polymers reinforced with various impurities are widely used in modern production practice. Major advantages of wood impurities (sawdust, chips) are their economic cost and availability [1, 2].

To determine ratios of the sawdust wood fibers, a vibrating unit with a nest of sieves was used. In the end, three volumes of sawdust (5 mm^3, 25 mm^3, 120 mm^3) were selected [2, 3, 4]. Through the experiments, the samples were subjected to three types of load (pressure, shear, and bending) to determine the effect of the sawdust volume on the strength characteristics of the composite materials.

In 2001, samples with wood filler were subjected to the tests, the purpose of which was to determine the quality of adhesion between fibers and binder. The results suggest that reinforcement with wood fibers increases the material [3].

In 2002, during the experiments, wood and wood fiber was chemically treated using MAPP (maleated polypropylene). It was found that these samples have higher tensile and flexural strength [5].

In 2006, tests were conducted on the surface treatment of NaOH and CICH2COOH wood. The experiments have shown that such an effect enables to obtain high values of tensile strength [6].

Within the framework of this study, it is planned to demonstrate the practicability of the chemical treatment to improve the properties of the composite materials.

Materials and Methods. Wood sawdust (5 mm^3, 25 mm^3, 120 mm^3) [1] was treated by water at room temperature for 2, 4, 6 and 8 days.

100 g of sawdust was placed in a plastic container covered with 1 liter of water and left for 2, 4, 6 and 8 days. Then the water was drained, and the mass was covered with distilled water for an hour. After that, the sawdust was removed and dried in the oven for 24 hours at $110\degree$ C. Further on, all tests were also conducted at room temperature.

Research Results.

Metering of weight loss of processed sawdust

10 g of sawdust of different volumes (5 mm^3, 25 mm^3, 120 mm^3) treated by the method described above were used. After processing, the samples were examined under an optical microscope.

In this case, the weight loss of sawdust is equal to the weight difference before and after processing. The weight loss ratio is calculated as follows:

$$\frac{W_0 - W_1}{W_1} = W\%,$$

where W_0 is the weight of the fiber sample before processing (g); W_1 is the weight of the fiber sample after treatment (g); $W\%$ is percentage of the weight loss (Fig. 1).
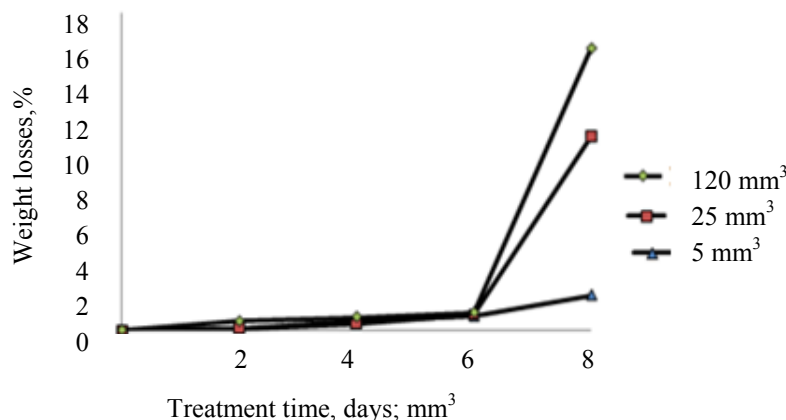
Fig. 1. Dependence of sawdust weight loss on time of treatment by water

The graph shows that 120 mm^3 sawdust does not lose much more weight than 25 mm^3 sawdust (the difference is about 4%). If we compare sawdust of 5 mm^3 and of 120 mm^3, the weight loss of the latter is 8 times higher. At this, in all samples, weight loss depends directly on the treatment time (the longer the test, the less weight). On exposure to water for long, some solubles go into the liquid, so, after washing and drying, the material weighs less.

In the succeeding experiments, three composite samples were considered. For that, sawdust of various volumes (5 mm^3, 25 mm^3, 120 mm^3) was impregnated with 10% polyurethane ether and mixed well. Then, a hardener was added, and the mixture was poured into dies. Polyester was 90% of the total mass of the sample.

<u>Bending test of composites</u>

For the tests, samples of the composite material of 8 × 15 × 160 mm according to ASTM D 790 [7, 8] were prepared.

Resistance to bending was measured at three points. Fig. 2 shows samples of the composite material reinforced with sawdust before the bending test.

Fig. 2. Samples of composite material reinforced with sawdust before bending test

Resistance of the specimen to bending (MPa) is determined by the formula:

$$\sigma_{u_{32}} = \frac{3 \cdot P \cdot L}{2 \cdot B \cdot t^2},$$

where P is load force (H), L is the sample length (mm), B is the sample width (mm), t is the sample height (mm).

<u>Compression test of composites</u>

For the tests, samples of the composite material of Ø12.7 × 25.4 mm were prepared. Resistance was measured under the compressed condition. The load was applied until a rupture occurred.

Samples of the composites reinforced with sawdust and prepared for testing are shown in Fig. 3. Resistance to compression (MPa) is determined by the formula [9]:

$$\sigma_{c_{\pi}} = \frac{P}{F},$$

where P is compression force (H), F is c/s area (mm^2).

Fig. 3. Samples of composites reinforced with sawdust before compression test

Bending test results

Fig. 4 shows that samples made of 5 mm³ sawdust are more resistant to bending.
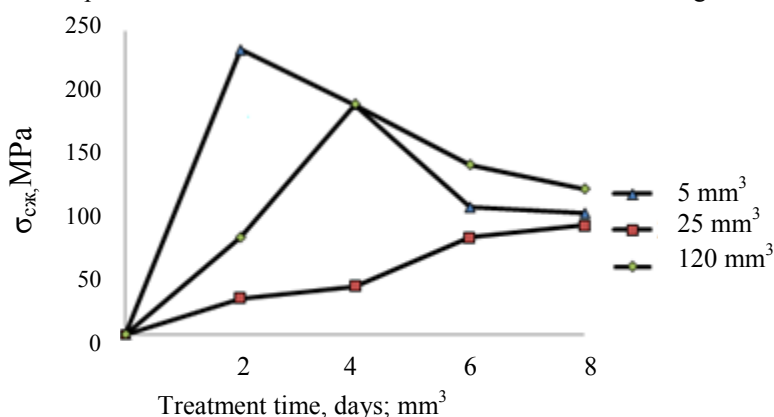
Fig. 4. Change in resistance to bending against specimen treatment time

Maximum bending resistance (230.88 MPa) was shown by the sample with 5 mm³ sawdust after treatment for two days. The sample of 25 mm³ exhibited maximum bending resistance (98.6 MPa) after the eight-day treatment. The sample of 120 mm³ exhibited maximum bending resistance (194.55 MPa) after the four-day treatment.

The increase in bending resistance in this case is explained as follows. Under the treatment with water, the roughness of the sawdust surface increases, and the area of interaction with the base expands. Thus, the adhesion between sawdust and polyester is strengthened and, as a consequence, the strength of the samples increases under bending.

Compression test results

The samples from sawdust of 5 mm³ are weaker in compression (compared to the samples of sawdust of 25 mm³ and 120 mm³) (Fig. 5).
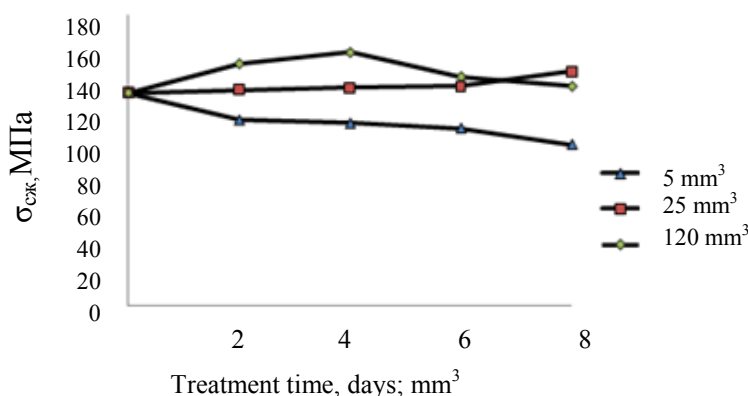
Fig. 5. Change in compression resistance depending on specimen treatment time

The peak value of compression strength (156.67 MPa) is shown by the samples with 120 mm³ sawdust treated within four days. This is due to the fact that under the water treatment, holes appear on the surface of larger wood sawdust. This leads to the increased adhesion between the sawdust and the basic polymer, and enhances the compression resistance of the composite.

Discussion and Conclusions. Testing of the composite samples reinforced with wood sawdust and treated with water allows for the following conclusions.

1. Samples of 120 mm³ sawdust lose more weight than samples of sawdust of 5 mm³ and 25 mm³.

2. Sample weight loss depends directly on the water treatment time.

3. Under treating samples with water, the first sharp increase in bending resistance is observed for two days.

Machine building and machine science

4. Maximum bending resistance (230.88 MPa) was shown by the sample with 5 mm^3 sawdust.

5. Maximum compressive strength (156.67 MPa) was performed by the sample with 120 mm^3 sawdust.

References

1. Antypas, I.-R., Dyachenko, A.G. Vliyanie soderzhaniya drevesnogo dispersnogo napolnitelya na dolgovechnost' kompozitsionnykh materialov. [Effect of wood particulate filler content on durability of composite materials.] Vestnik of DSTU, 2017, vol. 17, no. 1 (88), pp. 67–74 (in Russian). DOI: https://doi.org/10.23947/1992-5980-2017-17-1-67-74

2. Kharmanda, G., Antypas, I.-R. Tegration of reliability and optimization concepts into composite yarns. Sostoyanie i perspektivy razvitiya sel'skokhozyaystvennogo mashinostroeniya: sb. st. 10-y Mezhdunar. yubileynoy nauch.-prakt. konf. v ramkakh 20-y Mezhdunar. agroprom. vystavki «Interagromash-2017» [State and prospects of agricultural machinery development: Proc. 10th Int. Jubilee Sci.-Pract. Conf. within framework of the 20th Int. Agroindustrial Exhibition "Interagromash-2017".] Rostov-on-Don: DSTU Publ. House, 2017, pp. 174–176.

3. Thames, S. F., Zhou, L. Effect of preparation and processing on mechanical properties and water absorption of soy protein-based biocomposites. Proc. of ICCE-5 (Fifth International Conference On Composites Engineering), Las Vegas, USA, 1998, pp. 887-897.

4. Yibin Xue, et al. Mechanical Properties of Wood Fiber Composites under The Influence of Temperature and Humidity. Atlanta: Department of Engineering Clark Atlanta University, 2003, pp. 3906–3911.

5. Starck, N.-M., Rowlands, R.-E. Effects of Wood Fiber Characteristics on Mechanical Properties of Wood / Polypropylene Composites. Wood and fiber science, 2003, vol. 35 (2), pp. 167–174.

6. Dobreva, D., et al. Morphology and Mechanical Properties of Polypropylene — Wood Flour Composites. BioResources, 2006, no. 1 (2), pp. 209–219.

7. Antypas, I.-R., Sirotenko, A.N. Vliyanie formy gofrirovannogo kartona na amortiziruyushchie svoystva upakovki. [Effect of corrugated cardboard shape on the packing damping properties.] Sostoyanie i perspektivy razvitiya sel'skokhozyaystvennogo mashinostroeniya: sb. statey 7-y mezhdunar. nauch.-prakt. konf. v ramkakh 17-y Mezhdunar. agroprom. vystavki «Interagromash-2014» [State and prospects of agricultural machinery development: Proc. 7th Int. Sci.-Pract. Conf. within framework of the 17th Int. Agroindustrial Exhibition "Interagromash-2014".] Rostov-on-Don: DSTU Publ. House, 2014, pp. 200–202 (in Russian).

8. Antypas, I.-R., Dyachenko, A.G. Opredelenie kharakteristik komponentov kompozitnykh materialov, prednaznachennykh dlya proizvodstva detaley sel'skokhozyaystvennoy tekhniki. [Studies on characterization of composite materials components for part production in agricultural industry.] Vestnik of DSTU, 2017, vol. 17, no. 3 (90), pp. 60–69 (in Russian). DOI: https://doi.org/10.23947/1992-5980-2017-17-3-60-69

9. Kharmanda, G., Antypas, I.-R. System reliability based design optimization using optimum safety factor with application to multi failure fatigue analysis. Sostoyanie i perspektivy razvitiya sel'skokhozyaystvennogo mashinostroeniya: sb. st. 10-y Mezhdunar. yubileynoy nauch.- prakt. konf. v ramkakh 20-y Mezhdunar. agroprom. vystavki «Interagromash-2017» [State and prospects of agricultural machinery development: Proc. 10th Int. Jubilee Sci.-Pract. Conf. within framework of the 20th Int. Agroindustrial Exhibition "Interagromash-2017".] Rostov-on-Don: DSTU Publ. House, 2017, pp. 177–179.

Authors:

Dyachenko, Alexey G.,
associate professor of the Machine Design Principles
Department, Don State Technical University
(1, Gagarin sq., Rostov-on-Don, 344000, RF),
Cand.Sci. (Eng.),associate professor,
ORCID: http://orcid.org/0000-0001-9934-4193 ,
alvaic@mail.ru

Savostina, Tatyana P.,
senior teacher of the Machine Design Principles
Department, Don State Technical University
(1, Gagarin sq., Rostov-on-Don, 344000, RF),
ORCID: https://orcid.org/0000-0001-5550-7624
kovtanya@yandex.ru

Saed Bakir Imad,
associate professor of the Agricultural Engineering
Department, University of Aleppo (Faculty of Mechanics,
University of Aleppo, Aleppo, Syrian Arab Republic),
Dr.Sci. (Eng.), associate professor,
ORCID: https://orcid.org/0000-0003-3855-7691
bakir-111@mail.ru

Machine building and machine science

MACHINE BUILDING AND MACHINE SCIENCE
МАШИНОСТРОЕНИЕ И МАШИНОВЕДЕНИЕ

Ultrasonic effect on electric spark forming and development in electroacoustic spraying [*]

S. B. Kudryashev[1], A. A. Zakalyuzhny[2][**]
[1,2] Don State Technical University, Rostov-on-Don, Russian Federation

Влияние ультразвука на процессы формирования и развития электрической искры при электроакустическом напылении[***]

С. Б. Кудряшев[1], А. А. Закалюжный[2] [**]
[1,2] Донской государственный технический университет, г. Ростов-на-Дону, Российская Федерация

Introduction. The electroacoustic application of wear-resistance coatings is studied. The work objective is to obtain a mathematical model of the ultrasonic effect on the formation and development of an electric spark occurring in the process of the electroacoustic sputtering.

Materials and Methods. The effect of ultrasonic vibrations on the processes occurring during the formation and development of a spark discharge is analyzed; the equations of continuity, energy motion and transfer, with the ultrasonic field contribution are considered. Factors affecting the thermal conductivity and electrical conductivity of strongly ionized gas are studied.

Research Results. When obtaining the model, it was assumed that the heat removal from the channel is carried out by a "clear emitter". Then, for the channel region, a self-similar solution is made: pressure, temperature and density are constant over the cross-section, and velocity is proportional to the radius. A mathematical model that describes the processes occurring in the spark channel with the ultrasonic field energy effect is obtained.

Discussion and Conclusions. On the basis of the developed model, it is specified that under the ultrasonic radiation effect, the radius and temperature of the spark channel increase, and conditions of the double ionization under high ultrasonic energy are created.

Введение. Статья посвящена изучению процесса электроакустического нанесения износостойких покрытий. Целью работы является получение математической модели влияния ультразвука на процессы формирования и развития электрической искры, происходящей в процессе электроакустического напыления.

Материалы и методы. В основе анализа влияния ультразвуковых колебаний на процессы, протекающие при формировании и развитии искрового разряда, рассмотрены уравнения непрерывности, движения и переноса энергии с учетом вклада ультразвукового поля. Учтены факторы, влияющие на теплопроводность и электропроводность сильно ионизованного газа.

Результаты исследования. При получении модели были сделаны предположения, что отвод тепла из канала осуществляется «прозрачным излучателем». Тогда для области канала было принято автомодельное решение: давление, температура и плотность постоянны по сечению, а скорость пропорциональна радиусу. Получена математическая модель, описывающая процессы, протекающие в искровом канале с учетом влияния энергии ультразвукового поля.

Обсуждение и заключения. На основании построенной модели установлено, что под действием ультразвука увеличивается радиус и температура искрового канала, а также создаются условия двукратной ионизации при высоких энергиях ультразвука.

Introduction. When applying wear-resistant coatings by electroacoustic spraying, a relatively narrow conductive channel with high temperature and ionization is formed, in which Joule heat is released, which leads to an increase in pressure and expansion of the channel. The expanding channel acts like a piston on the rest of the gas, and, since the expansion occurs at supersonic speed, it causes a shock wave, which propagates in front of this kind of piston. The temperature in the shock wave region is much higher than in the undisturbed gas, and the temperature in the channel itself is many times higher than in the shock wave. Accordingly, the density of the gas in the channel is very small; the vast majority of the mass of the moving gas is displaced from it, which makes it possible to consider the channel boundary as a piston [1].

The very fact of the formation of a narrow channel can be understood as follows: under the ultrasound action, as well as after the gas breakdown and the appearance of conductivity in the places of the current flow, Joule heat is released. The electrical conductivity of the gas is known to increase strongly with temperature. Thus, at a high degree of ionization, when the collision of electrons with ions is significant, the electrical conductivity is proportional to $T^{3/2}$. With small ionization, this dependence is sharper, since with the growth of *T,* the degree of ionization rapidly increases, and, consequently, there is a tendency to the current concentration in a relatively narrow channel. In places where the temperature is higher, the conductivity of the current is greater, so there is more current flowing, and more heat is released. This leads to even more heating and so on [2].

Physical processes determining the width of the channel and the limit of current concentration is heat transfer from the channel and the extension of the heated area under the action of pressure. The channel can be considered to be the area to the point where the temperature and the degree of ionization decreases significantly. In the channel, the inertia of the gas can be neglected, but it is necessary to take into account the release and transfer of heat. In the shock wave region, inertia must be taken into account, but electrical and thermal conductivity can be neglected. These two areas are separated by a transition layer – the "shell" of the channel. Heating and ionization of the gas entering the channel occurs in the shell [3, 4].

Materials and Methods. The main equations are the equations of continuity, motion and energy transfer taking into account the action of the ultrasonic field. They have the form of [5, 6]

$$\frac{\partial \rho}{\partial t} = V \frac{\partial \rho}{\partial r} + \rho \frac{\partial (rV)}{r \partial r} = 0 \tag{1}$$

$$\text{(2)}$$

$$\rho \left(\frac{\partial V}{\partial t} + V \frac{\partial V}{\partial r} \right) + \frac{\partial p}{\partial r} = 0 \tag{3}$$

$$\frac{\partial}{\partial t} \left(\rho \varepsilon + \frac{\rho V^2}{2} \right) + \frac{1}{r} \frac{\partial}{\partial r} \left\{ r\rho V \left(\varepsilon + \frac{p}{\rho} + \frac{V^2}{2} \right) \right\} + \frac{\partial (rq)}{r \partial r} = jE + U$$

where ρ is density, V is velocity, p is pressure, ε is internal energy per unit mass of gas, q is heat flux, j is current density, E is electric field, U is contribution to the ultrasonic field.

The equation of state has the form

$$p = (n_e + n_i) T = \rho T (z+1) / m_a \tag{4}$$

where m_a is the average mass of an atom; n_e, n_i is the number of electrons and ions per unit volume; z is the average charge of an ion; $n_e = z n_i$. Temperature is expressed in energy units.

We assume that the ionization in the channel can be calculated by Saha ionization equation. The internal energy of the gas is

$$\varepsilon = \frac{3}{2} \frac{p}{\rho} + \frac{I}{m_a} = \frac{p}{\rho} \left[\frac{3}{2} + \frac{I}{(z+1)T} \right] \tag{5}$$

where I is the total ionization energy plus the dissociation energy per atom. The formula (5) is convenient to use in the case of full ionization; with incomplete ionization with increasing *T,* the value of *I* also increases. At the same time, as follows from Saha ionization equation, $I/T \approx const$, so for ε, the following formula is more convenient:

$$\varepsilon = \frac{1}{\gamma - 1} \frac{p}{\rho}$$

$$\text{(6)}$$

where γ is the effective adiabatic index; for air $\gamma = 1.22$.

Electrical conductivity σ and thermal conductivity χ of highly ionized gas are equal to

$$\sigma = \sigma_1(T)T^{3/2} = 3\sigma'(z)T^{3/2}\Big/\Big(4e^2\sqrt{2\pi m}\lambda\Big)$$

(7)

$$\chi = \chi_1(z)T^{5/2}$$

Here, *e, m* is the charge and mass of an electron, $\lambda = \ln\Big(3T^{3/2}\Big/\Big(ze^3\sqrt{4\pi n_e}\Big)\Big)$, $\sigma/(z)$ is the dimensionless coefficient. For *z*=1, the value is $\sigma/= 1.95$. The value $\chi\, e^2\big/\sigma T$, under the Wiedemann–Franz law, of the 1st order. For $\lambda=5$ $\sigma1(1)=3,4.1013$sec—$1eV$-3/2,

$\chi_1(1)=3,9.1020$ cm-1 sec-$1eV$-5/2.

Research Results. Let us suppose that the time dependence of the channel radius, the boundary of which plays the role of the piston displacing the gas, has the form of *a(t)=Atk*; the motion in the shock wave region is determined by two dimensional parameters A, ρ.

In the equations (4)–(6), we introduce dimensionless notation (a_c — the radius of the wave front)

$$x = r\big/a_c(t),\ \rho'(x) = \rho\big/\rho_0,\ V'(x) = V\big/a_c,\ p'(x) = p\big/\rho_0 a_c^2$$

(8)

Neglecting heat release and transfer, let us write the system (1)–(3) in the form

$$(V'-x)\frac{dp'}{dx} + \rho'\frac{dxV'}{xdx} = 0$$

$$\left(1-\frac{1}{k}\right)V' + (V'-x)\frac{dV'}{dx} + \frac{1}{\rho'}\frac{dp'}{dx} = 0$$

(9)

$$2\left(1-\frac{1}{k}\right)p' + (V'-x)\frac{dp'}{dx} + \gamma\, p'\frac{dxV'}{xdx} = 0$$

with boundary conditions at *x*=1

$$\rho' = (\gamma+1)\big/(\gamma-1),\ V' = 2\big/(\gamma-1),\ p' = 2(\gamma-1)$$

(10)

The position of the piston is determined by the point where $V'=x$. The pressure on p_k piston can be expressed through the piston speed.

$$p_k = K_p \rho_0 a^2,$$

(11)

where "resistance coefficient" $K_p \approx 0,9$ ($K_p=p'(a)a2/a2_c$) is deduced from the numerical solution of the system (9).

We neglect the radiation and assume that

$$q = -\chi\frac{dT}{dr}$$

(12)

Let the temperature *T* in the channel be much greater than that required for the complete ionization, therefore, on the edge, *T* is much less than in the center. Let us suppose that *T*=0 at *r*=*a*. We introduce dimensionless notations

$$s = \frac{r^2}{a^2(t)},\ \theta(s) = \frac{T}{T_0},\ u = \frac{1}{\theta}\frac{r}{2a}\left(\frac{r}{a}-\frac{V}{a}\right),\ y = \frac{r}{2a}\left\{\frac{q}{pa}+\frac{5}{2}\left(\frac{V}{a}-\frac{r}{a}\right)\right\},$$

(13)

where T_0 is the temperature on the axis. We consider the pressure to be constant along the channel cross-section.

If the heat is removed from the channel by a "clear emitter", a simple self-similar solution can be specified for the channel area: pressure, temperature and density are constant over the cross section, and the speed is proportional to the radius. The temperature drop is concentrated in the shell. In the same place, the radiation is absorbed and the ionization of the gas entering the channel takes place. Considering the shell to be thin, it is possible to obtain a system of equations for the main parameters of the channel. In general, you can use these equations to estimate them as a mathematical model that describes, although roughly, the main processes in the channel. This takes into account the approximate action of ultrasound and thermal conductivity [7].

The energy balance equations for the channel and the shell have the form

$$\frac{dW}{dt} = p\frac{d\pi a^2}{dt} = Q_j + Q_U,$$

(14)

$$\left(\varepsilon+\frac{p}{\rho}\right)\frac{dM}{dt} = Q_t + Q_R,$$

(15)

where *M, W* is the mass and energy of the gas in the channel. The equation (15) is obtained by integrating (3) over the cross section of the channel (including the shell) without assuming the form of distribution of values over the cross section. For a homogeneous model, let us suppose

$$W = M \cdot \varepsilon, \ M = \pi \cdot a^2 \rho .$$

The equations (14), (15) are the consequence of the law of energy conservation. The expressions for the release of heat Q_j due to the electric field and heat Q_U due to the ultrasonic field, as well as for the heat removal by radiation Q_R and thermal conductivity Q_T, can be taken as

$$Q_j = j^2 / \pi \, a^2 \sigma, \quad Q_U = \eta \omega \tag{16}$$

$$Q_R = \pi \, a^2 Q_R'(p, T), \quad Q_T = 1,3 \cdot 2\pi\chi \, T \tag{17}$$

where ω is the frequency of ultrasonic vibrations, η is the dimensional coefficient.

Comparing (14) and (15), we obtain that

$$Q_T + Q_R = \mu \left(Q_j + Q_U \right) , \tag{18}$$

where μ is a coefficient of the 1st order. If T is independent of t, then

$$\mu = \gamma \left[1 + (\gamma - 1) 2a^2 \left(\frac{d^2 a^2}{dt^2} \right)^{-1} \right]^{-1} \tag{19}$$

Let us consider the channel in air with the conductivity of $\sigma = 2 \cdot 10^{14} \mathrm{sec}^{-1}$; $Kp = 0.9$; $\gamma = 1.2$; $j \sim t$; hence $\xi = 4.5$. For the radius of the channel, we get the expression

$$a = 0,93 (1 + \theta)^{1/6} \rho^{-1/6} j^{1/3} t^{1/2} \tag{20}$$

Here, a is measured in mm, j – in kA, t – in μs; $\rho_0 = 1.29 \cdot 10^{-3}$ g / cm^3 under the atmospheric pressure. If the shock wave is weak, the radius is similarly deduced from (19).

Table 1 gives values of the radius calculated by the formula (20), with different values of θ and t (μs) at the discharge voltage $V = 30$ V, and the battery capacity $c = 0.15$ μF, and inductance of circuit $L = 4$ nH (corresponding to $j = V/L = 7.5 \ 10^9$ A/sec).

Table 1

The channel radius for different values of θ, t

T θ	0.3	0.5	1
0	0.65	1.00	1.62
1	0.73	1.12	1.82
2	0.78	1.20	1.95
3	0.82	1.26	2.04

Let us estimate the temperature in the channel. We believe that $\mu \sim 1$, for the same discharge as above at the time $t = 1$ μs at $L = 4$ nH we have that $Q_j + Q_U = (1 + \theta) 1,7 \cdot 10^{13}$ erg / cm sec. If we assume that all heat is transferred by the electronic thermal conductivity, and the radiation is neglected, we obtain that

$T \approx 4(1 + \theta)$eV. Taking T=4eV we find that the number of ions per unit volume in this case is $n_j = 9.10^{17}$, which in order corresponds to the experimental values.

Discussion and Conclusions. Based on the constructed approximate model, the following conclusions can be made about the effect of ultrasound on the development of the spark channel.

1. The radius of the channel increases by $(1+\theta)1/6$ times in comparison with the case when there is no ultrasound, where θ is the ratio of the energies of the electric and ultrasonic fields.

2. The temperature in the channel increases proportionally $(1+\theta)$ under the assumption that the outflow of heat is carried out by the electronic thermal conductivity.

3. Already at the moment of the shock wave formation, almost complete ionization occurs in the channel, and conditions for double ionization at high ultrasound energies can be created.

References

1. Zhdanov, G.S. Fizika tverdogo tela. [Solid-state physics.] Moscow: MSU, 1962, 500 p. (in Russian).
2. Gadalov, V.N., Emel'yanov, S.G., Safonov, S.V., Vornacheva, I.V., Filonovich, A.V. Electroacoustic coating application to improve the performance of composites based on heat-resistant nickel alloys. M: Allerton Press, Inc. Russian Engineering Research, 2017, vol. 37, iss. 9, pp. 751–753.

Machine building and machine science

3. Gurevich, A.G. Fizika tverdogo tela. [Solid-state physics.] St.Petersburg: BKhV-Peterburg, 2004, 320 p. (in Russian).

4. Kushner, V.S., et al. Materialovedenie. [Material science.] Omsk: OmGTU, 2008, 232 p. (in Russian).

5. Kudryashev, S.B. Razrabotka dinamiki prodol'no-krutil'nykh volnovodov primenitel'no k protsessu elektroakusticheskogo napyleniya pri uprochnenii rezhushchego instrumenta: avtoref. dis. … kand. tekhn. nauk. [Development of the dynamics of lengthwise-torsion waveguides by electroacoustic sputtering under hardening of cutting tools: Cand.Sci. (Eng.) diss., author's abstract.] Rostov-on-Don, 1998, 22 p. (in Russian).

6. Lozanskiy, E.D., Firsov, O.B. Teoriya iskry. [Theory of spark.] Moscow: Atomizdat, 1975, 272 p. (in Russian).

7. Maleev, D.N., Minakov, V.S. Elektroakusticheskoe napylenie uprochnyayushchikh pokrytiy. [Electroacoustic spraying of hardening coatings.] Rostov-on-Don: DSTU, 2014, 136 p. (in Russian).

8. Maleev, D.N., Al-Tibbi, W.H., Chilikin, D.A. Optimizatsiya protsessa elektroakusticheskogo napyleniya po kriteriyu mikrotverdosti. [Optimization of the electro-acoustic sputtering process by the microhardness criterion.] Vestnik of DSTU, 2010, vol. 10, no. 3(46), pp. 339–344 (in Russian).

9. Gadalov, V.N., Vornacheva, I.V., Makarova, I.A. Nekotorye svedeniya o sostoyanii sovremennykh uprochnyayushchikh tekhnologiy s aktsentom na elektroiskrovoe legirovanie. [On the state of modern hardening technologies with focus on electric spark alloying.] Auditorium, 2017, no. 4 (16) Available at: https://cyberleninka.ru/article/v/nekotorye-svedeniya-o-sostoyanii-sovremennyh-uprochnyayuschih-tehnologiy-s-aktsentom-na-elektroiskrovoe-legirovanie (accessed: 24.04.2018) (in Russian).

10. Belotskiy, A.V. Ul'trazvukovoe uprochnenie metallov. [Ultrasound hardening of metals.] Kiev: Tekhnika, 1989, 168 p. (in Russian).

Authors:

Kudryashev, Sergey B.,
associate professor of the Production Automation
Department, Don State Technical University (1, Gagarin
sq., Rostov-on-Don, 344000, RF), Cand.Sci. (Eng.),
associate professor,
ORCID: https://orcid.org/0000-0003-4767-470X
skudryshov@donstu.ru

Zakalyuzhny, Alexey A.,
graduate student of the Production Automation
Department, Don State Technical University (1, Gagarin
sq., Rostov-on-Don, 344000, RF),
ORCID: https://orcid.org/0000-0002-1888-3222
zakalizhnuy-95@yandex.ru

MACHINE BUILDING AND MACHINE SCIENCE
МАШИНОСТРОЕНИЕ И МАШИНОВЕДЕНИЕ

Repairing the main shaft of dryer toaster[*]

Y. G. Lyudmirsky[1], S. S Assaulenko[2][**]
[1, 2] Don State Technical University, Rostov-on-Don, Russian Federation

Ремонт главного вала тостера сушилки[***]

Ю. Г. Людмирский[1], С. С. Ассауленко[2][**]
[1, 2] Донской государственный технический университет, г. Ростов-на-Дону, Российская Федерация

Introduction. The sources of damage and wear of the main shaft of the drier toaster are analyzed. The repair know-how and welding operations execution limitations which must be considered when developing the technique providing the restoration of the structure performance features are studied. The work objective is to develop a technique of repair without dismantling for the main toaster shaft. To solve the task, a design repair structure was installed, and postwelding operations that meet the engineering and regulatory requirements for this structure were performed.

Materials and Methods. In "Kompas 3D" software, the following models were developed: integral shaft (project shaft design); damaged shaft as a result of long-term operation (more than 15 years); and damaged shaft with a welded repair structure. Numerical simulation of the stress-strain state (SSS) was carried out.

Research Results. Software for the computational modeling of the repair structure SSS is developed. The repair shaft structure in which the maximum stresses do not exceed the shaft stresses in the project design is obtained using the model. To eliminate the aggressive medium effect on the corrosion fatigue strength of the shaft, an insulating method is used. A technique for mounting the repair structure to the shaft allowing for the outrun limitation 0.12 mm is developed.

Discussion and Conclusions. Torsion shafts damaged deeply by wear and corrosion are considered. To restore their structural integrity, it is worthwhile using the following complex of techniques:

— constructive (consists in the installation of optional parts that compensate for insufficient strength, and provides a reduction in stress concentration in the most loaded zones);

— processing (reduces residual welding stresses due to the reasonable sequence of deformation that contributes to generating favorable residual compressive stresses);

— isolation (is based on the application of anticorrosion coatings).

Введение. Статья посвящена анализу причин повреждений и износа главного вала тостера сушилки. Рассмотрены специфика ремонтного производства и ограничения в выполнении сварочных работ, которые необходимо учитывать при создании технологии, обеспечивающей восстановление эксплуатационных свойств конструкции.

Цель работы — создание технологии ремонта главного вала тостера без его разборки. Для реализации этой задачи была установлена расчетная ремонтная конструкция и выполнены послесварочные операции, обеспечивающие требования технической и нормативной документации к данной конструкции.

Материалы и методы. В программной среде «Компас 3D» разработаны модели: целого вала (конструкция вала в проектном состоянии); вала, поврежденного в результате длительной эксплуатации (более 15 лет); поврежденного вала с приваренной ремонтной конструкцией. Проведено численное моделирование напряженно-деформированного состояния (НДС) моделей.

Результаты исследования. Разработано программное обеспечение для численного моделирования НДС ремонтной конструкции. С помощью модели получена конструкция ремонтного вала, в которой максимальные напряжения не превышают напряжений вала в проектном состоянии. Для исключения влияния агрессивной среды на коррозионную усталостную прочность вала использован изоляционный способ. Для присоединения ремонтной конструкции к валу разработана технология выполнения швов, позволяющая ограничить биение 0,12 мм.

Обсуждение и заключения. Рассмотрены работающие при кручении валы, поврежденные в результате износа и коррозии на большую глубину. Для восстановления их конструктивной прочности целесообразно использовать комплекс перечисленных далее методов. Конструктивный (заключается в установке дополнительных деталей, компенсирующих недостаточную прочность, и обеспечивает уменьшение концентрации напряжений в наиболее нагруженных зонах). Технологический (уменьшает остаточные сварочные напряжения за счет рациональной последовательности деформирования, способствующего наведению благоприятных остаточных напряжений сжатия). Изоли-

The economic expediency of the developed repair technique is obvious. The repairing of the shaft without dismantling costs 180,000 rubles, while a new shaft costs 3.8 million rubles.

рующий (основан на нанесении антикоррозионных покрытий).

Экономическая целесообразность разработанной технологии ремонта несомненна. Ремонт вала без его разборки стоил 180 тысяч рублей, а цена нового вала — 3,8 млн рублей.

Introduction. Failure of machines is often due to the negative impact of structural, technological or operational factors. To choose the type of repair, you need to know:

— operational aspect features ,

— conditions of its operation;

— possible failure causes of the main elements.

The specificity of the repair is that you have to deal with already created structures during work performance. This requires the selection of certain welding methods, the location of repair welds, restricts access to welding sites. In some cases, the possibility of heating the metal during welding and subsequent heat treatment of the welded joint is reduced [1]. All this leads to the need for developing special technical solutions in each case.

Oil extraction plants for the distillation of solvent (gasoline) from the meal (cake) use an evaporator (toaster), equipped with heating jackets and steam supply pipelines. The toaster, shown in Fig. 1, is a column apparatus assembled from vats (1) mounted one above the other.
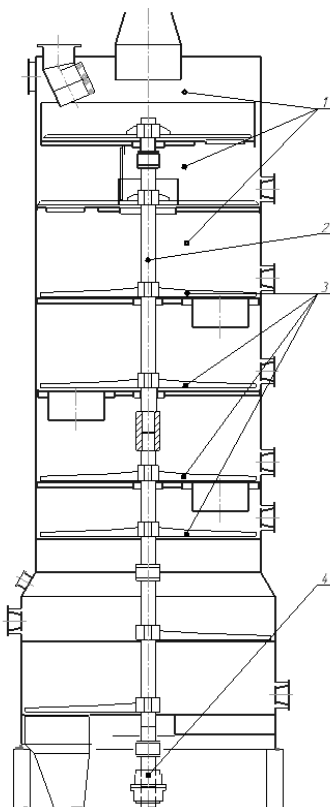
Fig 1. Scheme of dryer toaster

Through all the vats, shaft 2 passes, on which pair agitators of meal 3, installed above the bottoms of the vats with a small gap, are fixed. The shaft drive is provided through the reduction gear 4 of the engine capacity of 160 kW and rotates with a frequency of 10 Rev/min. Torque on the shaft of the toaster is 14500 kg•m.

Dryer toaster, investigated in the framework of this work, was in operation at the oil extraction plant of the "MEZ Yug Rusi" branch for 15 years, which led to significant local wear of the shaft.

The design dimensions of the shaft are as follows: diameter is 285 mm, length is 6860 mm. As the diagnostics had shown, the shaft wear was localized in the lower part, where it was in contact with the meal (acting as an abrasive). The temperature of the meal was 105 ºC. The contact point was blown with moist air. In this part of the shaft at the site of 700 mm, its diameter decreased to 245 mm as a result of corrosion and mechanical wear.

The worn part of the shaft is shown in Fig. 2.
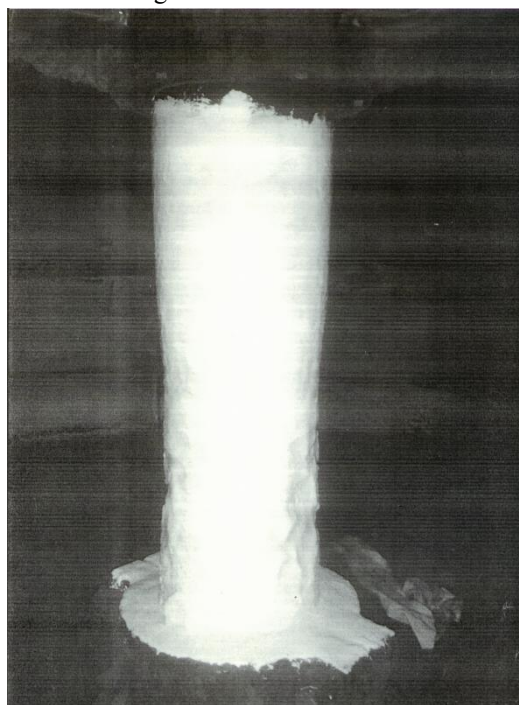
Fig. 2. Shaft wear after 15 years of operation

The calculations performed according to [2] showed that the polar moment of inertia of the shaft in the design was $6.6•10^4$ cm^4, and due to the operation, it decreased to $3.8•10^4$ cm^4. Further operation of the shaft without restoring its bearing capacity could lead to the destruction and explosion of gasoline vapor in the toaster. In this regard, various options for repair of the main shaft of the toaster were evaluated. Replacement was not considered due to the high cost of the individual shaft production. In addition, its dismantling required disassembly of the toaster and the room where it was installed, which was almost impossible.

Currently, the most widely used methods of repairing worn shafts are the following:

— welding metal over the damaged area [3] to restore the size and the carrying capacity of parts;

— replacement of the damaged section of the structure with a new one;

— installation of additional parts or structure repair [4].

The first repair option was rejected, because in this case it was required to weld a large amount of metal (more than 140 kg) on a vertically located shaft, which would inevitably lead to defects and large deformations.

The second method is difficult. In its implementation, there would be difficulties with cutting the damaged part off the shaft, cutting edges for welding, assembly and welding. This would result in unacceptable welding deformations. In this case, even with a successful replacement of the damaged area, the operational properties of the toaster would most probably be violated.

The third method is usually recommended for repair if the surface damage is large [4, 5]. Thus, it was decided to repair the main shaft of the toaster by installing a repair structure (Fig. 3).

Machine building and machine science
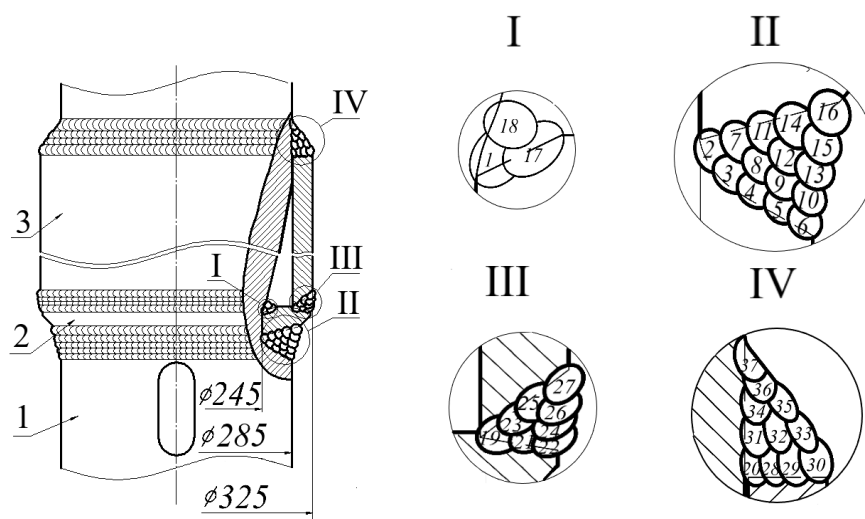
Fig 3. Scheme of repair structure

The design of the shaft 1 consists of two half-rings 2 and two half-couplings 3. The sizes of the coupling and the ring were determined according to strength and technological considerations. The length of the couplings equal to 800 mm, exceeded the length of the damaged section of the shaft by 100 mm. The inner couplings diameter is 285 mm, and the outer one is 325 mm. To restore the static strength of the shaft in its worn parts, it was needed to weld the element, the polar moment of inertia of which would make up for its wear loss ($6.6 \cdot 10^4$ cm^4 – $3.8 \cdot 10^4$ cm^4 = $2.8 \cdot 10^4$ cm^4). Then, the above-mentioned diameters of the polar moment of inertia of a coupling half is equal to $3.1 \cdot 10^4$ cm^4. Thus, the dimensions of the repair structure welded to the shaft not only restore the calculated moment of inertia of the shaft, but also increase it by 15 %, which provides static strength of the shaft.

The papers [6, 7, 8] show that the durability of the welded designs working at repeatedly static loadings in the damp environment, mainly depends on the stress-strain state (SSS) where weld metal comes to the basic metal. The finite element method (FEM) was used to estimate the effect of weld geometry on the SSS. When designing the repair structure, we sought to ensure that the stresses in the weld area did not exceed the stresses in the area of keyways on the shaft to transfer torque to the meal agitators.

The method of SSS calculation is presented in [9]. In the "Compass 3D" software environment, 3D-models of the complete shaft with the original keyway, damaged by the shaft corrosion, and the damaged shaft, were developed with account of the installation of the repair structure. The Ansys software product [10, 11] was used for the calculation. The 3D model was imported in Ansys Workbench. With the help of this software shell, pre-processing of geometry and selection of the material corresponding to the material of the shaft-17G1S was carried out (Table. 1).

Table 1

Parameters of the selected material

Property	Unit of measurement	Value
Density	kg/m^3	7850
Yield stress	mPa	250
Ultimate tensile strength	mPa	460

Further, the calculation was carried out, which includes the creation of a finite element mesh, as well as the determination of boundary conditions by applying torque from the reducer and rigid fastening of the shaft on the reverse side.

Fig. 4 provides the results of the calculated structures, and Table 2 - maximum stresses on the shaft: in the areas of keyways (Fig. 4, a), in the place of shaft wear (Fig. 4, b), in the most loaded area of the repair design (Fig. 4, c).

a)   b)   c)
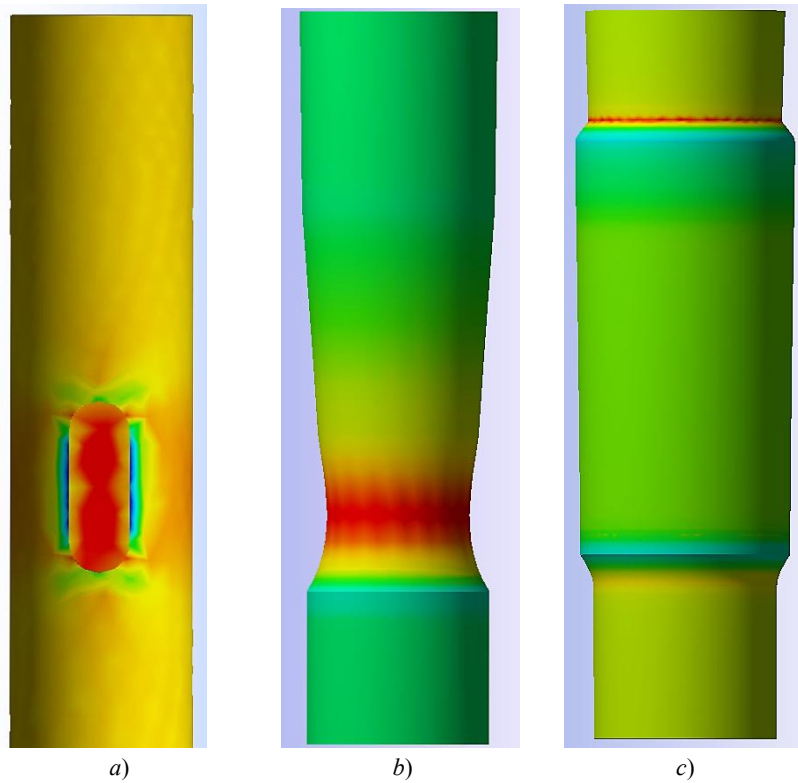
Fig. 4. Models of stress-strain state calculation in areas of: keyways (*a*); shaft corrosion (*b*); repair structure(*c*)

Table 2

Maximum calculated stresses

Area of stress calculation on the shaft	Maximum voltage, mPa
Keyways	74
Shaft corrosion	124
Repair structure	75

It can be seen that the stresses in the developed repair structure do not practically exceed the design stresses in the keyways areas.

SSS depends not only on the operating voltage, but also on the magnitude and the sign of residual stresses in the area of weld metal connection with the main metal. Therefore, the method of plastic deformation was used in the repair technology [12]. It allows you to reduce residual tensile stresses or even change them into favorable compressive stresses.

Before starting, degassing of the toaster and the shop where it was located was performed. The damaged part of the shaft and the welding site were cleaned with rotating brushes to the metallic sheen.

The assembly of the repair structure started with the installation of two half-rings 2 (see Fig. 3), their tightening up and tack welding. To weld the half-rings, the UONI electrodes 13/55 [13] were used in the modes specified in Table 3.

Table 3

Modes of manual arc welding with coated electrodes

Electrode brand	Diameter, mm	Recommended current strength when AWM * A, in the position:		
		bottom	vertical	horizontal and ceiling
UONI 13/45, UONI 13/55	3.0	80–100	60–80	70–90
	4.0	130–160	100–130	120–140
	5.0	170–200	140–160	150–170
* AWM-arc welding mode.				

After that, the welds were cleaned flush with the base metal.

Then the ring was set perpendicular to the shaft, as shown in Fig. 3, and welded; circular welds were welded connecting the ring 2 to the shaft, according to the scheme shown in Fig. 5, a.

a)

b)
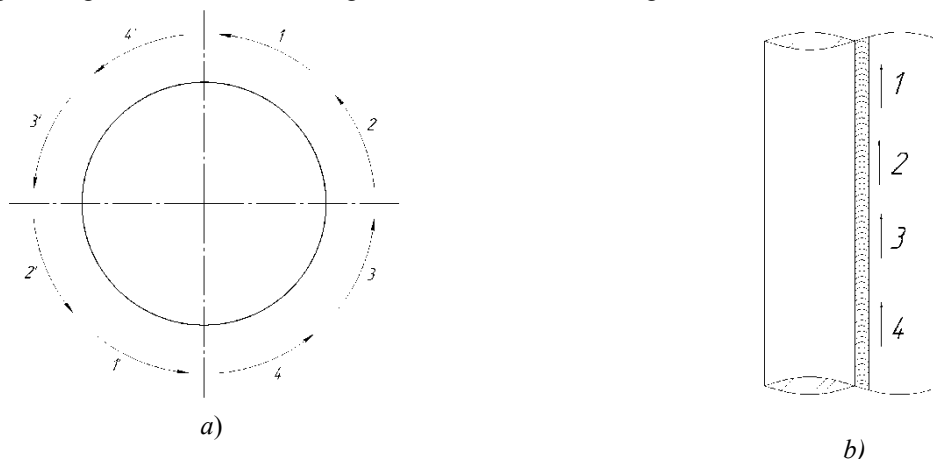
Fig. 5 Diagram of implementation of: circular welds (*a*), longitudinal welds (*b*)

The welding was performed simultaneously by two welders. The order of bead welding (1-18) is shown in Fig. 3.

Two coupling halves were assembled on the welded ring, so that the distance from the longitudinal welds of the ring to the longitudinal welds of the coupling was 120-130 mm. Half couplings were tightened around the shaft by the means of two centralizers; at each junction there were three tack welds with the length of 50-60 mm. To reduce the probability of occurrence of defects during welding, the beginning and the end of each tack weld was rubbed down with an abrasive tool. After this, the upper centralizer was removed, and the welding of longitudinal welds of the coupling started. The welding was performed by the step-back method [14] from the bottom up — in the order shown in Fig. 5, b. After performing 70 % of the length of the longitudinal weld, the lower centralizer was removed, and the root weld was completed. Filler and cap beads were done in the same order. Each subsequent layer was shifted relative to the previous one by 25-30 mm. The current strength recommended in Table 2 for vertical joints welding, was reduced by 10 %.

The circular welds connecting the coupling to the shaft and the ring were made simultaneously by two welders in diametrically opposite places relative to the shaft (see Fig. 5, a). First, the beads 19 to 27 and then, 28 to 37 (see Fig. 3) were welded. After circular welds were welded, their deseaming and plastic deformation at the edges of the weld metal with the base metal of the shaft was made. The quality of the welds was checked by the visual inspection in layers.

The radial-motion variation of the shaft was measured by hour-type indicators above the repair structure by 100 mm in two mutually perpendicular directions. Its value did not exceed 0.12 mm.

In order to protect the coupling and the shaft from corrosion, the space between them was filled with sunflower oil [15], and the outer surface of the shaft was insulated with epoxy glue of the EDP brand according to TS (technical specification) 07510508.90-94.

The integrity of the repaired shaft is monitored quarterly. It has been working reliably for four years with full compliance of functional indicators with the requirements of technical and regulatory documentation.

The economic feasibility of the developed technology is significant. The repair cost 180 thousand rubles, whereas the price of a new shaft is 3.8 million rubles.

Conclusions. To restore the structural strength of the shafts working in torsion, it is advisable to use a set of the following methods. The *constructive* method involves the installation of additional parts that compensates for the lack of strength, and provides a decrease in stress concentration in the most loaded areas. The *technological* method reduces residual welding stresses due to the rational sequence of deformation, which helps to induce favorable residual compression stresses. The *insulating* method is the application of anti-corrosion coatings.

References

1. Lukyanov, V.F., Lyudmirskiy, Yu.G., Dyurgerov, N.G. Remont konstruktsiy i vosstanovlenie detaley svarkoy i naplavkoy. [Repair of structures and restoration of parts by welding and surfacing.] Rostov-on-Don: DSTU Publ. Centre, 2011, 220 p. (in Russian).

2. Nikolayev, G.A., Vinokurov, V.A. Svarnye konstruktsii. Raschet i proektirovanie. [Welded constructions. Calculation and design.] Moscow: Vysshaya shkola, 1990, 446 p. (in Russian).

3. Dyurgerov, N.G., Kolesnikov, V.I. Tekhnologicheskie metody vosstanovleniya i povysheniya iznosostoykosti detaley mashin. Ch. 2. [Processing methods of restoration and increase in wear resistance of machine parts. Part 2.] Rostov-on-Don: RSTU Publ. Centre, 2007, 368 p. (in Russian).

4. VSN 012-88. Stroitel'stvo magistral'nykh i promyslovykh truboprovodov. Kontrol' kachestva i priemka rabot. Chast' I (s Izmeneniem № 1). [Industrial Construction Standards 012-88. Construction of main and field pipelines. Quality control and work acceptance. Part I (with Alteration No. 1).] VNIIST; Minneftegazstroy. Available at: http://docs.cntd.ru/document/1200001425 (accessed: 19.07.2018) (in Russian).

5. Instruktsiya po tekhnologiyam svarki pri stroitel'stve i remonte promyslovykh i magistral'nykh gazoprovodov. Chast' II: STO «Gazprom» 2.22-136 2007: STO 2-2.2-136-2007. [Instruction on welding technologies for construction and repair of field and main gas pipelines. Part II: "Gazprom" Industry Standard (IS) 2.22-136 2007: IS 2-2.2-136-2007.] Scientific & Research Institute of Natural Gases and Gas Technologies. Moscow: VNIIGAZ, 2007, 193 p. (in Russian).

6. Kudryavtsev, I.V., Naumchenkov, N.E. Ustalost' svarnykh konstruktsiy. [Fatigue of welded assemblies.] Moscow: Mashinostroenie, 1976, 270 p. (in Russian).

7. Nikolayev, G.A., Kurkin, S.A., Vinokurov, V.A. Svarnye konstruktsii. Prochnost' svarnykh soedineniy i deformatsii konstruktsiy. [Welded assemblies. Strength of welded joints and structure deformations.]. Moscow: Vysshaya shkola, 1982, 272 p. (in Russian).

8. Trufyakov, V.I., ed. Prochnost' svarnykh soedineniy pri peremennykh nagruzkakh. [Strength of welded joints under variable loads.] Kiev: Naukova dumka, 1990, 256 p. (in Russian).

9. Lukyanov, V.F., Assaulenko, S.S. Analiz prichin razrusheniya opornogo uzla strelovogo krana. [Failure analysis of boom seat metal structures.] Vestnik of DSTU, 2014, vol. 14, no. 4 (79), pp. 186–193 (in Russian).

10. Chigarev, A.V., Kravchuk, A.S., Smalyuk, A.S. ANSYS dlya inzhenerov. [ANSYS for engineers.] St.Petersburg: Piter, 2004, 512 p. (in Russian).

11. Bruyaka, V.A., et al. Inzhenernyy analiz v ANSYS Workbench. [Engineering analysis in ANSYS Workbench .] Samara: Samara State Tech. University Publ. Centre, 2010, 271 p. (in Russian).

12. Sagalevich, V.M. Metody ustraneniya svarochnykh deformatsiy i napryazheniy. [Methods for eliminating welding deformations and stresses.] Moscow: Mashinostroenie, 1974, 248 p. (in Russian).

13. Rekomendatsii po primeneniyu RD 03-615-03 (poryadok primeneniya svarochnykh tekhnologiy pri izgotovlenii, montazhe, remonte i rekonstruktsii). [Recommendations for the application of Guideline Document РД 03-615-03 (procedure for the use of welding technologies in the manufacture, installation, repair and reconstruction).] National Agency of NDT and Welding (NAKS); Federal Service for Ecological, Technological and Atomic Supervision. Moscow: NAKS, 2008, 280 p. (in Russian).

14. Lukyanov, V.F., Kharchenko, V.Ya., Lyudmirskiy, Yu.G. Proizvodstvo svarnykh konstruktsiy (izgotovlenie v zavodskikh usloviyakh). [Manufacture of welded structures (manufacturing in the factory).] Rostov-on-Don: Terra print, 2006, 336 p. (in Russian).

15. Shreier, L.L., ed. Korroziya. [Corrosion.] Moscow: Metallurgiya, 1981, 632 p. (in Russian).

Authors:

Lyudmirskiy, Yury G.,
professor of the Welding Fabrication Machines and
 Automation Department, Don State Technical
University (1, Gagarin Square, Rostov-on-Don, 344000,
RF), Dr.Sci. (Eng.), professor,
ORCID: https://orcid.org/0000-0003-0639-2597
lyudmirskiy40@mail.ru

Assaulenko, Semen S.,
senior lecturer of the Welding Fabrication Machines and
Automation Department, Don State Technical
University (1, Gagarin Square, Rostov-on-Don,
344000, RF),
ORCID: https://orcid.org/0000-0002-3529-1368
Assaulenko_s@mail.ru

Machine building and machine science

317

MACHINE BUILDING AND MACHINE SCIENCE
МАШИНОСТРОЕНИЕ И МАШИНОВЕДЕНИЕ

Technique of functional unification of adaptive hydraulic drive module capable of load stabilization on the working body of mobile machines[*]

V. A. Pershin[1], T. A. Khinikadze[2][**]

[1,2] Institute of Service and Business (DSTU branch), Shakhty, Russian Federation

Методика функциональной унификации адаптивного модуля гидропривода с функцией стабилизации нагрузки на рабочем органе мобильных машин[***]

В. А. Першин[1], Т. А. Хиникадзе[2][**]

[1,2] Институт сферы обслуживания и предпринимательства (филиал) г. Шахты Донского государственного технического университета, Российская Федерация

Introduction. Issues on the functional unification of the adaptive hydraulic drive module are studied. For the first time, self-adapting mechanisms are considered taking into account adaptive intercommunication of the load control and agreement of motions on the working body of the mobile machines. The work objective is to create and analyze the technique of the functional unification of the adaptive hydraulic drive module. In the furtherance of this goal, a number of tasks are solved. The selection of technical equipment – unified adaptive hydraulic drive modules of the mobile machines – is validated. The methodology and indicators of the module functional unification are described. Intercommunications are considered: direct positive and back negative ones. Their effect on the functional unification property of the adaptive module is shown.

Materials and Methods. For the synthesis and analysis of the functional unification indicators of the adaptive module, a similarity method of the technical systems operation is adopted.

Research Results. Techniques for structural-functional unification of the self-adapting modules are developed. Optional versions of the unified modules modification and proper combinations of hydraulic motors, regulating equipment, and mathematical models of adaptive communications are presented. Criteria and indicators of similarity are proposed. The functional unification of the adaptive intercommunications of the module and different types of the hydraulic motors and fluid throttling elements in the hydraulic system are analyzed. Recommendations for implementing the functional unification under typing and operation (adjustment) of the adaptive module are formulated.

Discussion and Conclusions. The methodology is recommended for the functional unification of the hydraulic self-adapting

Введение. Исследованы вопросы функциональной унификации адаптивного модуля гидропривода. Впервые рассмотрены принципы самоадаптации с учетом внутренних адаптивных связей управления нагрузкой и согласованности движений на рабочем органе мобильных машин.

Цель работы — создание и анализ методики функциональной унификации адаптивного модуля гидропривода. Для достижения поставленной цели решен ряд задач. Обоснован выбор технических устройств — унифицируемых адаптивных модулей гидропривода мобильных машин. Предложены методика и показатели функциональной унификации модуля. Рассмотрены внутренние связи: прямая положительная и обратная отрицательная. Показано их влияние на свойство функциональной унификации адаптивного модуля.

Материалы и методы. Для синтеза и анализа показателей функциональной унификации адаптивного модуля принят метод подобия функционирования технических систем.

Результаты исследования. Разработана методика проведения конструктивно-функциональной унификации модулей с самоадаптацией. Показаны возможные варианты модификации унифицируемых модулей и соответствующие им сочетания гидродвигателей, регулирующей аппаратуры и математических моделей адаптивных связей. Предложены критерии и индикаторы подобия. Выполнен анализ функциональной унификации внутренних адаптивных связей модуля с разными типами гидродвигателей и элементов дросселирования жидкости в гидросистеме. Сформулированы рекомендации проведения функциональной унификации при типизации и эксплуатации (наладке) адаптивного модуля.

Обсуждение и заключения. Методика рекомендована для функциональной унификации гидравлического модуля с

---

module. It can be used for the development of unit sizes and under its operation as an independent drive or a hydraulic drive subsystem of a multifunctional or combined machine.

самоадаптацией. Она может использоваться при разработке типоразмеров модуля и в процессе его эксплуатации в качестве автономного привода или подсистемы гидропривода многофункциональной или комбинированной машины.

Introduction. Multifunctional and combined mobile machines are abundantly used under difficult conditions: in road construction and agricultural work. As a rule, their operation involves manual or hard-programmed control. Thus, it is important to create simple functionally unified drives (modules) of mobile machines capable of adapting to the variable properties of the processed environment [1].

It should be noted that the issues of unification are related to the solution of a number of scientific and practical problems. One of them is the problem of standard sizes of functionally unified products. For its solution, the corresponding means of fundamental [2] and applied [3, 4, 5] mathematics is used. Studies on the adaptive systems of different structures and purposes [6], hydraulic drives of devices with adaptively coordinated movements of the working body taking up stochastic fluctuating loads are carried out [7, 8, 9, 10]. In the framework of this paper, the principle of functional unification in the modular hydraulic drive capable of load self-adaptation is considered. The research and practical testing of such a module is conducted for the first time.

Materials and Methods. A device for drilling rocks with variable properties [11] and a device for processing curved surfaces [12] are accepted as the basic objects of research (Fig. 1, 2).
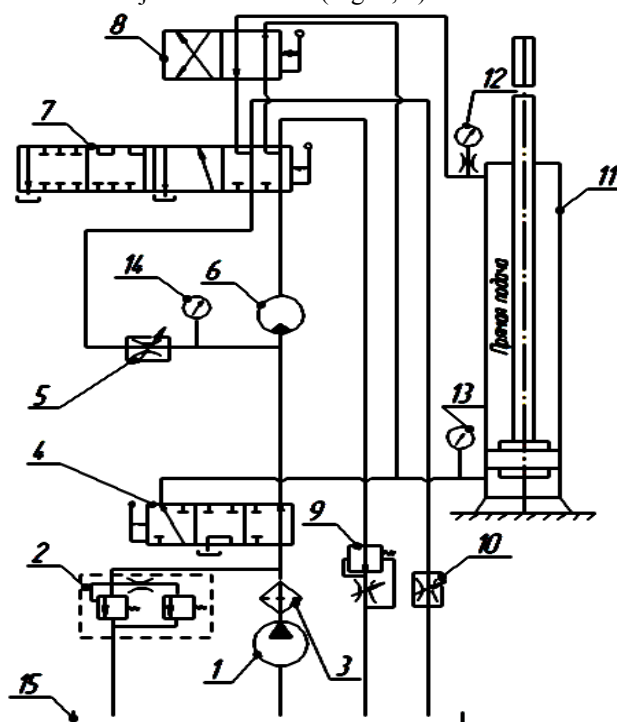
Fig. 1. Schematic diagram of device for drilling rocks with variable properties [3]
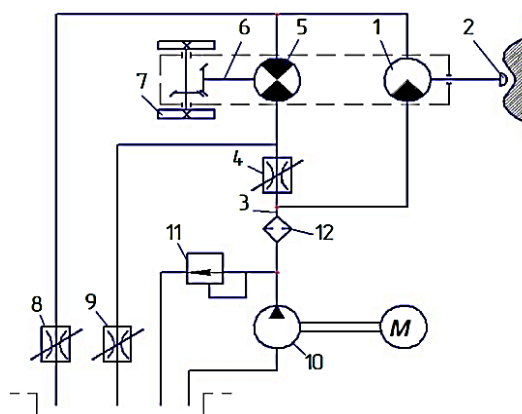
Fig. 2. Schematic diagram of device for processing curved surfaces [2]

The following elements are numbered in the diagrams (for Fig. 2, designations are given in brackets): 1 (10) — fixed displacement hydraulic pump; 2 (11) — safety valve; 3 (12) — filter; 4, 7, 8 — control valves; 5 (4) — choke (mode control); 6 (1) — main motion hydraulic motor; 9 — flow control; 10 — retaining adjustable choke; 11 — feed hydraulic cylinder; 12, 13, 14 — pressure gauges; 15 — tank; (2) — working body; (3) — hydraulic system; (5) — reversible feed motor; (6) — feed motor shaft; (7) — feed mechanism; (8, 9) — adjustable chokes.

The elements of the hydraulic system of these devices (including their modifications [13]) are structurally combined according to the differential scheme.

A hydraulic cylinder (see Fig. 1) or hydraulic motor (see Fig. 2) are additionally included between the return lines of the mode control and the main motion hydraulic motor. Thus, two communications are established: the back negative and the direct positive.

A flow control (see Fig. 1) is on the return line of the hydraulic motor of the main motion of the drilling device under consideration. An adjustable choke (see Fig. 2) is on the return line of the hydraulic motor of the main motion of the device for processing curved surfaces. This is the fundamental difference between these devices.

Such variations of the unified modules allow providing a combination of movements of the working body of the mobile machine: rotation-feed; rotation-rotation; feed-feed [14].

Design differences affect the characteristics of direct positive and back negative communications of the devices, both unified and modular (Table 1, 2).

Table 1

Functional dependences of adaptive communications between the module and the flow control

Types of hydraulic motors	Functions of module adaptive communications	
	Back negative	Direct positive
Hydraulic motor of the main motion — feed hydraulic motor	$\omega_{\text{гп}} = AM_0 - (BM_{\text{сгд}} + CM_{\text{сдп}})$	$\omega_{\text{гп}} = k_1\omega_{\text{гд}}$
Hydraulic motor of the main motion —feed hydraulic cylinder ω	$\omega_{\text{гп}} = AM_0 - (BM_{\text{сгд}} + CM_{\text{сдп}})$	$v_{\text{цп}} = k_2\omega_{\text{гд}}$
Hydraulic cylinder of the main motion — feed hydraulic cylinder	$v_{\text{цп}} = AM_0 - (BM_{\text{сгд}} + CM_{\text{сцп}})$	$v_{\text{цп}} = k_3 v_{\text{цп}}$

Functional dependencies of the adaptive communications of the module with an adjustable throttle

Types of hydraulic motors	Functions of module adaptive communications	
	Back negative	Direct positive
Hydraulic motor of the main motion — feed hydraulic motor	$\omega_{\text{гп}} = AM_0 - (BM_{\text{сгд}} + CM_{\text{сдп}})$	$\omega_{\text{гп}} = k_1\omega_{\text{гд}} - \mu\,\dfrac{f_{\text{др8}}}{f_{\text{цп}}}\sqrt{\dfrac{2\Delta P_{\text{др8}}}{\rho}}$
Hydraulic motor of the main motion —feed hydraulic cylinder	$\omega_{\text{гп}} = AM_0 - (BM_{\text{сгд}} + CF_{\text{сдп}})$	$v_{\text{цп}} = k_2\omega_{\text{гд}} - \mu\,\dfrac{f_{\text{др8}}}{f_{\text{цп}}}\sqrt{\dfrac{2\Delta P_{\text{др8}}}{\rho}}$
Hydraulic cylinder of the main motion — feed hydraulic cylinder	$v_{\text{цп}} = AM_0 - (BF_{\text{сгд}} + CF_{\text{сцп}})$	$v_{\text{цп}} = k_3 v_{\text{цгд}} - \mu\,\dfrac{f_{\text{др8}}}{f_{\text{цп}}}\sqrt{\dfrac{2\Delta P_{\text{др8}}}{\rho}}$

Let us note that the ratio of the velocities of the output elements of hydraulic motors (see Table 2) does not depend on the flow rate through the flow control, since this indicator does not depend on the pressure drop on the device, i.e. $Q_{\text{рп}} = const$.

Adaptive communications play a special role at action of working bodies of machines in modes with the required indicators of speed of performance of operations and stability [14]. The discussed above design and functional features of the devices (presence of an adjustable throttle or flow control) allow implementing such communications.

Tables 1 and 2 provide the legend: $v_{\text{цп}}$ — rod speed; $f_{\text{цп}}$ — cross sectional area of the feed hydraulic cylinder; $\omega_{\text{гд}}$ — angular velocity of the hydraulic motor main movement; A, B, C — constant coefficients depending on the moments of inertia, kinematic parameters and efficiency of the units of the main drive and feed drive module; M_0 — the nominal and the calculated total moment of resistance corresponding to the processing without adaptation; $f_{\text{др8}}$ — area of flow cross-section of the throttle Др$_8$; $M_{\text{сгд}}$, $M_{\text{сдп}}$ — the actual moments of resistance taken up respectively by the main drive shaft and the feed shaft; $F_{\text{сгд}}$, $F_{\text{сцп}}$ — the actual resistance forces, which are taken up respectively by the rod of hydraulic cylinders of main movement and the feed cylinder; $\Delta P_{\text{др8}}$ — the pressure differential on the throttle Др$_8$; ρ — density of the working medium in the hydraulic system (oil); k_1, k_2, k_3 — the coefficients of conversion of design features and dimensions of the speeds of movements.

Back negative communication allows stabilizing the actual total moment (force) of the resistance on the working body in the process of the module work. In this case, we automatically compare:

- the actual moment of resistance with the value set by the mode regulator;
- changes in feed rates and the main motion with the sign, reverse to the error signal.

The following are the relevant equations of back communication on accelerations of the shaft of the feed hydraulic motor.

If there is a flow regulator:

$$\varphi_{\text{гп}} = \frac{1}{k_{\text{сгп}}}\left[-A\,\frac{\pm\frac{d}{dt}\left(B\Delta M_{\text{сгд}}^0 + C\Delta M_{\text{сдп}}^0\right)}{\left(B\Delta M_{\text{сгд}}^0 + C\Delta M_{\text{сдп}}^0\right)^{0,5}}\right]. \tag{1}$$

If there is an adjustable throttle:

$$\varphi_{\text{гп}} = -\frac{1}{k_{\text{сгп}}}\left[\left(A\,\frac{\pm\frac{d}{dt}\left(B\Delta M_{\text{сгд}}^0 + C\Delta M_{\text{сдп}}^0\right)}{\left(B\Delta M_{\text{сгд}}^0 + C\Delta M_{\text{сдп}}^0\right)^{0,5}} + \right.$$
$$\left. +\mu_{\text{др3}}f_{\text{др3}}\frac{d}{dt}\sqrt{\frac{2(\Delta P_{\text{др3}}^0 \pm \delta(\Delta P_{\text{др3}}^0)}{\rho}}\right)\right]. \tag{2}$$

The methodology of functional unification is determined by its goals and features, as well as the stage of the module life cycle. However, we should note the overall steps of its implementation:

- clarification of the functional purpose and conditions of the unified module operation;
- preliminary data collection within the framework of constructive and functional unification of hydraulic devices of standard and unified module (including single-valuedness conditions; nominal and boundary values of operation parameters, especially pressure drops on hydraulic devices under the conditions of dynamic equilibrium of hydraulic system);
- clarification of the adaptive communication type according to the design features of the modules (in accordance with Tables 1 and 2).

In compliance with the mentioned general provisions, the functional unification of adaptive communications is performed in a certain sequence.

- According to the calculation or by the specification, the passport, we specify the values of working (or maximum) loadings on the working body of the mobile machine with the unified module.

- In relation to the standard module, we determine the functional and design values of the parameters of the hydraulic elements of the unified module. Here we use nomograms, graphs or calculations (for example, by the method of similarity of functioning) [15].

Research Results. When performing unification, the principle of superposition of functions is used.

Let us briefly consider an example of the method of functional unification of hydraulic motors of the module.

The output characteristics of the hydraulic motor and the hydraulic cylinder are angular velocity (rotation frequency) and torque on the shaft of the hydraulic motor, linear speed and force on the rod of the hydraulic cylinder. Functional dependencies that define these characteristics have the following form [16]:

a) for the hydraulic motor

$$M_{\textit{гм}} = f_1(P_{\textit{вх}}, q, \beta, J, M_{\textit{тр}}, \Delta P_{\textit{ут}}(Q_{\textit{ут}}, f_{\textit{щ}}, \rho)),$$
$$n_{\textit{гм}} = f_2(Q, q, \upsilon, E, Q_{\textit{ут}}(\Delta P_{\textit{ут}}, f_{\textit{щ}}, \rho));$$

$$(3)$$

b) for the hydraulic cylinder

$$V_{\textit{ш}} = f_1(Q, d_{\textit{ц}}, \delta, \rho, \Delta P_{\textit{ц}}, E, V_{\nu}),$$
$$F_{\textit{ш}} = f_2(\Delta P_{\textit{ц}}, \Delta F_n, m_{\textit{пд}}, F_{\textit{стр}}, \mu, F_{\textit{вт}}, \beta).$$

$$(4)$$

Here $n_{\textit{гм}}$ — shaft speed; q — volume of oil; Q — flow (supply) of oil; E — elastic modulus; μ — dynamic oil viscosity ρ — density of oil; $P_{\textit{вх}}$ — inlet pressure; $\Delta P_{\textit{ут}}$ — differential pressure on leakage element; $Q_{\textit{ут}}$ — leakage value; $f_{\textit{щ}}$ — the area of the slit through which passes a leak; J — moment of inertia; β — oil compression coefficient; ; $F_{\textit{стр}}, F_{\textit{вт}}$ — equivalent force of breakaway and internal friction in the cylinder; r — radius of rotation of the mass; ξ, v — structural coefficients; $M_{\textit{в}}$ — shaft torque; $M_{\textit{тр}}$ — friction torque; $\Delta P_{\textit{ц}}$ — differential pressure on hydraulic cylinder; $F_{\textit{ш}}$ —stress on the rod; ΔFn — the difference between the forces on the piston.

When carrying out constructive and functional unification, special criteria of similarity of unification [17] obtained by the dimensional analysis [15] are used.

For a hydraulic motor, the similarity criteria of unification have the form:

$$\pi_n = \frac{n}{Q} f_{\textit{ц}}^{1,5}; \pi_q = \frac{q}{Q} f_{\textit{ц}}^{1,5}; \pi_E = \frac{E}{\Delta P}; \pi_\beta = \beta P_{\textit{вх}},$$

$$\pi_{M_{\textit{тр}}} = \frac{M_{\textit{тр}} \rho^3}{P_{\textit{вх}} J^3}; \pi_{\Delta P} = \frac{\Delta P}{P_{\textit{вх}}}; _j = \frac{f_{\textit{ц}} \rho^2}{J^2};$$

$$(5)$$

$$\pi_{Qc} = \frac{Qc\mu^{0,33}}{P_{\textit{н}}^{0,33} q}; \ \pi_{pc} = \frac{\rho \, q^{0,67}}{P_{\textit{н}}^{0,33} \mu^{0,67}}.$$

Similarity criteria of unification have certain functional or structural sense, namely: π_n — the criterion of flow kinematic parameters; π_q — the criterion that characterizes the ratio of constructive and consumable (functional) characteristics; π_E — the criterion that characterizes the nominal stiffness of the working fluid; π_μ — the theoretical (indicator) criterion of the shaft torque of the pump; π_β — the criterion of elastic deformation of the working fluid; π_{Mm} — the criterion of friction losses in mates; π_J — the criterion of the loss of inertia hydraulic-mechanical resistance; π_{Q_c} — the criterion of the loss of hydrodynamic resistance of the working fluid; $\pi_{\Delta P_y}$ — the criterion of the loss to overcome the leakage of the working fluid; π_{pc} — the criterion of the loss on the inner (viscous) resistance of the working environment.

Thus, each criterion reflects the essence of one of the properties of the functional unification of the module, and any system of criteria reflects this property generally.

The generalized similarity criteria for unification obtained by combinations of separate criteria are presented in the form of:

$$M_{\textit{г}} = \frac{\pi_{\textit{м}} \pi_{P_{\textit{в}}} \pi_{\textit{ц}}}{\pi_E \pi_r \pi_y \pi_{N_T} \pi_Q \pi_\rho} \frac{Pq^{0,67} rJN_{\textit{тр}} Q\rho}{P_{\textit{в}} \mu Efy}; n_{\textit{г}} = \pi_n \pi_q \pi_\nu \pi_E^{-1} \pi_y \frac{Qf_{p\textit{э}} f_y^2 E\Delta P_y}{q^2 \nu P\rho Q_y}.$$

$$(6)$$

Particular similarity indicators of the functional unification of C_i, are obtained from the equations (5) for the unified model and standard modules [15]. In this case, the respective similarity number π_{yi} and π_{mi} for the standard and the unified modules should be equal:

$$\pi_{yi} = \pi_{mi} = idem. \tag{7}$$

In this example, separate indicators of similarity of functional unification have the following form:

$$1 = \frac{C_n}{C_q} C_{f_\text{ц}}{}^{1,5} \; ; \; 1 = \frac{C_q}{C_q} C_{f_\text{ц}}{}^{1,5}; \; 1 = \frac{C_E}{C_{\Delta P}} \; ; \; 1 = C_\beta C_{P_\text{вх}} \; ; \; 1 = \frac{C_{M_\text{тр}} C_{\rho}{}^{3}}{P_\text{вх} J^{3}}; \tag{8}$$

$$1 = \frac{C_{M_\text{гм}} \rho^{3}}{C_{P_\text{вх}} C_{J}{}^{3}}; \; 1 = \frac{\Delta P}{P_\text{вх}}; \; 1 = \frac{C_Q C_\mu{}^{0,33}}{P_\text{н}{}^{0,33} q}; \; 1 = \frac{C_Q}{C_q{}^{2}} \frac{C_{\Delta P_\text{гм}}}{C_\rho}.$$

As well as similarity criteria of functional unification, separate indicators can be combined into complexes, obtaining the effect of superposition.

The change of scale of parameters C_i of the unified module in indicators (8) in relation to similar parameters of the indicators of the standard module shall correspond to the condition of equality to 1 [15]. For example, for the output characteristic of $\Delta P_{\text{гм}}$ on the indicator

$$1 = \frac{C_Q}{C_q{}^{2}} \frac{C_{\Delta P_\text{гм}}}{C_\rho} \tag{9}$$

you can analyze the functional unification on the pressure drop, the characteristic (working) volume and flow of the hydraulic motor, oil density.

The required standard size of one of the parameters of the unified module is determined by the substitution in (5) and (8) of the known values of the parameters of the standard module hydraulic motor and a priori known (established by technical specifications, etc.) values of the parameters of the unified module.

The features of the procedure of functional unification research depend on the task. When carrying out unification of the module of a new standard size, first, you carry out constructively-functional unification, the choice of standard sizes of elements of the hydraulic system, and then you check their functional compliance to the internal adaptive intercommunications. To solve the first problem, we use particular criteria and indicators of functional unification similarity. To solve the second problem, generalized criteria, indicators, as well as the equations of direct and back adaptive intercommunications are used.

Other objectives of the unification of the adaptive module are: analysis of the causes of violations of functional unification in the process of operation of a single adaptive module, and the study of the effectiveness of functional unification in the modernization of the adaptive module of a hydraulic drive. The method of similarity of functioning of technical systems can also be used [18], [19].

Discussion and Conclusions. The urgency of development and application of the unified hydraulic drive of modular type in mobile machines is proved. This design allows you to adapt the power and kinematic parameters when the working body is exposed to fluctuating loads. The method of carrying out constructive and functional unification of modules with self-adaptation involves the use of mathematical models of adaptive intercommunications. Optional versions of modification of the unified modules with self-adaptation and the corresponding combinations of hydraulic motors, regulating equipment and mathematical models of adaptive intercommunications are shown. An example of the functional unification technique using the method of similarity of technical systems operation is given. The technique is recommended for the study of functional unification in the development of standard sizes and in the operation of the proposed type of module.

References

1. Yanson, R.A. Sistemnaya unifikatsiya samokhodnykh stroitel'nykh mashin. [Systemic unification of self-propelled construction machines.] Moscow: Izd-vo Mos. gos. stroit. un-ta, 2005, 95 p. (in Russian).

2. Latyev, S.M. Konstruirovanie tochnykh (opticheskikh) priborov. [Design of precision (optical) devices.] St. Petersburg: Politekhnika, 2007, 580 p. (in Russian).

3. Unifikatsiya izdeliy. Osnovnye polozheniya: GOST 23945.0-80. [GOST 23945.0-80: Product unification. Basic principles.] Interstate Council for Standardization, Metrology and Certification (ISC). Moscow: Standartinform, 1980. Available at: http://www.internet-law.ru/gosts/gost/14244 (accessed: 02.02.18) (in Russian).

4. Babayan, G.G., Degoyan, A.S., Ovakemyan, I.R. Modul'nyy printsip unifikatsii v postroenii struktury avtomaticheskikh rotorno-konveyernykh liniy. [Modular principle of unification in the construction of the structure of automatic rotor-conveyor lines.] Available at: http://elib.sci.am/2000_2/04/04r.htm (accessed 02.02.18) (in Russian).

5. Yurevich, E.I. Osnovy robototekhniki. [Basics of Robotics.] St. Petersburg: BKhV, 2005, 416 p. (in Russian).

Machine building and machine science

6. Zhmud, V.A. Adaptivnye sistemy avtomaticheskogo upravleniya s edinstvennym osnovnym konturom. [Adaptive systems of automatic control with the only main loop.] Automatics & Software Enginery, 2014, no. 2 (8), pp. 106–122 (in Russian).

7. Ginsbourg, A.A., Pichouk, V.V. Kriterii vybora parametrov ispolnitel'nykh organov gidroprivodov s adaptatsiey k nagruzke. [The criteria of selecting the parameters of hydraulic drive actuators adaptable for the load hydraulic systems of technological equipment.] Vestnik GGTU im. P.O. Sukhogo, 2007, no. 3 (30), pp. 38–44 (in Russian).

8. Nekrashevich, K.Ya. Matematicheskaya model' gidrosistemy, realizovannoy s primeneniem kombinirovannogo printsipa adaptatsii k nagruzke. [Mathematical model of hydraulic system designed with using of combined principle of adaptation to load.] Mechanics of Machines, Mechanisms and Materials, 2014, no. 1 (26), pp. 21– 31 (in Russian).

9. Pershin, V.A., Solovyev, S.G. Povyshenie kachestva protsessa khoningovaniya tsilindrov DVS putem stabilizatsii ego silovykh i adaptatsii kinematicheskikh parametrov. [Improving the quality of the honing process of the internal combustion engine by stabilizing its power parameters and adapting the kinematic factors.] Progressivnye tekhnologii v transportnykh sistemakh: sb. dokl. IX Ros. nauch.-prakt. konf. [Advanced technologies in transport systems: Proc. IX Russian Sci.-Pract. Conf.] Orenburg, 2009, pp. 267–270 (in Russian).

10. Pershin, V.A., Soloviev, S.G., Guguev, I.K. Adaptivnyy modul' gidroprivoda burovoy ustanovki. [Adaptive module hydraulic drive rig.] University News. North-Caucasian region. Technical Sciences Series, 2015, no. 1, pp. 102–106 (in Russian).

11. Pershin, V.A., et al. Sposob bureniya porody s peremennymi svoystvami i ustroystvo dlya ego osushchestvleniya: patent № 2582691 Ros. Federatsiya: E21B 44/00. [Method of drilling rock with variable properties and a device for its implementation.] RF Patent, no. 2582691, 2016 (in Russian).

12. Drovnikov, A.N., Vodyanik, G.M., Pershin, V.A Ustroystvo dlya stabilizatsii tolshchiny snimaemogo sloya pri mekhanicheskoy obrabotke krivolineynykh poverkhnostey: a. s. № 483224 SSSR: 23q 5/06, B24b 5/16. [Device for stabilizing the thickness of the skimmed layer under machining of curved surfaces.] USSR Authorship certificate no. 483224, 1975 (in Russian).

13. Golubets, V.I., et al. Sposob intensifikatsii protsessa rezaniya: a. s. № 929331 SSSR: B 23 B 1/00. [Method of enhancement of the cutting process.] USSR Authorship certificate no. 929331, 1982 (in Russian).

13. Khinikadze, T.A., et al. Issledovanie ustoychivosti adaptivnogo modulya gidroprivoda oborudovaniya dlya mekhanicheskoy obrabotki materialov. [Study of the stability of the adaptive hydraulic drive module of the equipment for machining materials.] Teoreticheskie i prakticheskie aspekty razvitiya sovremennoy nauki: mat-ly XVIII mezhdunar. konf. [Theoretical and practical aspects of the modern science development: Proc. XVIII Int. Conf.] Moscow: TsNIK, 2015, pp. 12–17 (in Russian).

14. Khinikadze, T.A. Issledovanie sootvetstviya kharakteristik adaptivnogo modulya gidroprivoda tekhnologicheskim parametram mashin. [Study of the conformity of the characteristics of the adaptive hydraulic drive module to the technological parameters of machines.] Young Researcher of the Don, 2018, no. 2 (11), pp. 107–112 (in Russian).

15. Pershin, V.A. Metodologiya podobiya funktsionirovaniya tekhnicheskikh sistem. [Methodology of similarity of the technical system operation.] Novocherkassk: UPTs "Nabla" SRSTU (NPI); Shakhty: SRSUES Publ. House, 2004, 227 p. (in Russian).

16. Pershin, V.A., Guguev, I.K., Priskoko, S.S. Modeli formirovaniya i upravleniya tekhnicheskim sostoyaniem gidroprivoda transportnykh mashin. [Models of formation and control of the technical condition of hydraulic drive of transport machines.] Politransportnye sistemy: mat-ly VI Vseros. nauch.-tekhn. konf. [Polytransport systems: Proc. VI All-Russian Sci.-Tech. Conf.] Novosibirsk: STU Publ. House, 2009, 426 p. (in Russian).

17. Khinikadze, T.A., Pershin, V.A. Issledovanie pokazateley funktsional'noy unifikatsii tekhnicheskikh sistem na printsipakh podobiya funktsionirovaniya. [Study of functional unification factors of technical systems on the principles of operation similarity.] Sovremennye problemy nauki, tekhnologiy i innovatsionnoy deyatel'nosti: sb. nauch. tr. mezhdunar. nauch.-prakt. konf. 31 avgusta 2017 goda. [Modern problems of science, technology and innovation:

Proc. Int. Sci.-Pract. Conf., August 31, 2017.] Tkacheva, E.P., ed. Belgorod: APNI, 2017, part I, pp. 112–117 (in Russian).

18. Pershin, V.A. Similarity of Functioning Technical Systems as the Condition Support of Effectiveness in the Process of their Life Cycle. Europäische Fachhochschulle. European Applied Sciences, 2013, no. 12, pp. 87–89.

19. Bulgakow, A., Drownikow, A., Pershin, V. Criteria of Taking Decisions at Machinery in Conditions of the Construction Plant.19th International Symposium on Automation and Robotics in Construction. Washington: U.S. Government printing office, 2002, pp. 103–107.

Authors:
Pershin, Victor A.,
Chief Research Scholar of the Department for Training
Scientific Personnel and of Scientific Research, Institute of
Service and Business (DSTU branch), (147, Shevchenko
St., Shakhty, Rostov Region, RF), Dr,Sci. (Eng.),
professor,
ORCID: https://orcid.org/0000-0002-7313-4371
vpershin2013@gmail.com

Khinikadze, Tengiz A.,
postgraduate student of the Technical Systems of Housing
and Public Utilities and Service Department, Institute of
Service and Business (DSTU branch), (147, Shevchenko
St., Shakhty, Rostov Region, RF),
ORCID: https://orcid.org/0000-0003-1709-9505
khinikadze@mail.ru

Machine building and machine science

INFORMATION TECHNOLOGY, COMPUTER SCIENCE, AND MANAGEMENT
ИНФОРМАТИКА, ВЫЧИСЛИТЕЛЬНАЯ ТЕХНИКА И УПРАВЛЕНИЕ

Forecasting the groundwater level of cement raw materials deposit based on dynamic neighborhood models[*]

I. A. Sedykh[1][**]

[1] Lipetsk State Technical University, Lipetsk, Russian Federation

Прогнозирование уровня подземных вод месторождения цементного сырья на основе динамических окрестностных моделей[***]

И. А. Седых[1][**]

[1] Липецкий государственный технический университет, г. Липецк, Российская Федерация

Introduction. The development of a mathematical model for the groundwater level of a deposit of cement raw materials located in the Zadonian-Yelets aquifer, which is the principal domestic water supply source for the city of Lipetsk, is considered. Therefore, it is necessary to provide ongoing monitoring and to have the possibility to predict the water level under the field development. The work objectives are the identification and study of a dynamic neighborhood model with variable hierarchical neighborhoods of the groundwater level that enables to adequately predict value of the water level in the examined wells.

Materials and Methods. The definition of a dynamic neighborhood model with variable hierarchical neighborhoods is given, differing by time-varying double-level neighborhood communications between the first- and second-level nodes. At each next discrete instant of time, the neighborhood model nodes change their state under the influence of the online parameters and node states included in their neighborhood. As a subcase, we consider a model with line state recalculation functions. Parametric identification of the dynamic neighborhood model consists in finding the system parameters for each second-level node, and is based on the ordinary least squares.

Research Results. A linear dynamic neighborhood model with variable hierarchical neighborhoods for predicting the groundwater level in a cement raw material deposit located in the Zadonian-Yelets aquifer is developed. The software using C++ is developed for the parametric identification and simulation of the functioning of the dynamic neighborhood model under consideration. It enables to determine parameters of the node state recalculation functions for a given structure,

Введение. Статья посвящена разработке математической модели уровня подземных вод месторождения цементного сырья, расположенного в задонско-елецком водоносном горизонте, являющимся основным источником хозяйственно-питьевого водоснабжения города Липецка. Поэтому на стадии разработки месторождения необходимо проводить постоянный мониторинг и иметь возможность прогнозирования уровня подземных вод. Цель работы — идентификация и исследование динамической окрестностной модели с переменными иерархическими окрестностями уровня подземных вод, позволяющей с достаточной точностью прогнозировать значение уровня вод в обследуемых скважинах.

Материалы и методы. Приведено определение динамической окрестностной модели с переменными иерархическими окрестностями, отличающейся изменяющимися во времени двухуровневыми окрестностными связями между узлами первого и второго уровня. В каждый следующий дискретный момент времени узлы окрестностной модели меняют свое состояние под воздействием текущих управлений и состояний узлов, входящих в их окрестности. В качестве частного случая рассмотрена модель с линейными функциями пересчета состояний. Параметрическая идентификация динамической окрестностной модели заключается в нахождении параметров системы для каждого узла второго уровня и основана на методе наименьших квадратов.

Результаты исследования. Разработана линейная динамическая окрестностная модель с переменными иерархическими окрестностями для прогнозирования уровня подземных вод месторождения цементного сырья, расположенного в задонско-елецком водоносном горизонте. Для параметрической идентификации и моделирования функционирования рассматриваемой динамической окрестностной модели разработано программное обеспечение на языке С++, позволяющее для заданной

and also to predict the model behavior in the operation process. A hierarchical structure is given, and a parametric identification of the linear dynamic neighborhood model of the groundwater level is carried out. After the parametric identification on the teaching data selection, the mathematical model is checked on the test sample.

Discussion and Conclusions. The obtained average ratio errors of the identification and forecast suggest the developed model validity and enable to recommend it for predicting the underground water level of a cement raw materials deposit.

структуры находить параметры функций пересчета состояний узлов, а также прогнозировать поведение модели в процессе функционирования. Приведена иерархическая структура и проведена параметрическая идентификация линейной динамической окрестностной модели уровня подземных вод. После выполнения параметрической идентификации на обучающей выборке данных математическая модель проверена на контрольной выборке.

Обсуждение и заключения. Полученные средние относительные ошибки идентификации и прогноза свидетельствуют об адекватности разработанной модели и позволяют рекомендовать ее для прогнозирования уровня подземных вод месторождения цементного сырья.

Introduction. Zadonian-Yelets horizon is the main productive complex of limestone suitable for cement and metallurgical industries [1]. Limestone is light and light gray, with a yellowish tinge, medium-hard, fractured, fine-grained. You can often find hard limestone represented by silicified varieties. Limestone is often porous and cavernous. Clay rocks suitable for cement production lie among the quaternary deposits covering the limestone.

Overburden rocks are represented by a fertile layer of soil, loam, substandard clay, sand and a layer of crushed stone in the upper part of the destroyed limestone.

Hydrogeological conditions of the deposit are simple. Sokolsco-Sitovsky deposit is in in geomorphological terms in the slope part of the valley of the Voronezh River, which determines the hydrogeological situation in the field area [2].

The aquifer is fed by infiltration of atmospheric precipitation and by absorption of flood flow through the valleys of gullies and ravines. Groundwater discharge is in the Voronezh River.

The current position of the groundwater level was studied by monitoring observations in 7 wells evenly located on the field area. The level of groundwater in the low-water period varies from 102.5 m to 109.7 m.

Currently, the Zadonian-Yelets aquifer is the main source of the domestic and drinking water supply of the Lipetsk city. In this regard, the development of limestone can be made only in the water-free part of them with high pillar of at least 2.0 m, which is recommended by the sanitary service of the Lipetsk region.

Water inflow into the developed pit of the deposit occurs only due to atmospheric precipitation. In this regard, at the stage of development of the field, it is necessary to constantly monitor the state of groundwater of the Zadonian-Yelets aquifer and to be able to predict the groundwater level.

Dynamic neighborhood models with variable hierarchical neighborhoods are used in this paper to model the groundwater level of the field under consideration. These models allow modeling complex spatially distributed processes and objects that change their state in time [3-8].

Neighborhood models were first proposed in the late 90-ies of XX century [9]. The basic definitions and algorithms of the theory of neighborhood modeling are given in [9-12]. The concepts of "neighborhood", "neighborhood communications" are considered in [13-14]. They use agents that move around the neighborhood and interact with each other according to certain rules. Today, the theory of neighborhood modeling is being actively developed. There appeared dynamic [6-8], non-deterministic models [11], models with variable neighborhoods [15].

Materials and Methods. In this paper, we use dynamic neighborhood models to predict the state of spatially distributed systems. In them, each node is an independent object, functioning in time and related by neighborhood communications to the other objects of the system. This distinguishes the models under consideration from the widely used today neural networks, which can be used to simulate the operation of each object or node separately. The method of neighborhood modeling is intended for simultaneous joint modeling and prediction of the behavior of all elements of a distributed system.

Information technology, computer science, and management

Next, we consider the dynamic neighborhood models "input-state" with variable hierarchical neighborhoods. They differ in time-varying double-level neighborhood communications between the first- and second-level nodes, and in line state recalculation functions. They enable, in comparison with the known one-level neighborhood models, to perform forecasting with higher accuracy.

The dynamic neighborhood "input-state" model with variable [15] hierarchical neighborhoods can be specified by the set $NS_{IER} = (N, X, V, G, X[0], t)$, where:

1) $N = (A, O_x, O_v, O_{ier})$ is a two-level structure of the neighborhood model; $A = \{a_1, a_2, ..., a_n\}$ is a set of nodes of the first level; O_x and O_v are neighborhoods of communications of nodes by states and by controls, respectively; O_{ier} are hierarchical neighborhood communications between nodes. Each node $a_i \in A$ has its own neighborhood defined by states $O_x[a_i] \subseteq A$ and controls $O_v[a_i] \subseteq A$; $O_x = \overset{n}{\underset{i=1}{\cup}} O_x[a_i]$, $O_v = \overset{n}{\underset{i=1}{\cup}} O_v[a_i]$.

Some nodes of the first level $a_i \in A$ are assigned a set of nodes of the second level $O_{ier}[a_i] = \{a_i^1, ..., a_i^c\}$. All nodes $a_j \in O_x[a_i]$, $a_k \in O_v[a_i]$ have an impact on the second level nodes $a_i^b \in O_{ier}[a_i]$.

At each point in time, only a single active node is defined $b = 1, ..., c$ such that $a_i^b \in O_{ier}[a_i, t]$.

The node a_i^b is active at the time t if it meets the specified activation condition $f_i^b[t] = \text{true}$. For all nodes of the second level a_i^b $O_x[a_i^b] = O_x[a_i]$; $O_v[a_i^b] = O_v[a_i]$.

2) $X \in R^{\overset{n}{\underset{i=1}{\sum} p_i}}$ is a block vector of states of the neighborhood model in real time, each block of which $X[a_i] = X[i] \in R^{p_i}$ is a vector of states in the node a_i of the system $i = 1, ..., n$.

3) $V \in R^{\overset{n}{\underset{i=1}{\sum} m_i}}$ is a block vector of controls in real time, each block of $V[a_i] = V[i] \in R^{m_i}$ is a vector of controls in the node a_i of the system $i = 1, ..., n$.

4) $G : X_{O_x} \times V_{O_v} \to X$ is a vector function of states recalculating of the neighborhood model, where X_{O_x} is a set of states of the nodes of the first level, included in the neighborhood O_x; V_{O_v} is a set of controls of the nodes of the first level, included in the neighborhood O_v.

For the nodes of the first level $a_i \in A$, the function G_i will be:

$$X[t+1, i] = G_i[t] = \sum_{b=1}^{c} X[t+1, i^b] = \sum_{b=1}^{c} G_i^b[t], \tag{1}$$

where $G_i^b : X_{O_x[a_i^b]} \times V_{O_v[a_i^b]} \to X[i^b]$ is a state recalculation function for the second-level node a_i^b.

For each node of the second level $a_i^b \in O_{ier}[a_i, t]$, the function G_i^b in real time in the linear case has the form:

$$X[t+1, i^b] = \sum_{a_j \in O_x[a_{i^b}]} g_x^b[i^b, j] X[t, j] + \sum_{a_k \in O_v[a_{i^b}]} g_v^b[i^b, k] V[t, k] + g_c^b[i^b], \tag{2}$$

where $a_j, a_k \in A$ $(j, k = 1, ..., n)$ are nodes of the first level of the model; $X[t, i^b] \in R^{p_i}$ is the state in the node a_i^b at time t; $V[t, i^b] \in R^{m_i}$ is the control in the node a_i^b at time t; $g_x^b[i^b, j] \in R^{p_i \times p_j}$, $g_v^b[i^b, k] \in R^{p_i \times m_k}$, $g_c^b[i^b] \in R^{p_i \times 1}$ are model matrix-parameters.

For each second-level node $a_i^b \notin O_{ier}[a_i, t]$, the function G_i^b is currently zero, that is $X[t+1, i^b] = G_i^b[t] = 0$.

5) $X[0] \in R^{\overset{n}{\underset{i=1}{\sum} p_i}}$ is the initial state of the model.

6) t is the current discrete time of the model.

The structure of the neighborhood model can be represented as a single two-level graph of the structure of the neighborhood model-oriented graph with two types of arcs: state and control actions — or two-oriented graphs — external and internal structures.

Parametric identification of the dynamic neighborhood model [16-17] is in finding the system parameters for each node of the second level, and it is based on the least squares method:

$$E = \sum_{i=1}^{n} \| X[t+1, i] - G_i[t] \| \to \min.$$

Research Results. Let us consider the linear dynamic neighborhood model of the level of cement raw materials underground waters deposits. Fig. 1 shows the graph of the external structure of the model. Node a_1 is external environment. Currently, 7 wells are used for groundwater level monitoring purposes, which in Fig. 1 correspond to the nodes $a_2 - a_8$. The control actions of the nodes $V[t,i] \in R^{10}$ consist of the amount of precipitation in mm and of the average daily air temperature in °C for the last 5 days before the measurement of the water level in the wells at time t. The states of the nodes $X[t,i] \in R$ are equal to the water level in the well i at time t, $i = 2,...,8$.
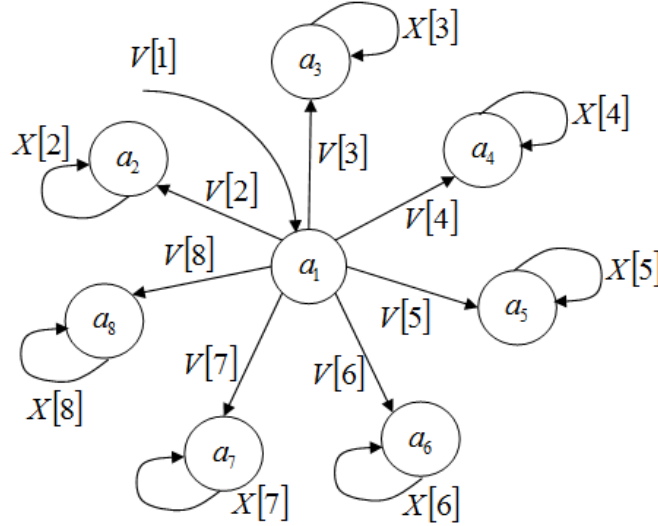
Fig. 1. Graph of the outer structure of the neighborhood model

The first level nodes of the neighborhood model a_i ($i = 2,...,8$) are hierarchical: $O_{ier}[a_i] = \{a_i^1, a_i^2\}$ and correspond to the positive and negative average daily air temperature. Their structure is shown in Fig. 2.
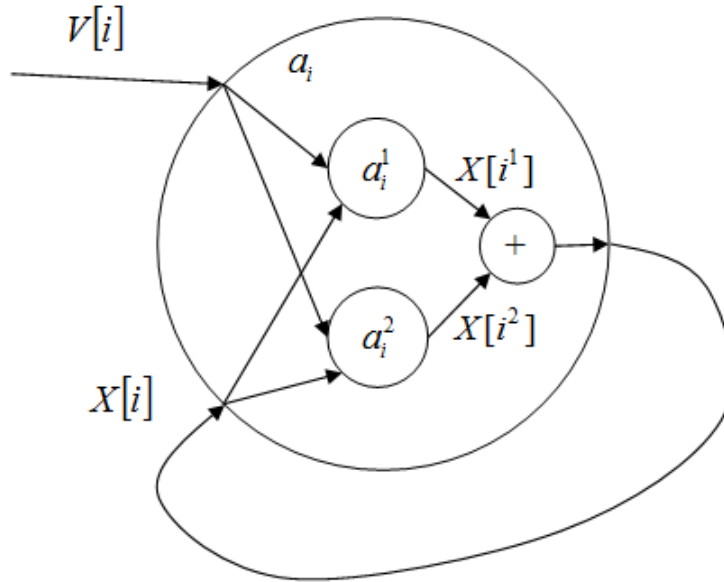
Fig. 2. Graph of the inner structure of the first level nodes

The system (2) for each node of the second level a_i^b of the surrounding groundwater level model will have the following form:

$$X[t+1,i^b] = g_x^b[i,i^b]X[t,i^b] + g_v^b[i,i^b]V[t,i^b] + g_c^b[i^b], \tag{3}$$

where $g_x^b[i,i] \in R$; $g_v^b[i,i] \in R^{1 \times 10}$; $g_c^b[i] \in R$; $i = 2,...,8$; $b = 1,2$.

The program in C++is developed for the parametric identification and performance simulation of the considered dynamic neighborhood model. The initial data for identification are the structure and the training sample. The program allows you to find parameters of the recalculation functions of node states, as well as to predict the behavior of the mathematical model in the process of operation.

After the parametric identification on the training data sample, the obtained model was tested on the control sample. The normalized initial and model values of the groundwater level for the node a_2 for training and control sampling are shown, respectively, in Fig. 3 and Fig. 4.
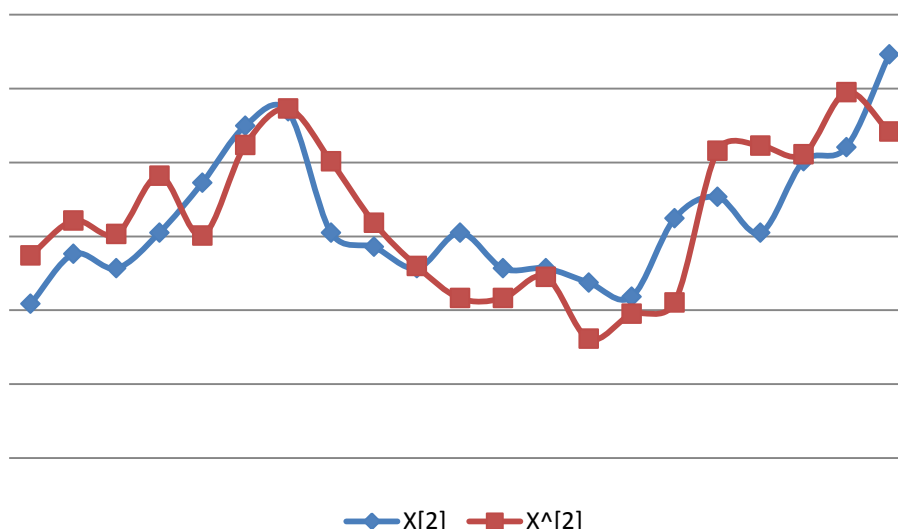
Fig. 3. Normalized source and model values of the groundwater level for the node a_2
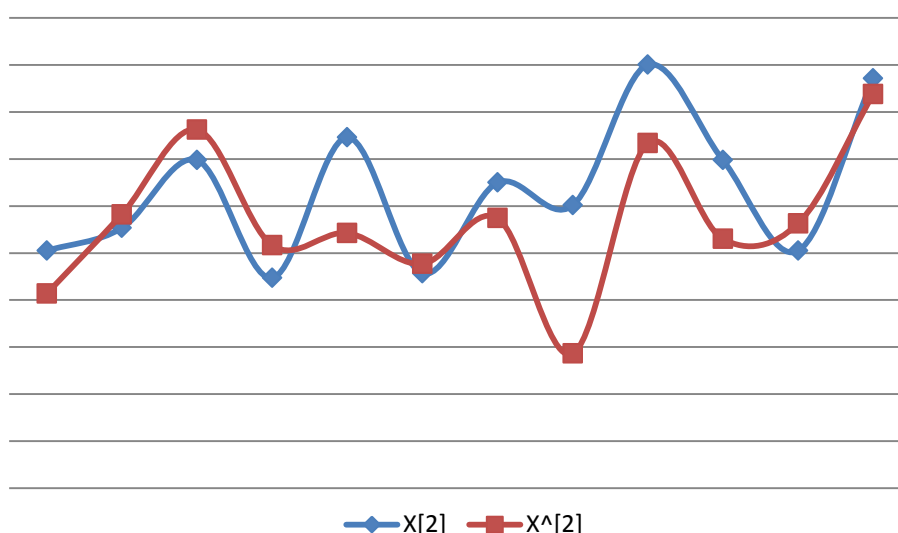
Fig. 4. Normalized source and predicted values of the groundwater level for the node a_2

The average relative error of identification (prediction) of the neighborhood model is calculated by the formula:

$$A = \frac{1}{Mn}\sum_{k=1}^{M}\sum_{i=1}^{n}\left|\frac{\hat{X}_m[t+1,i] - X_m[t+1,i]}{X_m[t+1,i]}\right| \cdot 100\%,$$

where $X_m[t+1,i]$ is the state of the node in the m-th training (control) sample tuple; $\hat{X}_m[t+1,i]$ are model values of the node state a_i; M is the volume of the training (control) sample.

The average relative error of prediction is shown in Fig. 5.
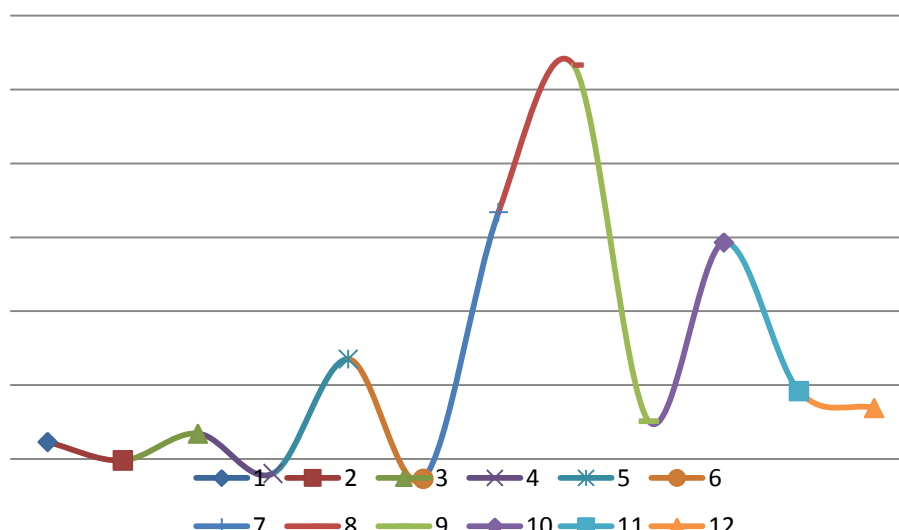
Fig. 5. Average relative prediction error for each tuple of the control sampling

The average relative error of identification was 0.19%, the average relative error of prediction was 0.23%, which indicates the adequacy of the developed model and allows us to recommend it for predicting the level of underground waters of the cement raw material field.

Conclusion. A linear dynamic neighborhood model with variable hierarchical surroundings to predict groundwater level deposits of cement raw materials, located in Zadonian-Yelets aquifer, is developed.

The software in C++programming language is developed for the parametric identification and performance simulation of the considered dynamic neighborhood model.

The implemented model predicts the level of groundwater in the analyzed wells with sufficient accuracy and can be effectively used to predict the level of groundwater deposits of cement raw materials.

References

1. Tkachenko, N.N. Evlanovsko-livenskiy vodonosnyy gorizont kak al'ternativa eletsko-zadonskomu dlya vodosnabzheniya g. Lipetska. [Evlanovsko-Livensky water horizon as alternative Eletsko-Zadonsky water supply.] Proceedings of Voronezh State University, Series: Geology, 2006, no. 2, pp. 255–257 (in Russian).

2. Kosinova, I.I., Zaridze, M.G. Otsenka stepeni preobrazovaniya otdel'nykh elementov ekologo-geologicheskoy sistemy v rayone razrabotki Sitovskogo kar'yera Sokol'sko-Sitovskogo mestorozhdeniya izvestnyakov. [Estimation of a degree of conversion of separate units of eco-geological system around development of the Sitovsky open-cast mine of Sokolovsko-Sitovsky limestone deposit.] Proceedings of Voronezh State University, Series: Geology, 2010, no. 1, pp. 264–269 (in Russian).

3. Sedykh, I.A., Shmyrin, A.M. Matematicheskoe modelirovanie maksimal'noy kontsentratsii vybrosov pri proizvodstve klinkera. [Mathematical modeling of the maximum concentration of emissions under the production of clinker.] V.I. Vernadskiy: ustoychivoe razvitie regionov. Materialy Mezhdunarodnoy nauch.-prakt. konf. V 5 t. T. 4. [V.I. Vernadskiy: sustainable development of regions. Proc. Int. Sci.-Pract. Conf. In 5 volumes. Vol. 4.] Tambov: TSTU Publ. Centre, 2016, pp. 127–131 (in Russian).

4. Shmyrin, A.M., Yartsev, A.G., Pravilnikova, V.V. Trilineynaya okrestnostnaya model' protsessa formirovaniya temperatury smotki goryachekatanoy polosy. [Trilinear neighborhood model of the process of forming the temperature of hot-rolled strip coiling.] Tambov University Reports. Series Natural and Technical Science, 2016, vol. 21, iss. 2, pp. 463–469 (in Russian).

5. Shmyrin, A.M., et al. Okrestnostnoe modelirovanie protsessa ochistki stochnykh vod. [Neighborhood modeling of wastewater treatment processes.] Tambov University Reports. Series Natural and Technical Science, 2017, vol. 22, iss. 3, pp. 596–604 (in Russian).

6. Sedykh, I.A., Smetannikova, A.M. Proverka ustoychivosti lineynykh dinamicheskikh okrestnostnykh modeley protsessa ochistki stochnykh vod. [Verification of stability of linear dynamic neighborhood models of wastewater treatment.] Materialy oblastnogo profil'nogo seminara «Shkola molodykh uchenykh» po problemam tekhn. nauk 17.11.2017 g. [Proc. Regional Profile Seminar "School of Young Scientists" on techn. sci. problems, 11/17/2017.] Lipetsk, 2017, pp. 125–129 (in Russian).

7. Sedykh, I.A. Okrestnostnoe modelirovanie predela tekuchesti stali posle nepreryvnogo otzhiga. [Neighborhood modeling of steel yield stress after continuous annealing.] Виртуальное моделирование, прототипирование и промышленный дизайн: мат-лы IV междунар. научно-практ. конф. (15–17 ноября 2017 г.). В 3 т. Т. 1[Virtual modeling, prototyping and industrial design: Proc. IV Int. Sci.-Pract. Conf. (November 15-17, 2017). In 3 vol. V. 1.] Tambov: TSTU Publ. Centre, 2017, pp. 378–383 (in Russian).

8. Sedykh, I.A., Smetannikova, A.M. Kriteriy Gurvitsa dlya proverki ustoychivosti lineynykh dinamicheskikh okrestnostnykh modeley protsessa ochistki stochnykh vod. [Hurwitz criterion for testing the stability of linear dynamic neighborhood models of the wastewater treatment process.] XXI vek: itogi proshlogo i problemy nastoyashchego plyus. [XXI century: Review of the past and problems of the present plus.] 2018, vol.7, no. 1(41), pp. 67–71 (in Russian).

9. Blyumin, S.L., Shmyrin, A.M. Okrestnostnye sistemy. [Neighborhood systems.] Lipetsk: LEGI, 2005, 132 p. (in Russian).

10. Blyumin, S.L., Shmyrin, A.M., Shmyrina, O.A. Bilineynye okrestnostnye sistemy. [Bilinear neighborhood systems.] Lipetsk: LEGI, 2006, 131 p. (in Russian).

11. Blyumin, S.L., et al. Okrestnostnoe modelirovanie setey Petri. [Neighborhood simulation of Petri nets.] Lipetsk: LEGI, 2010, 124 p. (in Russian).

12. Shmyrin, A.M., Sedykh, I.A., Shcherbakov, A.P. Obshchie bilineynye diskretnye modeli. [General bilinear discrete models.] Bulletin of Voronezh State Technical University, 2014, vol. 10, no. 3–1, pp. 44–49 (in Russian).

13. Shang, Y. Multi-agent coordination in directed moving neighborhood random networks. Chinese Physics B, 2010, vol. 19, no. 7, Article ID 070201.

14. Shang, Y. Consensus in averager-copier-voter networks of moving dynamical agents. Chaos, 2017, no. 27 (2), Article ID 023116.

15. Sedykh, I.A. Upravlenie dinamicheskimi okrestnostnymi modelyami s peremennymi okrestnostyami. [Control of dynamic neighborhood models with variable neighborhoods.] Control Systems and Information Technologies, 2018, no. 1(71), pp. 18–23 (in Russian).

16. Sedykh, I.A. Parametricheskaya identifikatsiya lineynoy dinamicheskoy okrestnostnoy modeli. [Parametric identification of a linear dynamic neighborhood model.] Innovatsionnaya nauka: proshloe, nastoyashchee, budushchee: sb. statey mezhdunar. nauch.-prakt. konf. [Innovative science: past, present, future: Proc. Int. Sci.-Pract. Conf.] Ufa, 2016, pp. 12–19 (in Russian).

17. Sedykh, I.A. Identifikatsiya i upravlenie dinamicheskimi okrestnostnymi modelyami. [Identification and management of dynamic neighborhood models.] Sovremennye slozhnye sistemy upravleniya (HTCS'2017): mat-ly XII mezhdunar. nauch.-prakt. konf. 25–27 oktyabrya 2017 g. V 2 ch. Ch. 1. [Modern sophisticated control systems (HTCS'2017): Proc. XII Int. Sci.-Pract. Conf., October 25-27, 2017, in 2 parts. Part 1.] Lipetsk, 2017, pp. 138–142 (in Russian).

Author:

Sedykh, Irina A.,
associate professor of the Higher Mathematics
Department, Lipetsk State Technical University (30,
Moskovskaya St., Lipetsk, RF), Cand.Sci. (Phys.-Math.),
associate professor,
ORCID: https://orcid.org/0000-0003-0012-8103
sedykh-irina@yandex.ru

INFORMATION TECHNOLOGY, COMPUTER SCIENCE, AND MANAGEMENT
ИНФОРМАТИКА, ВЫЧИСЛИТЕЛЬНАЯ ТЕХНИКА И УПРАВЛЕНИЕ

Selecting safety package components of enterprise information system following requirements of standard legal documents[*]

E. A. Vitenburg[1], A. A. Levtsova[2]**

[1,2] Volgograd State University, Volgograd, Russian Federation

Выбор элементов комплекса защиты информационной системы предприятия на основе требований нормативно-правовых документов[***]

Е. А. Витенбург[1], А. А. Левцова[2]**

[1,2] Волгоградский государственный университет, г. Волгоград, Российская Федерация

Introduction. Production processes quality depends largely on the management infrastructure, in particular, on the information system (IS) effectiveness. Company management pays increasingly greater attention to the safety protection of this sphere. Financial, material and other resources are regularly channeled to its support. In the presented paper, some issues on the development of a safety enterprise information system are considered.

Materials and Methods. Protection of the enterprise IS considers some specific aspects of the object, and immediate threats to IT security. Within the framework of this study, it is accepted that IS are a complex of data resources. A special analysis is resulted in determining categories of threats to the enterprise information security: hacking; leakage; distortion; loss; blocking; abuse. The connection of these threats, IS components and elements of the protection system is identified. The requirements of normative legal acts of the Russian Federation and international standards regulating this sphere are considered. It is shown how the analysis results enable to validate the selection of the elements of the IS protection system.

Research Results. A comparative analysis of the regulatory literature pertinent to this issue highlights the following. Different documents offer a different set of elements (subsystems) of the enterprise IS protection system. To develop an IS protection program, you should be guided by the FSTEC Order No. 239 and 800-82 Revision 2 Guide to ICS Security.

Discussion and Conclusions. The presented research results are the basis for the formation of the software package of intellectual support for decision-making under designing an enterprise information security system. In particular, it is possible to develop flexible systems that allow expanding the composition of the components (subsystems).

Введение. Качество производственных процессов во многом зависит от инфраструктуры управления — в частности, от эффективности информационной системы (ИС). Менеджмент компаний уделяет все большее внимание обеспечению безопасности этой сферы, на ее поддержку регулярно направляются финансовые, материальные и другие ресурсы. В представленной работе рассмотрены вопросы построения комплекса защиты информационной системы предприятия.

Материалы и методы. Охрана ИС предприятия учитывает особенности объекта защиты и актуальные угрозы информационной безопасности. В рамках данного исследования принято, что ИС представляет собой комплекс информационных ресурсов. По результатам специального анализа определены категории угроз информационной безопасности предприятия: взлом; утечка; искажение; утрата; блокирование; злоупотребление. Выявлена связь данных угроз, компонентов ИС и элементов комплекса защиты. Рассмотрены требования нормативно-правовых актов Российской Федерации и международных стандартов, регулирующих данную сферу. Показано, каким образом результаты данного анализа позволяют обосновать выбор элементов комплекса защиты ИС.

Результаты исследования. Сравнительный анализ регламентирующей литературы, относящейся к данному вопросу, позволил выявить следующее. Разные документы предлагают разный набор элементов (подсистем) комплекса защиты ИС предприятия. Разрабатывая программу защиты ИС, следует руководствоваться Приказом ФСТЭК № 239 и стандартом 800-82 Revision 2 Guide to ICS Security.

Обсуждение и заключения. Результаты представленного исследования являются основой для формирования программного комплекса интеллектуальной поддержки принятия решений при проектировании системы защиты информации на предприятии. В частности, можно разрабатывать гибкие комплексы, позволяющие расширять состав элементов (подсистем).

Information technology, computer science, and management

Introduction. Information systems (IS) are increasingly used in the production and management processes. Accordingly, the problem of cyber security (CS) of IS gets worse. In particular, IS weak isolation simplifies an unauthorized access to them [1, 2, 3]. The consequences of fraudulent attacks on IS may be production downtime, financial losses, and on the worst-case scenario – even man-made disasters [4]. Thus, the crucial task is to establish a protective system for the industrial IS which could effectively militate against malicious acts.

Materials and Methods. The development of an information security system is based on the results of a pre-project study during which the setup of the asset to be protected and the immediate threats are determined.

The asset of protection is represented as a set of information resources:

$$Object_{Sec} = \{NE, CC, IS, Sts, WS, PE, OS, SS, AS, IP, Sn, RSM, SM, IA\}.$$

Here, NE is a set of network hardware; CC is a number of communications lines; IS is an array of infrastructure servers; Sts a set of data storage systems; WS is number of localhosts; PE is a number of external equipment; OS is an array of operating systems; SS is a set of system software; AS is a set of application software; IP is number of information processes running in the tech companies; Sn is subnets; RSM is a number of removable media; SM is electronic data storage devices; IA is information assets.

Number of immediate CS threats $Threat$ is determined [5]:

$$Threat = \{Breaking, Leak, Distortion, Loss, Blocking, Abuse\}.$$

Here, $Breaking$ is hacking threats; $Leak$ is information leakage threatening; $Distortion$ is threats of distortion; $Loss$ is threats of loss; $Blocking$ is threats of blocking the information resources of a tech company; $Abuse$ is risks of abuse.

The system which meets these threats is an enterprise IP protection system (ISPS) (Fig. 1).
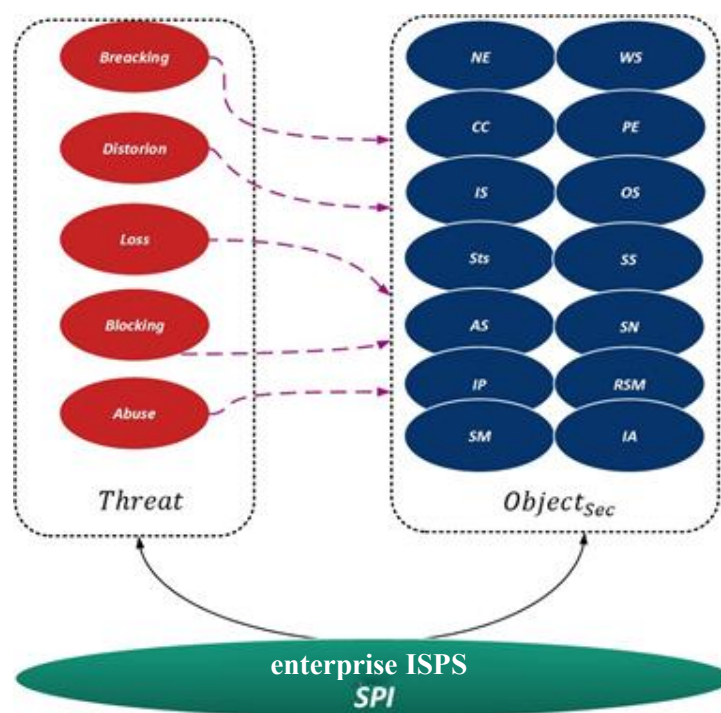

Fig. 1. Security objects – threats relations in ISPS diagram

SPI (*system of protection of information*) is two-tiered, and it includes subsystems (components) [6]:
— a set of subsystems (*Subsystem*) of information security;
— number of information security facilities (*MP*, *means of protection*).

Fig. 2 shows a general form of the ISPS structure.
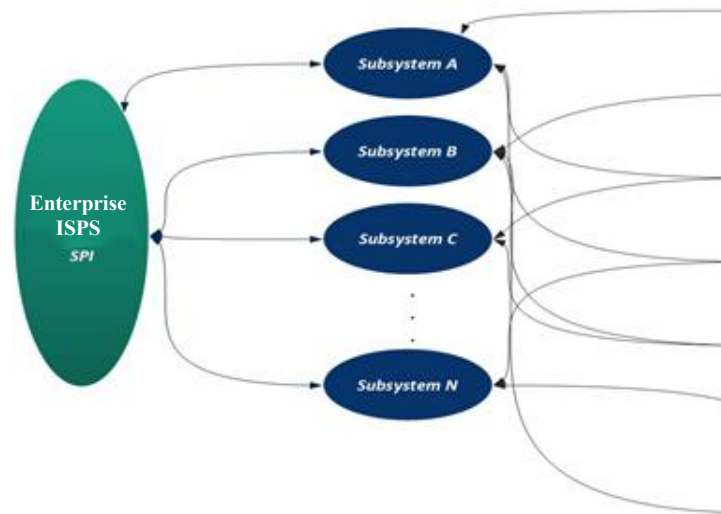
Fig. 2. Generalized structure of enterprise ISPS

When determining the components of the information protection system, experts proceed from the analysis of available regulatory documentation and standards operating at the enterprise. International experience should be taken into account as well. 800-82 Revision 2 Guide to Industrial Control Systems (ICS) Security [1] is widely used in the foreign and domestic practice. This standard was developed by the US National Institute of Standards and Technology. It, in particular, contains recommendations on improving safety in the industrial inspection systems, including the supervisory control and data acquisition systems. It shows how the organizational processes and business functions are subjected to threats, and it describes usual vulnerabilities. Special attention is given to security measures and counters that should be undertaken in a hostile situation.

Research Results. Domestic regulatory legal acts (RLA) handling the enterprise IS protection can be conditionally divided into two categories [6]:
— RLA on maintenance of information safety of the automatic process control system (APCS);
- RLA on the security of critical information infrastructure (CII).

Crucially, vulnerabilities in the CII protection can cause major material and environmental damage. Inadequate CII protection is fraught with social and military-political problems.

Designing the information security system (in particular, when modeling the intellectual support for decision-making) requires a preliminary comparative analysis of the profile regulatory legal acts of the Russian Federation. As for example, the following documents should be considered:
— Order no. 31 of the Federal Service for Technology and Export Control (FSTEC of Russia) of March 14, 2014, "On Approving Requirements for Providing Information Protection in Automated Control Systems of Production and Technological Processes at Critical Objects, Potentially Hazardous Facilities, and Objects posing high threat to life and health of people and the environment" [7];
— Order no. 239 of FSTEC of Russia of December 25, 2017, "On Approval of Requirements for Ensuring the Security of Significant Facilities of the Information Infrastructure of the Russian Federation" (draft) [8];
— International standard 800-82 Revision 2 Guide to Industrial Control Systems (ICS) Security [9].

Comparative analysis of the Orders of FSTEC of Russia no. 31 and no. 239 is presented in Table 1.

Table 1

Elements (subsystems) of enterprise IS protection system in
Orders of FSTEC no. 31 and no. 239

	FSTEC Order no. 31 of 14.03.14	FSTEC Order no. 239 of 25.12 2017
ISPS Subsystems	Identification and authentication of access subjects and access objects (IAF)	
	Access control of access subjects and access objects (UPD)	
	Restriction of software environment (OPS)	
	Protection of machine-readable media (ZNI)	
	Secure event logging (RSB)	Security audit (AUD)
	Antivirus protection (AVZ)	
	Intrusion detection (OV)	Intrusion prevention (PV)
	Infosecurity control (analysis) (ANZ)	Protection of information (automated) system and its components (ZIS)
	Integrity control (OTsL)	
	Information assurance (ODT)	
	Event planning to ensure information protection (PLN)	
	Protection of technical facilities and systems (ZTS)	
	Security assurance of software development (OBR)	Information security incident response (INTs)
	Virtualization environment protection (ZSV)	Personnel informing and training (IPO)
	Software update control (OPO)	
	Security protection of emergency procedures (DNS)	
	Analysis of threats to information security and risks from their implementation (UBI)	—
	Configuration control of data processing system and its security system (UKF)	
Note. For greater clarity, variances are not only placed in different cells, but are also highlighted in gray		

So, FSTEC Order no. 239 provides for the following subsystems in the IS protection system:
— security audit (AUD);
— protection of information (automated) system and its components (ZIS);
— information security incident response (INTs);
— staff informing and training (IPO).
It should be mentioned that the decision on the ISPS completeness to a certain extent depends on the financial capacities of the enterprise. However, if the cost of the protected resources and the potential damage from hazards is higher than the cost of the ISPS, then it makes sense to implement AUD and ZIS.
Comparative analysis of the FSTEC Order no. 239 of December 25, 2017, and 800-82 Revision 2 Guide to Industrial Control Systems (ICS) Security is given in Table 2.

Table 2

Elements (subsystems) of enterprise IS protection system in
FSTEC Order no. 239 of December 25, 2017, and in 800-82 Revision 2
Guide to Industrial Control Systems (ICS) Security)

	FSTEC Order no. 239 of 25.12.17	800-82 Revision 2 Guide to ICS Security
ISPS Subsystems	Identification and authentication (IAF) Identification and authentication	
	Access control (UPD) System and communications protection, Security assessment and authorization	
	Restriction of software environment (OPS)	System and information integrity
	Protection of machine-readable media (ZNI) Media protection	
	Security audit (AUD) Auditing and accountability	
	Antivirus protection (AVZ)	System and information integrity
	Intrusion prevention (hacking) (SOV)	System and information integrity
	Protection of information (automated) system and its components (ZIS)	System and information integrity
	Integrity control (OTsL)	System and information integrity
	Information assurance (ODT) System and services acquisition	
	Event planning to ensure information protection (PLN) Planning, contingency planning	
	Protection of technical facilities and systems (ZTS) Maintenance	
	Information security incident response (INTs) Incident response	
	Personnel informing and training (IPO) Personnel security	
	Software update control (OPO)	Organization — wide information security program management controls
	Security protection of emergency procedures (DNS) Physical and environmental protection Awareness and training	
	Configuration control (UKF) Configuration management	
	—	Risk assessment
	—	System and communications protection

Note. For greater clarity, variances are not only placed in different cells, but are also highlighted in gray.

In this case, the following differences are most obvious:
— 800-82 Revision 2 Guide to ICS Security combines the functional of the subsystems of OPS, AVZ, SOV, OTsL, ZIS defined in the FSTEC Order, in the subsystem of "System and information integrity";
— 800-82 Revision 2 Guide to ICS Security provides a subsystem for the protection of communication systems — "System and communications protection";
— The FSTEC Order combines the functional of the subsystems "System and communications protection" and "Security assessment and authorization" in the "Access control subsystem (UPD)";
— The FSTEC Order combines the functional of the "Planning" and "Contingency planning" subsystems in the subsystem of "Event planning to ensure information protection (PLN)";
— The FSTEC Order combines the functional of the subsystems of "Physical and environmental protection" and "Awareness and training" in the subsystem of "Security protection of emergency procedures (DNS)".

Special mention should be made of the subsystems for risk assessment and protection of communication systems [10]. These are the critical items of the enterprise IS protection system among those that are not provided for by domestic regulatory documents. Their implementation will enable to enhance protection; to respond promptly to incidents that arise in the enterprise IS; to counteract attacks timely and accurately.

Discussion and Conclusions. The analysis results of the IS protection system components will be used to build a model of intellectual support for decision-making when designing the ISPS. Particularly, it is planned to foresee the possi-

bility of expanding the ISPS subsystem setup. The selection of the system units will depend on the risk assessment, the extent of potential damage by injurious actions, and the cost of the ISPS components.

References

1. Ovsyanitskaya, L.Yu., Podpovetnaya, Yu.V., Podpovetnyy, A.D. Information security of small business: modern condition, problems and the ways of their colutions. Bulletin of the South Ural State University (Series "Computer Technologies, Automatic Control & Radioelectronics"), 2017, no. 4, pp. 77–84.

2. Glukhov, V.V., Ilin, I.V., Anisiforov, A.B. Problems of data protection in industrial corporations enterprise architecture. SIN'15: Proceedings of the 8th International Conference on Security of Information and Networks. New York ACM, 2015, pp. 34–37.

3. Pishchik, B.N. Bezopasnost' ASU TP. [Security of automated control systems for technological processes.] Computational   Technologies,   2013,   vol. 18,   spec.iss.,   pp. 170–175.   Available   at: file:///C:/Users/User/Downloads/23%20Pishik_n.pdf (accessed: 22.07.18) (in Russian).

4. Gritsay, G., et al. Bezopasnost' promyshlennykh sistem v tsifrakh. [Safety of industrial systems in figures.] Moscow: Positive   Technologies,   2012,   37 c.   Available   at: http://www.ptsecurity.ru/download/SCADA_analytics_russian.pdf (accessed: 22.07.18) (in Russian).

5. Mukminov, V.A., Khutsishvili, V.M., Lobuzko, A.V. Metodika otsenki real'nogo urovnya zashchishchennosti avtomatizirovannykh system. [Methods of the assessment of mis real protection levels.] Software & Systems, 2012, no. 1 (97), pp. 39–42 (in Russian).

6. Lukatskiy, A. Obzor mirovykh standartov IB ASU TP i sovety po ikh primenimosti v rossiyskikh usloviyakh. [Survey of IS world standards of automatic process control systems and hints on their applicability in Russia's circumstances.] Cisco Systems: Docplayer. Available at: http://docplayer.ru/33122677-Obzor-mirovyh-standartov-ib-asu-tp-i-sovety-po-ih-primenimosti-v-rossiyskih-usloviyah.html (accessed: 22.07.18) (in Russian).

7. Ob utverzhdenii trebovaniy k obespecheniyu zashchity informatsii v av-tomatizirovannykh sistemakh upravleniya proizvodstvennymi i tekhnologicheskimi protsessami na kriticheski vazhnykh ob"ektakh, potentsial'no opasnykh ob"ektakh, a takzhe ob"ektakh, predstavlyayushchikh povyshennuyu opasnost' dlya zhizni i zdorov'ya lyudey i dlya okruzhayushchey prirodnoy sredy : Prikaz Federal'noy sluzhby po tekhnicheskomu i eksportnomu kontrolyu ot 14 marta 2014 g. № 31. [On Approving Requirements for Providing Information Protection in Automated Control Systems of Production and Technological Processes at Critical Objects, Potentially Hazardous Facilities, and Objects posing high threat to life and health of people and the environment: Order no. 31 of the Federal Service for Technology and Export Control of March 14, 2014.] Federal Service for Technology and Export Control. Available at: https://fstec.ru/tekhnicheskaya-zashchita-informatsii/dokumenty/110-prikazy/864-prikaz-fstek-rossii-ot-14-marta-2014-g-n-31 (accessed: 22.07.18) (in Russian).

8. Ob utverzhdenii trebovaniy po obespecheniyu bezopasnosti znachimykh ob"ektov kriticheskoy informatsionnoy infrastruktury Rossiyskoy Federatsii: Prikaz Federal'noy sluzhby po tekhnicheskomu i eksportnomu kontrolyu ot 25 dekabrya 2017 g. № 239. [On Approval of Requirements for Ensuring the Security of Significant Facilities of the Information Infrastructure of the Russian Federation: Order no. 239 of Federal Service for Technology and Export Control of December 25, 2017.] Federal Service for Technology and Export Control. Available at: https://fstec.ru/tekhnicheskaya-zashchita-informatsii/dokumenty/110-prikazy/1593-prikaz-fstek-rossii-ot-25-dekabrya-2017-g-n-239 (accessed: 22.07.18) (in Russian).

9. Stouffer, K., et al. Guide to Industrial Control Systems (ICS) Security. U. S. Department of Commerce; National Institute of Standards and Technology. Gaithersburg: NIST, 2015, 247 p.

10. Singhal, A., Ou, X. Security risk analysis of enterprise networks using probabilistic attack graphs. Network Security Metrics. Cham: Springer, 2017, pp. 53–73.

Authors:

Vitenburg, Ekaterina A.,
postgraduate student of the Information Security
Department, Volgograd State University (100,
Universitetskiy pr., Volgograd, 400062, RF),
ORCID: https://orcid.org/0000-0002-1534-8865
e.vitenburg@ec-rs.ru

Levtsova, Alexandra A.,
student of the Information Security Department,
Volgograd State University (100, Universitetskiy pr.,
Volgograd, 400062, RF),
ORCID: https://orcid.org/0000-0002-4798-9704
alexandra.levtsova@yandex.ru

INFORMATION TECHNOLOGY, COMPUTER SCIENCE, AND MANAGEMENT
ИНФОРМАТИКА, ВЫЧИСЛИТЕЛЬНАЯ ТЕХНИКА И УПРАВЛЕНИЕ

Differentiation of polynomials in several variables over Galois fields of fuzzy cardinality and applications to Reed-Muller codes[*]

V. M. Deundyak[1,2], N. S. Mogilevskaya[2]**

[1] Research Institute "Spetsvuzavtomatika", Rostov-on-Don, Russian Federation.
[2] Southern Federal University, Rostov-on-Don, Russian Federation

Дифференцирование полиномов нескольких переменных над полями Галуа нечетной мощности и приложения к кодам Рида-Маллера[***]

В. М. Деундяк[1,2], Н. С. Могилевская[2]**

[1] НИИ «Спецвузавтоматика», г. Ростов-на-Дону, Российская Федерация.
[2] Южный федеральный университет, г. Ростов-на-Дону, Российская Федерация.

Introduction. Polynomials in several variables over Galois fields provide the basis for the Reed-Muller coding theory, and are also used in a number of cryptographic problems. The properties of such polynomials specified over the derived Galois fields of fuzzy cardinality are studied. For the results obtained, two real-world applications are proposed: partitioning scheme and Reed-Muller code decoder.

Materials and Methods. Using linear algebra, theory of Galois fields, and general theory of polynomials in several variables, we have obtained results related to the differentiation and integration of polynomials in several variables over Galois fields of fuzzy cardinality. An analog of the differentiation operator is constructed and studied for vectors.

Research Results. On the basis of the obtained results on the differentiation and integration of polynomials, a new decoder for Reed-Muller codes of the second order is given, and a scheme for organizing the partitioned transfer of confidential data is proposed. This is a communication system in which the source data on the sender is divided into several parts and, independently of one another, transmitted through different communication channels, and then, on the receiver, the initial data is restored of the parts retrieved. The proposed scheme feature is that it enables to protect data, both from the nonlegitimate access, and from unintentional errors; herewith, one and the same mathematical apparatus is used in both cases. The developed decoder for the second-order Reed-Muller codes prescribed over the derived odd Galois field may have a constraint to the recoverable error level; however, its use is advisable for a number of the communication channels.

Введение. Полиномы нескольких переменных над полями Галуа лежат в основе теории кодов Рида-Маллера, а также используются в ряде криптографических задач. В работе изучаются свойства таких полиномов, заданных над произвольными полями Галуа нечетной мощности. Для полученных результатов предложены два практических приложения: схема разделения данных и декодер кодов Рида-Маллера.

Материалы и методы. С использованием линейной алгебры, теории полей Галуа и общей теории полиномов нескольких переменных получены результаты, связанные с дифференцированием и интегрированием полиномов нескольких переменных над полями Галуа нечетной мощности. Для векторов построен и изучен аналог оператора дифференцирования.

Результаты исследования. На основе полученных результатов о дифференцировании и интегрировании полиномов предложен новый декодер для кодов Рида-Маллера второго порядка и предложена схема организации разделенной передачи конфиденциальных данных, т.е. такой системы связи, в которой исходные данные на стороне отправителя разделяются на несколько частей и, независимо друг от друга, передаются по различным каналам связи, а на стороне получателя из принятых частей восстанавливаются исходные данные. Особенностью предлагаемой схемы является то, что она позволяет защищать данные, как от нелегитимного доступа, так и от непреднамеренных ошибок, при этом в обоих случаях используется один и тот же математический аппарат. Разработанный декодер для кодов Рида-Маллера второго порядка, заданных над произвольным нечетным полем Галуа, может иметь некоторое ограничение по числу исправляемых ошибок, однако, его использование целесообразно для ряда каналов связи.

Information technology, computer science, and management

Discussion and Conclusions. The proposed practical applications of the results obtained are useful for the organization of reliable communication systems. In future, it is planned to study the restoration process of the original polynomial by its derivatives, in case of their partial distortion, and the development of appropriate applications.

Обсуждение и заключения. Предложенные практические приложения полученных результатов представляются полезными для организации надежных систем связи. В дальнейшем планируется исследование процесса восстановления исходного полинома по его производным, в случае их частичного искажения, и разработка соответствующих приложений.

Introduction. Polynomials of several variables over Galois fields and their derivatives are used in several information security domains. Some issues on the integration and differentiation of polynomials of several variables are considered in a number of papers. Thus, in [1], polynomials defined over simple Galois fields are studied, in [2-4], results for Boolean functions are obtained, and in [5-6], results for polynomials given over ternary Galois fields are described.

In this paper, we consider polynomials of several variables specified over the derived Galois fields of fuzzy cardinality. For such polynomials, the results related to the calculation of the directional derivatives, as well as to the restoration of the polynomial from the set of its derivatives calculated in the basic directions are obtained. For the results, two possible practical applications are proposed: a partitioning scheme and a decoder for Reed-Muller codes (PM codes).

The partitioning scheme can be used to organize the partitioned transmission of confidential data, i.e. such a communication system in which the initial data on the sender is divided into several parts and, independently of one another, transmitted through different communication channels, and then, on the receiver, the original data is restored from the collected parts. The proposed scheme feature is that it enables to protect data, both from the nonlegitimate access, and from unintentional errors. At this, in both cases, one and the same mathematical apparatus associated with PM codes and polynomial differentiation is used. Partitioned transmission can be used both to improve the communication speed, and to ensure data security by complicating the task of interception from several communication lines. Some issues on data partition are considered in [7-11].

For PM-codes of the second order, deterministic decoders are known only for certain values of the Galois field cardinality q. Such as, quite a lot of decoders are known for the case of $q = 2$, for example [12-13], for the case of $q = 3$ and the use of a semicontinuous communication channel, a decoder [5] is constructed. In [14], a second-order Reed-Muller decoder for the codes preset over Galois fields of cardinality 2, 4, and 8 is proposed. The second-order PM code decoder defined above the derived fuzzy Galois field proposed in this paper is based on reduction to first-order Reed-Muller codes. Their codewords can be decoded by any suitable decoder. In the case of PM codes specified over the fields with cardinality of more than three, the proposed decoder has some limitation on the recoverable error rate. It should be mentioned that the use of the proposed decoding scheme in case of field cardinality of more than three, may be advisable at a low noise pollution level of the communication channels used despite the limitation.

Differentiation of polynomials in several variables

Suppose $q = p^s$, where p is an odd prime, $s \in \mathbb{N}$, F_q is a Galois field of q cardinality. Let us consider a polynomial ring in m variables $F_q[x_1, ..., x_m]$ over F_q field. Let us denote the polynomial linear space of $F_q[x_1, ..., x_m]$ degree not more than r as $F_q^{(r)}[x_1, ..., x_m]$. Suppose F_q^m is m-linear space over F_q.

The result of the differentiation operator action is the polynomial derivative $f \in F_q^{(r)}[x_1, ..., x_m]$ along $\bar{b} \in F_q^m$:

$$(D_{\bar{b}} f)(\bar{x}) = f_{\bar{b}}(\bar{x}) - f(\bar{x}), \quad \bar{x} \in F_q^m, \tag{1}$$

where $f_{\bar{b}}(\bar{x}) = f(\bar{x} + \bar{b})$. It is easy to see that $D_{\bar{b}} f \in F_q^{(r-1)}[x_1, ..., x_m]$, and the operator

$$D_{\bar{b}}f : F_q^{(r)}[x_1,...,x_m] \rightarrow F_q^{(r-1)}[x_1,...,x_m] \tag{2}$$

is a linear one. Let us denote the vector coordinate sum $\bar{\alpha} \in F_p^m$, where p is prime, as a sum of natural numbers, by $\rho(\bar{\alpha})$. The polynomials $f \in F_q^{(2)}[x_1,...,x_m]$ may be written in a canonical form

$$f(\bar{x}) = \sum_{\bar{\alpha} \in F_q^m} f_{\bar{\alpha}} \bar{x}^{\bar{\alpha}} = a_{\bar{0}} \bar{x}^{\bar{0}} + \sum_{\rho(\bar{\alpha})=1} a_{\bar{\alpha}} \bar{x}^{\bar{\alpha}} + \sum_{\rho(\bar{\alpha})=2} a_{\bar{\alpha}} \bar{x}^{\bar{\alpha}}, \tag{3}$$

where, when writing the monomial $\bar{x}^{\bar{\alpha}} = x_1^{\alpha_1}...x_m^{\alpha_m}$, the indices α_i will be identified with the elements of the field F_p, and the summands in each sum will be arranged in an lexicographic order of magnitude. If the last sum in (3) is zero, we obtain a polynomial in $F_q^{(1)}[x_1,...,x_m]$.

Lemma 1. Suppose $q = p^s$, p is an odd prime, $f(\bar{x}) \in F_q^{(2)}[x_1,...,x_m]$ is a polynomial in a canonical form (3), $\bar{b} = (b_1,...,b_m) \in F_q^m$. Then

$$f(\bar{x}) = f_{00...00} + \bar{x}\left(f_{10...00}, f_{01...00},...,f_{00...01}\right)^T + \bar{x}A\bar{x}^T, \tag{4}$$

$$(D_{\bar{b}}f)(\bar{x}) = \bar{b}\left(f_{10...00}, f_{01...00},...,f_{00...01}\right)^T + 2\bar{x}A\bar{b}^T + \bar{b}A\bar{b}^T = 2\bar{x}A\bar{b}^T + f(\bar{b}) - f_{00...00}, \tag{5}$$

where

$$A = \begin{pmatrix} f_{200..00} & f_{110..00}/2 & f_{101..00}/2 & \cdots & f_{100..10}/2 & f_{100..01}/2 \\ f_{110..00}/2 & f_{020..00} & f_{011..00}/2 & \cdots & f_{010..10}/2 & f_{010..01}/2 \\ f_{101..00}/2 & f_{011..00}/2 & f_{002..00} & \cdots & f_{001..10}/2 & f_{001..01}/2 \\ \cdots & \cdots & \cdots & \ddots & \cdots & \cdots \\ f_{100..10}/2 & f_{010..10}/2 & f_{001..10}/2 & \cdots & f_{000..20} & f_{000..11}/2 \\ f_{100..01}/2 & f_{010..01}/2 & f_{001..01}/2 & \cdots & f_{000..11}/2 & f_{000..02} \end{pmatrix},$$

Proof. In the case of a prime Galois field, the proof is contained in [1]. Using (1), (4) and matrix symmetry, we obtain:

$$f_{\bar{b}}(\bar{x}) = f(\bar{x}+\bar{b}) = f_{00...00} + (\bar{x}+\bar{b})\left(f_{10...00}, f_{01...00},...,f_{00...01}\right)^T + (\bar{x}+\bar{b})A(\bar{x}+\bar{b})^T,$$

$$(D_{\bar{b}}f)(\bar{x}) = f_{\bar{b}}(\bar{x}) - f(\bar{x}) = \bar{b}\left(f_{10...00}, f_{01...00},...,f_{00...01}\right)^T + \bar{x}A\bar{b}^T + \bar{b}A\bar{x}^T + \bar{b}A\bar{b}^T,$$

$$(D_{\bar{b}}f)(\bar{x}) = \bar{b}\left(f_{10...00}, f_{01...00},...,f_{00...01}\right)^T + 2\bar{x}A\bar{b}^T + \bar{b}A\bar{b}^T = 2\bar{x}A\bar{b}^T + f(\bar{b}) - f_{00...00}. \bullet$$

Let us prove the theorem that determines the restoring method up to a polynomial constant term in $F_q^{(2)}[x_1,x_2,...,x_m]$ by the set of its derivatives calculated in the basic directions.

Theorem 1. Suppose $\beta = \{\bar{b}_i = (b_1^i, b_2^i,...,b_m^i)\}_{i=1,...,m}$ is some basis of space F_q^m, where q is odd. Let us consider the polynomial $f \in F_q^{(2)}[x_1,x_2,...,x_m]$ of (4):

$$f(\bar{x}) = f_{00...00} + \bar{x}\left(f_{10...00}, f_{01...00},...,f_{00...01}\right)^T + \bar{x}A\bar{x}^T.$$

If

$$\left\{\left(D_{\bar{b}_i}f\right)(\bar{x}) = \alpha_1^i x_1 + \alpha_2^i x_2 + ... + \alpha_m^i x_m + \alpha_0^i\right\}_{i=1,...,m}, \tag{6}$$

Then,

$$A = \frac{1}{2}\begin{pmatrix} \alpha_1^1 & \alpha_1^2 & \cdots & \alpha_1^m \\ \alpha_2^1 & \alpha_2^2 & \cdots & \alpha_2^m \\ \vdots & \cdots & \ddots & \vdots \\ \alpha_m^1 & \alpha_m^2 & \cdots & \alpha_m^m \end{pmatrix}\begin{pmatrix} b_1^1 & b_1^2 & \cdots & b_1^m \\ b_2^1 & b_2^2 & \cdots & b_2^m \\ \vdots & \cdots & \ddots & \vdots \\ b_m^1 & b_m^2 & \cdots & b_m^m \end{pmatrix}^{-1}, \tag{7}$$

$$\begin{pmatrix} f_{10...00} \\ f_{01...00} \\ \vdots \\ f_{00...01} \end{pmatrix} = \begin{pmatrix} \alpha_0^1 - \bar{b}_1 A \bar{b}_1^T \\ \alpha_0^2 - \bar{b}_2 A \bar{b}_2^T \\ \vdots \\ \alpha_0^m - \bar{b}_m A \bar{b}_m^T \end{pmatrix}\begin{pmatrix} b_1^1 & b_2^1 & \cdots & b_m^1 \\ b_1^2 & b_2^2 & \cdots & b_m^2 \\ \vdots & \vdots & \ddots & \vdots \\ b_1^m & b_2^m & \cdots & b_m^m \end{pmatrix}^{-1}. \tag{8}$$

Proof. From (5), (6), we obtain:

$$\forall \ i = 1, ..., m: \ 2A\bar{b}_i^T = (\alpha_1^i, \alpha_2^i, ..., \alpha_m^i)^T, \ f(\bar{b}_i) - f_{00...00} = \alpha_0^i. \tag{9}$$

Then,

$$2A\begin{pmatrix} b_1^1 & b_1^2 & \cdots & b_1^m \\ b_2^1 & b_2^2 & \cdots & b_2^m \\ \vdots & \vdots & \ddots & \vdots \\ b_m^1 & b_m^2 & \cdots & b_m^m \end{pmatrix} = \begin{pmatrix} \alpha_1^1 & \alpha_1^2 & \cdots & \alpha_1^m \\ \alpha_2^1 & \alpha_2^2 & \cdots & \alpha_2^m \\ \vdots & \cdots & \ddots & \vdots \\ \alpha_m^1 & \alpha_m^2 & \cdots & \alpha_m^m \end{pmatrix}.$$

Hence, the formula (7) comes out right.

It follows from (4) that for any $\bar{b} \in \mathrm{F}_q^m$:

$$f(\bar{b}) - f_{00...00} = \bar{b}\left(f_{10...00}, f_{01...00}, ..., f_{00...01}\right)^T + \bar{b}A\bar{b}^T .$$

For $\bar{b}$, we take the vectors $\bar{b}_i \in \beta$ and use the equation $f(\bar{b}_i) - f_{00...00} = \alpha_0^i$ from (9). Then,

$$\forall \ i = 1, ..., m: \ \alpha_0^i - \bar{b}_i A\bar{b}_i^T = \bar{b}_i \left(f_{10...00}, f_{01...00}, ..., f_{00...01}\right)^T .$$

Consequently,

$$\begin{pmatrix} \alpha_0^1 - \bar{b}_1 A\bar{b}_1^T \\ \alpha_0^2 - \bar{b}_2 A\bar{b}_2^T \\ \vdots \\ \alpha_0^m - \bar{b}_m A\bar{b}_m^T \end{pmatrix} = \begin{pmatrix} b_1^1 & b_2^1 & \cdots & b_m^1 \\ b_1^2 & b_2^2 & \cdots & b_m^2 \\ \vdots & \vdots & \ddots & \vdots \\ b_1^m & b_2^m & \cdots & b_m^m \end{pmatrix}\begin{pmatrix} f_{10...00} \\ f_{01...00} \\ \vdots \\ f_{00...01} \end{pmatrix}$$

And the formula (8) is proved. •

Reed-Muller q-ary codes $RM_q(r,m)$. Let us consider RM-codes over the finite field F_q where $q = p^s$, p is an odd prime, $s \in \mathrm{N}$ [15–16]. The elements $\mathrm{F}_q^{(r)}[x_1,...,x_m]$ are information polynomials of the code $RM_q(r,m)$; we suppose that $m \geq r > 0$, $m \geq 2$. Vector $\bar{f}$ made up from the information polynomial coefficients is called an information vector.

In the vector space F_q^m , let us fix some ordering

$$\{\bar{\alpha}_1, ..., \bar{\alpha}_n\} \ (\bar{\alpha}_j = (\alpha_{j1}, \alpha_{j2}, ..., \alpha_{jm})) , \ n = q^m. \tag{10}$$

The arbitrary information polynomial $f(\bar{x}) \in \mathrm{F}_q^{(r)}[x_1,...,x_m]$ is coded by its evaluation at the ordered space F_q^m points:

$$C(f) = (f(\bar{\alpha}_1), ..., f(\bar{\alpha}_n)) , \tag{11}$$

and so, the coder-operator is defined

$$C: \ \mathrm{F}_q^{(r)}[x_1,...,x_m] \to \mathrm{F}_q^n .$$

Reed-Muller codes are defined by the natural parameters r and m (r<m)

$$RM_q(r,m) = \{(f(\bar{\alpha}_1),...,f(\bar{\alpha}_n)) \ | f(\bar{x}) \in \mathrm{F}_q[x_1,...,x_m], \deg(f) \leq r\} \subset \mathrm{F}_q^n ,$$

The parameter *r* is called a code order. They form a family of linear [n, k, d] q-codes whose length and dimension are determined from the formulas

$$n = q^m, \ k = \sum_{i=0}^{r} \sum_{j=0}^{\lfloor i/q \rfloor} (-1)^j C_m^j C_{i-qj+m-1}^{m-1} ,$$

where $\lfloor \ \rfloor$ is rounding up to the smaller whole number, and the minimum code distance d of the code $RM_q(r,m)$ is convenient to calculate using the dual code $RM_q(r^\perp,m)$ parameters where $r^\perp = m(q-1) - r - 1$. Suppose ρ is residue of division $r^\perp + 1$ by $q - 1$: $r^\perp + 1 = \sigma(q-1) + \rho$ where $\rho < q - 1$, then the parameter d of the code $RM_q(r,m)$ is given by the expression

$$d = (\rho + 1)q^\sigma. \tag{12}$$

Note that the arbitrary [n, k, d] $_q$-code enables to correct $t = \lfloor (d-1)/2 \rfloor$ errors in one codeword [17].

Next, let us consider PM-codes of orders 1 and 2 given over Galois fields of fuzzy cardinality, write the corresponding information polynomials in the form (3), and use ordering (10) for numbering the information vector coordinates.

Lemma 2. Let $r \in \{1; 2\}$, $q \geq 3$, then the minimum code distance of the code $RM_q(r,m)$ is calculated by the formula:

$$d_r = (q-r)q^{m-1},$$ (13)

and values of the recoverable $t_r = \lfloor (d-1)/2 \rfloor$ - by the codes $RM_q(r,m)$, $r \in \{1; 2\}$, are related as follows:

$$t_1/2 \leq t_2.$$ (14)

Proof. Let us make use of the fact that $r < q$ and calculate σ and ρ - subquotient and the remainder of the division $r^{\perp} + 1$ by $q-1$ respectively:

$$\sigma = (m(q-1)-r)\operatorname{div}(q-1) = m-1;$$

$$\rho = (m(q-1)-r)\operatorname{mod}(q-1) = q-1-r.$$

Then, from the formula (12) we obtain (13). From the equalities $d_1 = (q-1)q^{m-1}$, $d_2 = (q-2)q^{m-1}$, we get that the desired inequality (14) is as follows

$$\frac{1}{2} \cdot \left\lfloor \frac{(q-1)q^{m-1}-1}{2} \right\rfloor \leq \left\lfloor \frac{(q-2)q^{m-1}-1}{2} \right\rfloor.$$

Note that d_2 is odd, and d_1 is even, hence

$$\left\lfloor \frac{(q-2)q^{m-1}-1}{2} \right\rfloor = \frac{(q-2)q^{m-1}-1}{2},$$

$$\left\lfloor \frac{(q-1)q^{m-1}-1}{2} \right\rfloor = \frac{(q-1)q^{m-1}-2}{2},$$

Consequently, the inequality (14) takes the form

$$\frac{1}{2}\left(\frac{(q-1)q^{m-1}-2}{2} \right) \leq \frac{(q-2)q^{m-1}-1}{2},$$

It is easily seen that it is equal to the inequality $q \geq 3$. ●

Consequence. If q>3, then there is a strict and when q=3, then there is an equality in (14).

Table 1 lists parameters of some PM-codes. The top three lines contain the parameters q, m, n of the code in question $RM_q(r,m)$. The following three lines contain the values: k_1 is code dimension, d_1 is minimum code distance, and t_1 is the number of recoverable errors for the codes $RM_q(1,m)$. And the following three lines show similar values of k_2, d_2, t_2 for the codes $RM_q(2,m)$.

Table 1

Parameter values of some RM-codes

q		3				5				7			
m		2	3	5	7	2	3	5	7	2	3	4	5
n		9	27	243	2187	25	125	3125	78125	49	343	2401	16807
r=1	k_1	3	4	6	8	3	4	6	8	3	4	5	6
	d_1	6	18	162	1458	20	100	2500	62500	42	294	2058	14406
	t_1	2	8	80	728	9	49	1249	31249	20	146	1028	7202
r=2	k_2	6	10	21	36	6	10	21	36	6	10	15	21
	d_2	3	9	81	729	15	75	1875	46875	35	245	1725	12005
	t_2	1	4	40	364	7	37	937	23437	17	122	857	6002

Now, we introduce the analog of the differentiation operator $D_{\bar{b}}$ operating in the space of polynomials (see (2)), for the space F_q^n where $n = q^m$. The vector coordinates from F_q^n will be numbered by vectors from the ordered set F_q^m (see (10)). Let us consider the shift operator $\tau_{\bar{b}} : F_q^n \to F_q^n$ following the formula

$$\tau_{\bar{b}}(\bar{a}) = (a_{\bar{\alpha}_1 + \bar{b}}, ..., a_{\bar{\alpha}_n + \bar{b}}),$$

where $\bar{a} = (a_{\bar{\alpha}_1}, ..., a_{\bar{\alpha}_n}) \in F_q^n$, $\bar{b} = (b_1, ..., b_m) \in F_q^m$. Note that the shift operator $\tau_{\bar{b}}$ is mixing bijection. The linear operator $\Delta_{\bar{b}} : F_q^n \to F_q^n$, that is the analog to $D_{\bar{b}}$, is defined by the formula:

$$\Delta_{\bar{b}}(\bar{a}) = \tau_{\bar{b}}(\bar{a}) - \bar{a}, \ \bar{a} = (a_{\bar{\alpha}_1}, ..., a_{\bar{\alpha}_n}) \in F_q^n. \tag{15}$$

We call $\Delta_{\bar{b}}(\bar{a})$ a vector derivative of vector $\bar{a}$ along $\bar{b}$.

Lemma 3. Let us consider the polynomial $f \in F_q^{(2)}[x_1, x_2, ..., x_m]$, vector $\bar{b} = (b_1, ..., b_m) \in F_q^m$, operators $\Delta_{\bar{b}}$, $D_{\bar{b}}$ and C. Then,

$$\tau_{\bar{b}}(C(f)) = C(f_{\bar{b}}), \ C(D_{\bar{b}} f) = \Delta_{\bar{b}}(C(f)). \tag{16}$$

The proof is carried out by the direct calculations, and for $q = 3$ is available in [6].

Note that from (2) and (16), it follows that if $C(w) \in RM_q(2, m)$, then $\Delta_{\bar{b}}(C(w)) \in RM_q(1, m)$.

Below, we consider examples of practical applications of the theoretical results obtained.

Data partitioning scheme. For partitioning and restoring data in the proposed scheme, we use $[n, k_1, d_1]_q$-code, $RM_q(1, m)$ and $[n, k_2, d_2]_q$-code $RM_q(2, m)$, specified over the derived Galois field F_q of fuzzy cardinality. Values q and m are parameters of this scheme.

Data partitioning algorithm.

Input: information vector $\bar{w} \in F_q^{k_2}$ of the code $RM_q(2, m)$ and an ordered set of basic vectors

$$\beta = \{\bar{b}_i = (b_1^i, b_2^i, ..., b_m^i) \in F_q^m\}_{i=1,...,m}, \tag{17}$$

That is a private key of the scheme under consideration.

Output: vectors $\bar{S}_i \in F_q^{n+1}$, $i = \overline{1, m}$.

Step 1. Let us assign the information polynomial $w = w(\bar{x})$ to the input vector $\bar{w}$ and encode it using (11) into the vector $C(w) \in F_q^n$ of the code $RM_q(2, m)$.

Step 2. Let us form m of the vector derivatives (see (15)):

$$\Delta_{\bar{b}_i}(C(w)) = C(D_{\bar{b}_i}(w)) \in F_q^n, \ i = \overline{1, m}, \ \bar{b}_i \in \beta.$$

Note that $C(D_{\bar{b}_i}(w)) \in RM_q(1, m)$.

Step 3. We concatenate each vector $C(D_{\bar{b}_i}(w)) \in F_q^n$, $i = \overline{1, m}$ with the coefficient $f_{00..00} := w(\bar{0})$ of the code vector $C(w)$:

$$\bar{S}_i = C(D_{\bar{b}_i}(w)) \| f_{00..00} \in F_q^{n+1}.$$

Then, vectors $\bar{S}_i \in F_q^{n+1}$, $i = \overline{1, m}$ are transmitted along m different communication lines. Obviously, during the transmission, vectors $\bar{S}_i$, $i = \overline{1, m}$ can be distorted. Thus, from the communication channel, vectors $\bar{S}_i'$ will be obtained:

$$\bar{S}_i' = (C(D_{\bar{b}_i}(w)))' \| f_{00..00}' \in F_p^{n+1}, \ i = \overline{1, m}.$$

where $(C(D_{\bar{b}_i}(w)))'$ is supposedly distorted vector $C(D_{\bar{b}_i}(w))$, scalar $f_{00..00}'$ is supposedly distorted value $f_{00..00}$. Let us denote scalar $f_{00..00}'$ corresponding to $\bar{S}_i'$ by $f_{00..00_i}'$.

Data recovery algorithm.

Input: vectors $\bar{S}_i'$, $i = \overline{1, m}$ and private key β (see (17)).

Output: vector $\bar{w}' \in F_q^{k_2}$.

Step 1. We isolate two components: $(C(D_{\bar{b}_i}(w)))' \in F_q^n$ and $f_{00..00_i}'$, $i = \overline{1, m}$ from each vector $\bar{S}_i'$, $i = \overline{1, m}$.

Step 2. We direct the vectors $(C(D_{\bar{b}_i}(w)))'$ to the decoders of the code $RM_q(1, m)$. Note that you can use arbitrary decoders, for example, [16], [18]. At the output of the decoders considered, polynomials $D_{\bar{b}_i}'(w) \subset F_q^{(1)}[x_1, x_2, ..., x_m], i = 1, ..., m$ are generated.

Step 3. We develop vector $(f_{00..00,1}', f_{00..00,2}', ..., f_{00..00,m}')$ from the coefficients $f_{00..00,i}'$ and feed it to the decoder input of the code $RM_q(0, m)$ which actually coincides with the code of m-tuple repetition. The result of this decoder performance is the scalar $f_{00..00}''$.

http://vestnik.donstu.ru

Step 4. We substitute the values of the coefficients of the polynomials $D_{\bar{b}_i}^{'}(w) \subset F_q^{(1)}[x_1, x_2,...,x_m]$, $i = \overline{1,m}$ and the key β (see (17)) into the formulas (7) and (8), and derive the polynomial $f(\bar{x})$ from the results obtained. Then we calculate the desired polynomial $w'(\bar{x}) = f(\bar{x}) + f_{00..00}^{"}$.

Step 5. The message recipient is given the information vector $\bar{w}' \in F_q^k$ corresponding to the polynomial $w'(\bar{x})$.

Note 1. The correctness of the data recovery algorithm depends on the number of errors that damage the vectors $\bar{S}_i \in F_q^{n+1}$ during their transmission along the communication lines, as well as on the correcting capacity of the first-order PM-codes used. It is plain that if the decoders used reconstruct the vectors $C(D_{\bar{b}_i}(w))$ and the value $f_{00..00}$ correctly, then the initial data restoration using the results of Theorem 1 will be correct, hence the vector $w'(\bar{x})$ obtained at the output of the data recovery algorithm will coincide with the original information vector $\bar{w} \in F_q^{k_2}$. Note that operation of the decoder for recovery $C(D_{\bar{b}_i}(w))$ is correct, if

$$\forall i = \overline{1,m}: \quad d_h(C(D_{\bar{b}_i}(w)),(C(D_{\bar{b}_i}(w)))') \le \lfloor (d_1 - 1)/2 \rfloor,$$

where $d_h(\bar{x}, \bar{y})$ is Hamming distance between the vectors $\bar{x}, \bar{y}$. The scalar $f_{00..00}$ is restored correctly if the vector $(f_{00..00,1}^{'}, f_{00..00,2}^{'}, ..., f_{00..00,m}^{'})$ formed in step 3 of the algorithm contains fewer than m/2 coordinates differing from the value $f_{00..00} = w(\bar{0})$. If, in $\bar{S}_i \in F_q^{n+1}$, $i = \overline{1,m}$, more errors occurred than can be restored by the decoders used, then the recovery $\bar{w} \in F_q^{k_2}$ is not guaranteed.

Note 2. The proposed partition and recovery algorithms employ Reed-Muller codes of both the first and second orders, but the decoders are used only for the first-order codes.

Note 3. The transmission confidentiality is provided not only by the need for knowledge of the key, but also by using several communication lines, because in this case, data interception is more challenging for an intruder than illegal data capture from a single communication line.

Decoder of Reed-Muller codes of the second order. First, let us consider the idea of the decoding algorithm organization, and then we describe the algorithm step-by-step. Let us fix some basis $\beta = \{\bar{b}_i = (b_1^i, b_2^i,...,b_m^i) \in F_q^m\}_{i=1,...,m}$ in the space F_q^m where $q = p^s$, p is an odd prime. Suppose that the decoder input receives $\bar{Y} = C(w) + \bar{e} (\in F_q^n)$ where w is the information polynomial, $C(w)$ is the code vector of the $[n, k_2, d_2]_q$-code, $RM_q(2,m)$, $\bar{e} \in F_q^n$ is the error vector for which

$$wt_h(\bar{e}) \le t_2, \tag{18}$$

where $wt_h(.)$ is Hamming weight, $t_2 = \lfloor (d_2 - 1)/2 \rfloor$. Employing vector $\bar{Y}$, we construct m vector derivatives calculated in the basic directions using the operator $\Delta_{\bar{b}}$:

$$\Delta_{\bar{b}_i}(\bar{Y}) = \Delta_{\bar{b}_i}(C(w) + \bar{e}) = \Delta_{\bar{b}_i}(C(w)) + \Delta_{\bar{b}_i}(\bar{e}), \quad i = 1,...,m$$

each of which is the vector $\Delta_{\bar{b}_i}(C(w)) \in RM_q(1,m)$ distorted by the error vector $\Delta_{\bar{b}_i}(\bar{e}) \in F_q^n$, and can be unerringly decoded by an arbitrary decoder of the $[n, k_1, d_1]_q$-code $RM_q(1,m)$ operating up to half the code distance (see, e.g., [16], [18]), if the error level is less than $t_1 = \lfloor (d_1 - 1)/2 \rfloor$, i.e. when

$$wt_h(\Delta_{\bar{b}_i}(\bar{e})) \le t_1. \tag{19}$$

If the vectors are decoded correctly, then the desired information polynomial of the code can be reconstructed using Theorem 1 up to one coordinate which can be then found, for example, by maximum likelihood decoding. Thus, for proper decoding $\bar{Y}$, according to the proposed scheme, the fulfillment of the condition (19) is required.

Algorithm for decoding the code $RM_q(2,m)$.

Input: parameters of $[n, k_2, d_2]_q$-code $RM_q(2,m)$, $\bar{Y} = (Y_{\alpha_1}, Y_{\alpha_2},...Y_{\alpha_n}) \in F_q^n$.

Output: decoded information vector $\bar{w}$.

Step 1. Let us fix some basis $\beta = \{\bar{b}_i = (b_1^i, b_2^i,...,b_m^i) \in F_q^m\}_{i=1,...,m}$ of the space F_q^m and calculate the derived vectors along all the directions $\bar{b}_i \in \beta$:

$$\Delta_{\bar{b}_i}(\bar{Y}) = \tau_{\bar{b}_i}(\bar{Y}) - \bar{Y}.$$

Step 2. Let us decode $\Delta_{\bar{b}_i}(\bar{Y})$, $i = 1,...,m$, using the arbitrary decoder of $RM_q(1,m)$-codes that operates up to half the code distance, and as a result, we obtain vectors $\bar{p}_{\bar{b}_i}$ and their polynomial representations

$$p_{\bar{b}_i}(\bar{x}) = \alpha_1^i x_1 + \alpha_2^i x_2 + ... + \alpha_m^i x_m + \alpha_0^i \subset F_p^{(1)}[x_1, x_2,...,x_m], \quad i = 1,...,m.$$

Step 3. Using the polynomials $p_{\bar{b}_i}(\bar{x})$, $i = 1,...,m$, we find the polynomial $f(\bar{x})$ with the intercept zeroth-order term from the formulas (7) and (8).

Step 4. For all $z \in F_q$, we calculate

$$\Psi(z) = \sum_{i=1}^{n} \left| C(f(\bar{x}) + z)_{\alpha_i} - Y_{\alpha_i} \right|,$$

where $C(f(\bar{x}) + z)_{\alpha_i}$ is α_i- th coordinate of the vector $C(f(\bar{x}) + z)$ (see (11)). Let us denote z_0 the value z on which the function $\Psi(z)$ attained its minimum.

Step 5. The decoding result is vector $\bar{w}$ that one-to-one corresponds to the information polynomial $w(\bar{x}) = f(\bar{x}) + z_0$.

Theorem 2. So that the derived algorithm of decoding the code $RM_q(2,m)$ can rectify all errors, it is sufficient to meet the conditions (18) and

$$wt_h(\bar{e}) \le t_1 / 2, \tag{20}$$

where $t_1 = \lfloor (d_1 - 1)/2 \rfloor$, d_1 is minimum distance of the code $RM_q(1,m)$.

Proof. At step 2, the decoder input receives vectors

$$\Delta_{\bar{b}_i}(\bar{Y}) = \tau_{\bar{b}_i}(\bar{Y}) - \bar{Y} = \tau_{\bar{b}_i}(C(\bar{w})) + \tau_{\bar{b}_i}(\bar{e}) - C(\bar{w}) - \bar{e} = \Delta_{\bar{b}_i}(C(w)) + \Delta_{\bar{b}_i}(e).$$

Recall that $\Delta_{\bar{b}_i}(C(w)) \in RM_q(1,m)$, and the decoders of the code $RM_q(1,m)$ operating up to half the code distance rectify up to t_1 errors in the codeword. From the condition (20), it follows that

$$wt_h(\Delta_{\bar{b}_i}(\bar{e})) \le wt_h(\tau_{\bar{b}_i}(\bar{e})) + wt_h(\bar{e}) = 2wt_h(\bar{e}) \le t_1$$

So, vectors $\bar{p}_{\bar{b}_i}$ which are developed at Step 2 coincide with $\Delta_{\bar{b}_i}(C(w))$. Hence it follows that at Step 3, owing to Theorem 1, the polynomial $f(\bar{x}) = w(\bar{x}) - w(\bar{0})$ is formed.

From the condition (18), it follows that the value z_0 calculated at Step 4 is equal to the constant term $w(\bar{0})$ of the desired information polynomial $w(\bar{x})$. Thus, the desired information vector $\bar{w}$ is obtained.

Note that for the correct decoding according to the proposed scheme, it is required to meet the condition (20), from which (19) follows, although the condition (18) is more natural. Let us consider the relationship between these conditions.

Lemma 4. For the codes $RM_q(2,m)$, in the case of $q = 3$, the condition (18) and (20) are equivalent, and in the case of $q > 3$, when the condition (18) is satisfied, the fulfillment of the condition (20) is not guaranteed.

Proof. From the consequence of Lemma 2, we obtain that at $q = 3$, the equality $t_1/2 = t_2$ is true; i.e. the right-hand sides of the inequalities (18) and (20) coincide; hence, the fulfillment of one of them implies the fulfillment of the other. At $q > 3$ from the consequence of Lemma 2, we obtain that $t_1/2 < t_2$, viz from the fulfillment of (18), the fulfillment of (20) does not follow.

Note 1. In [5-6], the decoder of the $RM_3(2,m)$-code is described, where, as in the proposed algorithm, derivative vectors are constructed for the noisy codeword. They are decoded by the maximum likelihood algorithm, and then the desired information word is restored from the values obtained. However, the derived vectors are constructed in all 3^m possible directions, not only in basic ones, in the decoder from [5-6]. And another mechanism is used to obtain the desired information vector.

Note 2. For codes $RM_q(2,m)$, $q = 3$, the proposed decoder operates up to half the code distance. For codes $RM_q(2,m)$, $q > 3$, the proposed decoder does not guarantee the correction of all errors, the number of which is less than t_2, but the decoder will operate well if the weaker condition (20) is satisfied. Note that the use of the proposed decoding scheme in case of the fields with cardinality of more than three may be appropriate, despite the determined limitation, for the following reasons. First, the theory of the decoders of the second-order PM-codes is ill-defined. But, if there is a first-order decoder, then the proposed decoder which is a suspension over it can fill in this gap. Secondly, when using the communication channels, the error probability in which is such that (20) is satisfied, the transition from the first-order PM-codes to the second-order codes reduces redundancy (see Table 1).

Conclusion. Theoretical results associated with restoring polynomials of several variables over Galois fields of fuzzy cardinality by their derivatives are obtained. As practical applications to the results obtained, a data partition scheme and a second-order PM-code decoder are proposed. In future, it is instructive to study the process of a polynomial recovery from distorted derivatives, and to develop appropriate modifications of the real-world applications proposed in this paper.

References

1. Deundyak, V.M., Knutova, A.V. Integriruemost' sistem polinomov neskol'kikh peremennykh pervoy i vtoroy stepeni nad prostymi polyami Galua. [Integrability of systems of the first and second degree polynomials of several variables over simple Galois fields.] Izvestiya vuzov. Severo-Kavkazskiy region. Natural Sciences. 2016, no. 2, pp. 41–46 (in Russian).

2. Ambrosimov, A.S. Svoystva bent-funktsiy q-znachnoy logiki nad konechnymi polyami. [Properties of bent-functions of q-valued logic over finite fields.] Discrete Mathematics, 1994, no. 3(6), pp. 50–60 (in Russian).

3. Logachev, O.A., Salnikov, A.A., Yashchenko, V.V. Bulevy funktsii v teorii kodirovaniya i kriptologii. [Boolean functions in coding theory and cryptology.] Moscow: MTsNMO, 2004, 470 p. (in Russian).

4. Mazurenko, A.V., Mogilevskaya, N.S. Sposob vosstanovleniya bulevoy funktsii neskol'kikh peremennykh po ee proizvodnoy. [Method of restoring multivariable Boolean function from its derivative.] Vestnik of DSTU, 2017, no. 1 (88), pp. 122–131 (in Russian).

5. Deundyak, V.M., Mogilevskaya, N.S. Model' troichnogo kanala peredachi dannykh s ispol'zovaniem dekodera myagkikh resheniy kodov Rida-Mallera vtorogo poryadka. [The model of the ternary communication channel with using the decoder of soft decision for Reed-Muller codes of the second order.] University News. North-Caucasian region. Technical Sciences Series, 2015, no. 1 (182), pp. 3–10 (in Russian).

6. Deundyak, V.M., Mogilevskaya, N.S. Ob usloviyakh korrektnosti dekodera myagkikh resheniy troichnykh kodov Rida-Mallera vtorogo poryadka. [On correctness conditions of s soft-decisions decoder for ternary Reed-Muller codes of the second order.] Vladikavkaz Mathematical Journal, 2016, vol. 18, iss. 4, pp. 23–33 (in Russian).

7. Mogilevskaya, N.S., Kulbikayan, R.V., Zhuravlev, L.A. Porogovoe razdelenie faylov na osnove bitovykh masok: ideya i vozmozhnoe primenenie. [Threshold file sharing based on bit masks: concept and possible use.] Vestnik of DSTU, 2011, vol.11, no. 10, pp. 1749–1755 (in Russian).

8. Tormasov, A.G., Khasin, M.A., Pakhomov, Y.I. Obespechenie otkazoustoychivosti v raspredelennykh sredakh. [Fault tolerance in distributed environments.] Programming, 2001, vol. 27, no. 5, pp. 26 (in Russian).

9. Mishchenko, V.A., Vilanskiy, Y.V. Ushcherbnye teksty i mnogokanal'naya kriptografiya. [Distorted texts and multichannel cryptography.] Minsk: Entsiklopediks, 2007, 292 p. (in Russian).

10. Deundyak, V.M., Popova, S.B. Model' organizatsii zashchishchennogo dokumentooborota na baze raspredelennoy peredachi dannykh s autentifikatsiey. [Secure document management model based on distributed data transmission with authentication.] Vestnik of DSTU, 2015, vol. 15, no. 4, pp. 101–106 (in Russian).

11. Mogilevskaya, N.S. O primenenii porogovogo razdeleniya dannykh dlya organizatsii razdelennoy peredachi na primere metoda bitovykh masok. [On application of threshold data partitioning for organization of split transmission using bitmask method as an example.] Engineering Journal of Don, 2017, no. 2. Available at: http://www.ivdon.ru/uploads/article/pdf/IVD_48_ Mogilevskaya.pdf_492254b6f1.pdf (accessed :12.08.2017) (in Russian).

12. Sidelnikov, V.M., Pershakov, A.S. Dekodirovanie kodov Rida-Mallera pri bol'shom chisle oshibok. [Decoding of Reed-Muller codes with a large number of errors.] Problems of Information Transmission, 1992, vol. 28, no. 3, pp. 80–94 (in Russian).

13. Karyakin, Yu.D. Bystroe korrelyatsionnoe dekodirovanie kodov Rida—Mallera. [Fast correlation decoding of Reed-Muller codes.] Problems of Information Transmission, 1987, vol. 23, no. 2, pp. 40–49 (in Russian).

14. Paterson, K.G., Jones, A.E. Efficient decoding algorithms for generalized Reed-Muller codes. IEEE Transactions on Communications, 2000, vol. 48, iss. 8, pp. 1272 – 1285.

15. Pellikaan, R., Wu, X.-W. List decoding of q-ary Reed-Muller Codes. IEEE Trans. On Information Theory, 2004, vol. 50, iss. 3, pp. 679-682.

16. Santhi, N. On Algebraic Decoding of q-ary Reed-Muller and Product Reed-Solomon Codes. ISIT 2007 Conference, June 24 -29, Nice, France, 2007.

Information technology, computer science, and management

17. Deundyak, V.M., Maevskiy, A.E., Mogilevskaya, N.S. Методы помехоустойчивой защиты данных [Methods of noisefree data protection.] Rostov-on-Don: SFU, 2014, 309 p. (in Russian).

18. Ashikhmin, A.E., Litsyn, S.N. Fast Decoding of Non-Binary First Order Reed-Muller Codes. Applicable Algebra in Engineering, Communication and Computing, 1996, vol. 7, iss. 4, pp. 299–308.

Authors:

Deundyak, Vladimir M.,
associate professor of the Algebra and Discrete
Mathematics Department, Vorovich Institute for
Mathematics, Mechanics, and Computer Science, Southern
Federal University, Senior Research Scholar, Southern
Regional Certification Centre, Research Institute
"Spetsvuzavtomatika" (51, Gazetny per., Rostov-on-Don,
344002, RF), Cand(Phys-Math), associate professor,
ORCID: http://orcid.org/0000-0001-8258-2419
vl.deundyak@gmail.com

Mogilevskaya, Nadezhda S.,
associate professor of Vorovich Institute for Mathematics,
Mechanics, and Computer Science, Southern Federal
University (8-a, ul. Milchakova, Rostov-on-Don,
344090, RF), Cand(Eng), associate professor,
ORCID: http://orcid.org/0000-0003-1357-5869
nadezhda.mogilevskaia@yandex.ru